

University of New Hampshire

University of New Hampshire Scholars' Repository

Doctoral Dissertations

Student Scholarship

Spring 2006

Assessing the accuracy of the MODIS LAI 1-km product in southeastern United States loblolly pine plantations: Accounting for measurement variance from ground to satellite

John Shepherd liames Jr.
University of New Hampshire, Durham

Follow this and additional works at: <https://scholars.unh.edu/dissertation>

Recommended Citation

liames, John Shepherd Jr., "Assessing the accuracy of the MODIS LAI 1-km product in southeastern United States loblolly pine plantations: Accounting for measurement variance from ground to satellite" (2006). *Doctoral Dissertations*. 317.

<https://scholars.unh.edu/dissertation/317>

This Dissertation is brought to you for free and open access by the Student Scholarship at University of New Hampshire Scholars' Repository. It has been accepted for inclusion in Doctoral Dissertations by an authorized administrator of University of New Hampshire Scholars' Repository. For more information, please contact Scholarly.Communication@unh.edu.

ASSESSING THE ACCURACY OF THE MODIS LAI 1-KM PRODUCT IN
SOUTHEASTERN UNITED STATES LOBLOLLY PINE PLANTATIONS:
ACCOUNTING FOR MEASUREMENT VARIANCE FROM GROUND TO
SATELLITE.

By

JOHN SHEPHERD IIAMES, JR.

B.S. Virginia Tech, 1984

M.S. North Carolina State University, 1999

DISSERTATION

Submitted to the University of New Hampshire
In Partial Fulfillment of the
Requirements for the Degree of

Doctor of Philosophy

in

Natural Resources and Environmental Studies

May, 2006

UMI Number: 3217425

INFORMATION TO USERS

The quality of this reproduction is dependent upon the quality of the copy submitted. Broken or indistinct print, colored or poor quality illustrations and photographs, print bleed-through, substandard margins, and improper alignment can adversely affect reproduction.

In the unlikely event that the author did not send a complete manuscript and there are missing pages, these will be noted. Also, if unauthorized copyright material had to be removed, a note will indicate the deletion.

UMI[®]

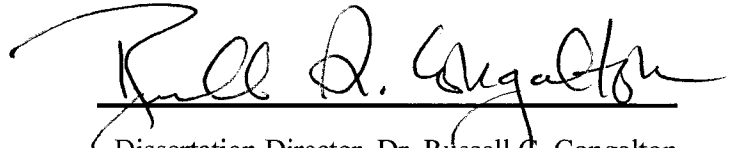
UMI Microform 3217425

Copyright 2006 by ProQuest Information and Learning Company.

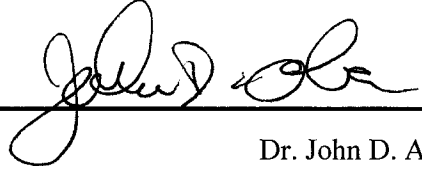
All rights reserved. This microform edition is protected against unauthorized copying under Title 17, United States Code.

ProQuest Information and Learning Company
300 North Zeeb Road
P.O. Box 1346
Ann Arbor, MI 48106-1346

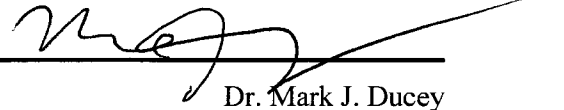
This dissertation has been examined and approved



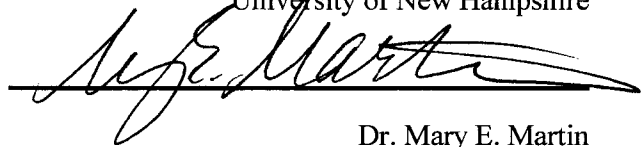
Dissertation Director, Dr. Russell G. Congalton
Professor of Natural Resources
University of New Hampshire



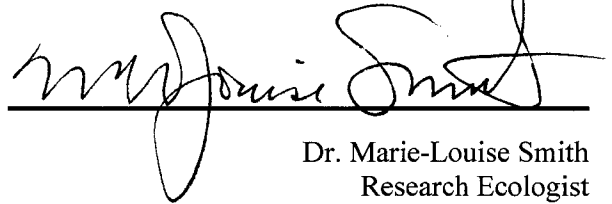
Dr. John D. Aber
Vice President for Research and Public Service
University of New Hampshire



Dr. Mark J. Ducey
Associate Professor of Natural Resources
University of New Hampshire



Dr. Mary E. Martin
Research Assistant Professor
Institute for the Study of Earth, Oceans, and Space
University of New Hampshire



Dr. Marie-Louise Smith
Research Ecologist
USDA Forest Service
Durham, NH

May 5, 2006
Date

ACKNOWLEDGEMENTS

First and foremost I am most grateful to God for providing this path of opportunity. Russ Congalton has had the most significant influence in encouraging my career in remote sensing. It seems like yesterday (1996) that we sat at lunch in Durham, NH and he discussed the incredible opportunities within this field. My colleagues at the US EPA have been especially supportive with this research giving their own time for various inputs into this project. I have appreciated input from Drew Pilant. He has consistently provided a sounding board from which to bounce ideas and thoughts. Others that I would like to thank include: Tim Lewis, Ross Lunetta, Joe Knight, Tim Wade, Megan Mahaffey, Jayantha Ediriwickrema, Dave Holland, and Govind Gawdi. I also want to thank Dr. John Lyon (Environmental Sciences Division, Director), Dr. Dorsey Worthy (Landscape Characterization Branch, Branch Chief), and Peter Principe (Acting LCB Branch Chief 2002) for supporting my long-term training at UNH.

My committee has been helpful even though we have been separated by seven states for the majority of my three and one-half years of work. I am thankful for their input into my project and stirring debate into other options for measuring forest productivity. I am thankful for the time and work provided by UNH graduate students in contributing to the assessment of land cover classification analyst differences. Those involved included: Jesse Bishop, Jennifer Bourgeault, Tina Cormier, Chris Czarneski, and Shawn Herrick. Also, a special thanks is given to Dr. Jeremiah Starling (Duke University) for proof reading this text.

Jeff Morisette and Jeff Privette at NASA Goddard (MD) have been instrumental with providing resources and insight into this research. Chapter II would not exist without the IKONOS data buy provided by NASA. The North Carolina Forest Nutritional Cooperative at NCSU allowed access to their long-term research plots. Specifically I would like to thank Tim Albaugh and Lee Allen. Yuri Knysthsfsff and Shabanov provided information on collection 4 and 5 MODIS LAI algorithm.

Finally, all of this extra work would not have been possible without support from my family. Michaela has been such a fan of my career development that without her support, I could not have accomplished this work. Ben and AJ also have been without a dad for the last couple of months as I finished this document. I also had great support from my mom and dad (John and Harriet Iiames, Wilmington, NC) and my sister, Whiz Iiames-Damutz and her husband Ted (Evanston, IL).

TABLE OF CONTENTS

ACKNOWLEDGEMENTS	iii
LIST OF TABLES	xi
LIST OF FIGURES	xiv
ABSTRACT	xvii
CHAPTER I: INTRODUCTION	1
CHAPTER II: LITERATURE REVIEW	4
Loblolly Pine (<i>Pinus taeda</i>)	4
<i>In Situ</i> Leaf Area Index	6
Direct and Semi-Direct Measures of LAI	7
Indirect Measures of LAI	9
Indirect Optical LAI Measurement Theory	9
Reported Distribution of Modified Beer-Lambert Law Inputs	14
Indirect Optical Instruments	14
TRAC	14
Digital Hemispherical Photography (DHP)	16
Satellite-Derived LAI	17
Vegetation Indices	17
Influence of Understory	22
MODIS MOD15A2 Description	23
Elements of Uncertainty	26

CHAPTER III: SITE DESCRIPTIONS AND SAMPLING	28
CHAPTER IV: LOBLOLLY PINE (<i>Pinus taeda</i>) LAI ANALYSIS INTEGRATING TWO INDIRECT OPTICAL INSTRUMENTS: THE TRACING RADIATION AND ARCHITECTURE OF CANOPIES (TRAC) AND DIGITAL HEMISPHERICAL PHOTOGRAPHY (DHP)	31
Abstract	31
Introduction	32
<i>In Situ</i> Measurement of LAI	34
Direct and Semi-Direct Measures of LAI	36
Indirect Measures of LAI	37
Indirect Optical LAI Measurement Theory	38
Reported Distribution of Modified Beer-Lambert Law Inputs	42
Indirect Optical Instruments	43
TRAC	43
Digital Hemispherical Photography (DHP)	44
Methods	46
Site Description	46
Optical TRAC-DHP and Field Measurements	49
TRAC Measurements	49
DHP Measurements	50
Needle-to-Shoot Area Ratio (λ_E)	52
Woody-to-Total Area Ratio (α).	53
Reference Stand-Level LAI: SETRES and Brunswick	54
Results	56
Element Clumping Index (Ω_E) and Effective LAI (L_e)	56

Needle-to-Shoot Area Ratio (γ_E)	56
Woody-to-Total Area Ratio (α)	59
TRAC-DHP derived LAI	59
Allometric Reference Stand-Level LAI	60
Comparison of LAI Estimates	62
Discussion	63
Conclusions	65
CHAPTER V: NDVI CHANGE DETECTION ANALYSIS OF IKONOS 4 M IMAGERY IN THE EVALUATION OF LEAF AREA INDEX (LAI) DIFFERENCES ON TWO LOBLOLLY PINE (<i>PINUS TAEDA</i>) STANDS FOLLOWING COMPLETE UNDERSTORY REMOVAL	66
Abstract	66
Introduction	67
Literature Review	68
Vegetation Indices	68
Influence of Understory	71
Methods	72
Site Descriptions	73
Understory harvest and herbicide application	77
<i>In situ</i> LAI Measurements	79
Sample Design	81
IKONOS Image Processing	82
Results	85
<i>In situ</i> LAI Measurements	85
Appomattox	86

Hertford	86
IKONOS Image Analysis	87
Georectification	87
Image-to-Image NDVI Change Detection	88
Within Image NDVI Change Analysis	88
Spatial averaging window size	90
Other Vegetation Indices	90
Discussion	91
Conclusions	94
CHAPTER VI: UNCERTAINTY ANALYSIS OF A FINE RESOLUTION LEAF AREA INDEX (LAI) SURFACE MAP FOR MODIS LAI VALIDATION IN SOUTHCENTRAL VIRGINIA	95
Abstract	95
Introduction	97
Literature Review	100
Uncertainty: Indirect <i>in situ</i> optical LAI estimation methods	103
Uncertainty: Inter-analyst differences in LC classification	104
MODIS MOD15A2 Description	106
Methods	109
Process 1: TRAC-DHP <i>in situ</i> variability	110
MODIS LAI validation and TRAC-DHP parameterization site; Appomattox, Virginia	110
TRAC-DHP parameterization sites; Brunswick (Va), SETRES (NC), and Schenck (NC)	112
Optical Instrument Descriptions: TRAC and DHP	115

Sampling Design	117
TRAC measurements (Ω_E)	120
DHP measurements (L_e).	123
Needle-to-shoot area measurements (γ_E)	124
Woody-to-total area ratio measurements (α)	124
TRAC-DHP LAI variability assessment: Monte Carlo Simulation in <i>P. taeda</i> (unthinned)	125
Appomattox Validation Site TRAC-DHP LAI estimation measurements 2002	126
Summary: TRAC-DHP <i>in situ</i> variability method	127
Process 2: Classification variance between analysts	127
Landsat ETM ⁺ Georectification	129
Data Exploration	130
Data Analysis: Techniques	131
Data Analysis: Classification	132
Classification Assessment	133
Classification Assessment: Classification-to-Classification Comparison	133
Classification Assessment: Reference Creation and Analysis	134
Classification Assessment: Classification-to-Reference Comparison	135
Classification Assessment: Training Site Assessment	136
Process 3: RSM Aggregation and Comparison	137

Appomattox Validation of MODIS MOD15A2 LAI 1 km ² cell	138
Results	141
TRAC-DHP variability analysis	141
LC Classification Variability	145
Classification-to-Classification Comparison	145
Reference Creation and Analysis	146
Classification-to-Reference Comparison	149
Training Site Assessment	157
RSM aggregation and comparison	160
Discussion	162
Indirect <i>in situ</i> optical estimation of LAI	162
Classification differences	163
Aggregation and comparison	164
Conclusions	165
CHAPTER VII: FINAL CONCLUSIONS	167
LITERATURE CITATIONS	170
APPENDICES	181
APPENDIX A: Point-in-Time LAI Estimation (Sampson et al., 2003)	182
APPENDIX B: MakeGrid AML	184

LIST OF TABLES

Table 1.	Regression correlations for vegetation indices (NDVI and SR)	21
Table 2.	LAI research sites and associated measurements	30
Table 3.	Forest biometric summary for both sites: SETRES and Brunswick.	48
Table 4.	Needle-to-Shoot area ratio (γ_E) measurements on SETRES S1P	57
Table 5.	Needle-to-Shoot area ratio (γ_E) measurements on SETRES S2P	57
Table 6.	Needle-to-Shoot area ratio (γ_E) measurements on SETRES S2P	58
Table 7.	Needle-to-Shoot area ratio (γ_E) measurements across three plots, crown position	58
Table 8.	ANOVA ($\alpha = 0.05$) for (γ_E) three plots	59
Table 9.	Parameter inputs for TRAC-DHP integration calculation of LAI	60
Table 10.	Control plot LAI derived from SETRES allometric equations at two sites: (SETRES and Brunswick).	62
Table 11.	TRAC-DHP: Allometric LAI comparison	63
Table 12.	Regression correlations for vegetation indices (NDVI and SR)	70
Table 13.	Image-to-image analysis of May 23 and August 3, 2002 images (Appomattox)	88
Table 14.	Vegetation indices differences evaluating biomass change detection for the August 13, 2002 Hertford IKONOS NDVI image	91
Table 15.	Global LAI products.	99
Table 16.	Forest biometric summary for all sites (UP – unthinned pine; TP – thinned pine; H – hardwood)	115
Table 17.	Plot coordinates, Appomattox (UTM, NAD 83, Zone 17, meters) U – unthinned, P -thinned)	120

Table 18.	Weather conditions measured at RDU for the period of 8/5/2004 – 8/12/2004	121
Table 19.	Natural variability measured over three forest types, Appomattox, Va. (NV = Natural Variation)	123
Table 20.	L_e natural variability measured over three forest types, Appomattox, Va. (NV = Natural Variation)	124
Table 21.	Derivative bands created from original 6-band ETM+ imagery	131
Table 22.	<i>P. taeda</i> variability for the modified Beer-Lambert light extinction model input parameters	143
Table 23.	<i>P. taeda</i> inputs for Monte Carlo simulation at Appomattox Q1P	144
Table 24.	<i>In situ</i> LAI measurements on Appomattox validation site 2002	145
Table 25.	Land cover reference data sets by cell resolution	147
Table 26.	Patch size analysis for 19.4 km ² classified Ikonos 1 m (resolution) image. PLPG is the proportion of the largest patch area to the total patch area.	149
Table 27.	Overall classification accuracy results for six analysts across 8 cell resolutions (150 m – 1200 m) as compared to 19.4 km ² reference classification	149
Table 28a.	Analyst 1-3 error matrices for 150 m cell resolution. LC = Land Cover (1 – Deciduous, 2 – Coniferous, 3 – Mix, 4 – Water, 5 – Other Vegetation).	151
Table 28b.	Analyst 4-6 error matrices for 150 m cell resolution. LC = Land Cover (1 – Deciduous, 2 – Coniferous, 3 – Mix, 4 – Water, 5 – Other Vegetation).	152
Table 29.	Kappa analysis of all six analyst-derived classifications (150 m cell resolution)	152
Table 30.	Testing for significant differences between 15 analyst pair-wise comparisons using a Bonferonni adjusted t-value of 2.58 (150 m)	153
Table 31a.	Analyst 1-3 error matrices for 90 m cell resolution. LC = Land Cover (1 – Deciduous, 2 – Coniferous, 3 – Mix, 4 – Water, 5 – Other Vegetation).	154

Table 31b.	Analyst 4-6 error matrices for 90 m cell resolution. LC = Land Cover (1 – Deciduous, 2 – Coniferous, 3 – Mix, 4 – Water, 5 – Other Vegetation).	155
Table 32.	Kappa analysis of all six analyst-derived classifications at the 90 m cell resolution	155
Table 33.	Testing for significant differences between 15 analyst pair-wise comparisons	156
Table 34.	Testing for significant differences between 90 m and 150 m matrices per analyst	157
Table 35.	Summary of training site data collected by six analysts.	158
Table 36.	Training site separability analysis for six analysts employing the Euclidean Distance algorithm.	159
Table 37.	Transformed Divergence analysis for six analysts for training site data	159
Table 38.	Jeffries-Matusita for six analysts for training site data	159
Table 39.	Signature overlap (%) for six analysts for training site data	159
Table 40.	Calculation of RSM mean LAI from combining LC types	161
Table 41.	RSM and MODIS 1 km ² LAI values with uncertainties	161
Table 42.	Classification variability between six analyst-derived classifications	161

LIST OF FIGURES

Figure 1.	LAI validation site map	29
Figure 2.	Location map of two sampling sites in North Carolina (SETRES) and Virginia (Brunswick).	47
Figure 3.	Plot design for SETRES and Brunswick Sites.	49
Figure 4.	Main axis measured to determine HSA-to-Projected conversion factor.	60
Figure 5.	Seasonal LAI derived from destructive harvest data for the SETRES site (2003).	61
Figure 6.	Seasonal LAI derived estimated using the SETRES allometric Equations for Brunswick site (2003).	61
Figure 7.	Mean seasonal LAI derived from SETRES-derived allometric equations for two sites, Brunswick and SETRES (2003).	62
Figure 8.	North Carolina and Virginia <i>P. taeda</i> site locations.	75
Figure 9.	Distribution of understory tree species sampled on the Appomattox site	76
Figure 10.	Distribution of understory tree species sampled on the Hertford site	76
Figure 11.	Understory Harvest, Appomattox, VA (A) showing pre-harvest (B) and post harvest (C) conditions.	78
Figure 12.	100 x 100 m (1 ha) quadrant design	82
Figure 13.	Sun and IKONOS collection azimuths from Appomattox image pairs.	84
Figure 14.	Sun and IKONOS collection azimuths from Hertford image pairs	84
Figure 15.	True color and false color composites	85

Figure 16.	Appomattox May 23, 2002 NDVI (A) and 5x5 NDVI (B). Appomattox August 3, 2002 NDVI (C) and 5x5 NDVI (D).	89
Figure 17.	Hertford May 12, 2002 NDVI (A) and 5x5 NDVI (B). Hertford August 13, 2002 NDVI (C) and 5x5 NDVI (D).	89
Figure 18.	Comparison of various spatial averaging windows on Hertford August 13, 2002 NDVI image	90
Figure 19.	The MODIS MOD15A2 validation procedure	102
Figure 20.	MOD15A2 LAI validation site (yellow square) constrained within a 100 km ² Landsat ETM ⁺ image, Appomattox, Virginia.	110
Figure 21.	Location map of three sampling sites in North Carolina and Virginia	114
Figure 22.	Elements of <i>P. taeda</i> uncertainty within the TRAC-DHP indirect <i>in situ</i> optical LAI estimation method.	118
Figure 23.	100 x 100 m quadrant sampling unit	119
Figure 24.	100 m subplot sampling unit	119
Figure 25.	The August 12, 2002 100 km ² Landsat ETM ⁺ image classified by 6 UNH analysts.	129
Figure 26.	Calculation of the percentage of training site overlap.	137
Figure 27.	MODIS MOD15A2 LAI Tile (vertical 05, horizontal 11)	140
Figure 28.	Three-year average of Appomattox validation site MODIS 1 km ² cell	141
Figure 29.	Atmospheric changes and the effect on measured Ω_E	143
Figure 30.	Effect of solar zenith angle changes on Ω_E	144
Figure 31.	LC agreement across eight cell resolutions for six analyst-derived LC maps	146
Figure 32.	Reference land cover variability across ten cell resolutions	148
Figure 33.	Reference land cover homogeneity analysis over multiple scales	148
Figure 34.	Percent overall agreement between six analyst-derived Classifications across varying scales	150

Figure 35.	Omission and Commission error for all analyst derived classifications across all land cover classes at the 150 m cell resolution	153
Figure 36.	Omission and Commission error for all analyst derived classifications across all land cover classes at the 90 m cell resolution.	156
Figure 37.	Spectral pattern analysis for training site data collected by six analysts	158
Figure 38.	Primary algorithm, back-up algorithm, or failure for MODIS LAI retrieval over 3 x 3 km area	165

ABSTRACT

ASSESSING THE ACCURACY OF THE MODIS LAI 1-KM PRODUCT IN SOUTHEASTERN UNITED STATES LOBLOLLY PINE PLANTATIONS: ACCOUNTING FOR MEASUREMENT VARIANCE FROM GROUND TO SATELLITE.

by

JOHN SHEPHERD IIAMES, JR.

University of New Hampshire, May, 2006

Leaf area index (LAI), defined here as one-half of the total leaf area per unit ground surface area (Chen, 1996), has been estimated at a global scale from spectral data processed from the Moderate Resolution Imaging Spectroradiometer (MODIS) sensor aboard two NASA EOS-AM spacecraft, Terra (launched in 1999) and Aqua (launched in 2002). The MOD15A2 LAI product is a 1 km global data product composited over an 8-day period and is derived from a three-dimensional radiative transfer model driven by an atmosphere corrected surface reflectance product (MOD09), a land cover product (MOD12) and ancillary information on surface characteristics. The United States Environmental Protection Agency (US EPA) initiated validation research (2002) in the evergreen needle leaf biome, as defined in the MOD12 classification, in a regional study located in the southeastern United States. The validation effort was prompted by the potential use of MODIS LAI inputs into atmospheric deposition and biogenic emission models developed within the US EPA Office of Research and Development. The MODIS LAI validation process involves the creation of a high spatial resolution LAI surface

map, which when scaled to the MOD15A2 resolution (1 km) allowed for comparison and analysis with the 1 km MODIS LAI product. Creation of this LAI surface map involved: (1) the collection of *in situ* LAI measurements via indirect optical measurements, (2) the correlation of land cover specific LAI estimates with spectral values retrieved from high resolution imagery (20 m - 30 m), and (3) the aggregation of these 30 m cells to 1 km spatial resolution, matching the resolution of the MODIS product and enabling a comparison of the two LAI values (Morisette et al. 2006).

This research assessed the uncertainty associated with the creation of the high-resolution LAI reference map, specifically addressing uncertainty in the indirect *in situ* optical measurements of LAI and the uncertainty in the land cover classification process. Also addressed was the influence of vegetative understory on satellite-derived vegetation indices from the IKONOS sensor.

CHAPTER I

INTRODUCTION

The advent of remotely sensed data from satellite platforms has enabled the examination of vegetative spatial distributions over regional and global scales. This assessment of ecosystem condition through the synoptic monitoring of terrestrial vegetation extent, biomass, and seasonal dynamics has begun to answer questions related to carbon sequestration and the expansion of greenhouse gases, biogenic emissions and the inputs into air quality, and other significant environmental issues. One input of interest, leaf area index (LAI) defined here as one-half the total green leaf area per unit ground surface area (Chen and Black, 1992a), has been used for the quantification of surface photosynthesis, evapotranspiration, and annual net primary production used in the calculation of terrestrial energy, carbon, water cycle processes, and biogeochemistry of vegetation. LAI has been identified as the variable of greatest importance for quantifying energy and mass exchange by plant canopies over landscapes (Running et al., 1986) and has been shown to explain 80% - 90% of the variation in the aboveground net primary production for forests in the United States (Gholz, 1982; Gower et al., 1992; Fassnacht and Gower, 1997).

The significance of LAI as source data for process-based ecological models has been well documented. Running and Coughlan (1988) ranked LAI as the most important attribute of vegetation structure for characterizing forest canopies over large areas at broad spatial scales using satellite remote sensing data. The leaf surface area has been identified as the main surface of exchange between the plant canopy and the atmosphere and has been related to canopy interception, transpiration, net photosynthesis, gas, water, carbon, and energy exchange, net primary productivity (NPP), biomass, rainfall interception, and dry deposition (Aber, 2001;

Gholz, 1982; Pierce and Running, 1988; Gower and Norman, 1991; Hall et al., 2003; Chason et al., 1991). Gower et al. (1999) notes that most ecosystem process models that simulate carbon and hydrogen cycles require LAI as an input variable. By controlling terrestrial mass and energy fluxes, vegetation plays a vital role in global climate change. Interest in tracking LAI phenology includes the role forests play in the sequestration of carbon from carbon emissions (Johnsen et al., 2001), and the formation of tropospheric ozone from biogenic emissions of volatile organic compounds (BVOC) naturally released into the atmosphere (Geron et al., 1994).

Researchers from the United States Environmental Protection Agency (US EPA) Landscape Characterization Branch under the auspices of the Environmental Sciences Division along with researchers from US EPA Atmospheric Modeling Division (AMD) are currently evaluating satellite derived LAI as a potential input into a number of air quality models. Two local scale AMD models, the Multilayer Model (MLM) and the Multilayer Biochemical Model (MLBC), estimate water vapor and carbon dioxide (MLBC only), along with ozone, SO₂, and nitric acid fluxes across the Clean Air Status and Trends Network (CASTNET). The MLM and MLBC models input a generalized annual leaf area index (LAI) profile developed from periodic leaf-on and leaf-off field sampled optical point measurements. Both of these dry deposition models were shown to be highly sensitive to the annual LAI profile parameters generated from these point measurements. On a regional scale, the Community Multiscale Air Quality Model (CMAQ) relies on output from the mesoscale model (MM5) where LAI, a function of solar radiation, root level moisture, air temperature, and air humidity deficit, are inputs to determine stomatal resistance. LAI inputs from the Moderate Resolution Imaging Spectroradiometer (MODIS) LAI product potentially may improve model returns due to the improved spatial and temporal resolution of the MODIS data.

LAI has been estimated at a global scale from spectral data processed from the Moderate Resolution Imaging Spectroradiometer (MODIS) sensor aboard two NASA EOS-AM spacecraft; Terra (launched in 1999) and Aqua (launched in 2002). The MOD15A2 LAI product is a 1 km

global data product composited over an 8-day period and is derived from a three-dimensional radiative transfer model driven by an atmosphere corrected surface reflectance product (MOD09), a land cover product (MOD12) and ancillary information on surface characteristics. The US EPA initiated validation research (2002) in the evergreen needle leaf biome, as defined in the MOD12 classification, in a regional study located in the southeastern United States. The evergreen needle-leaf biome has been evaluated in northern boreal forests but has not been validated in the southern pine region.

The MODIS LAI validation process involves the creation of a high spatial resolution LAI surface map, which when scaled to the MOD15A2 resolution (1 km) allows for comparison and analysis with the 1 km MODIS LAI product. Creation of this LAI surface map involved: (1) the collection of *in situ* LAI measurements via indirect optical measurements, (2) the correlation of land cover specific LAI estimates with spectral values retrieved from high resolution imagery (20 m - 30 m), and (3) the aggregation of these 30 m cells to 1 km spatial resolution, matching the resolution of the MODIS product and enabling a comparison of the two LAI values (Morisette et al., 2006).

This research addressed: (1) the assessment of *in situ* optical estimates of LAI, (2) the contribution of LAI from understory vegetation as assessed from *in situ* measurements and satellite-derived empirical relationships, and (3) the uncertainty associated with the creation of a fine-resolution LAI reference map.

CHAPTER II

LITERATURE REVIEW

This literature review documents *Pinus taeda* growth characteristics and physiology, *in situ* LAI estimation techniques “both direct, semi-direct, and indirect”, indirect optical LAI estimation theory employing the Beer-Lambert Law, satellite-derived LAI from vegetation indices, influence of understory, MODIS MOD15A2 description, and issues of uncertainty and error in geospatial and measurement processes.

Loblolly Pine (*Pinus taeda*)

Approximately 58% of the southeastern United States is forested, of which 20% is owned by forest industry (Johnsen et al., 2001). *Pinus taeda* is the dominant tree species within this region comprising over half the standing pine volume in the south. This tree species is capable of establishment and growth on wide variety of soils and is highly plastic with respect to resource availability (Maier et al., 2002). In particular, the area of commercial forestlands in *P. taeda* has increased 15.3% in 29 years (1960-1989) (Schultz, 1997). This tree species is intermediate to shade intolerant. Highly prolific growth may occur on average site quality, with a 0.6-0.9 m growth increment per year, typically attaining heights of 23-26 m at age 50.

P. taeda needles are 8-18 cm in length with 2-3 needles per fascicle. Within a fully stocked stand, approximately 10-20% of incident radiation reaches the forest floor. The canopy architecture for *P. taeda* exhibits significant variation due to indeterminate growth (multiple flushes) and high plasticity, i.e. developmental patterns, in foliage accretion and abscission in response to site fertility and drought (Dougherty et al., 1995; Herbert and Jack, 1998; Vose, 1988;

Vose and Allen, 1988; Sampson et al., 2003). Sampson et al. (2003) found that *P. taeda* varied twofold interannually with a minimum LAI in March-April and a maximum in September.

Needle abscission and accretion were found to impact a current year foliage cohort beginning at bud initiation (July) and continuing through the third year, though only 7-9% of the foliage could be attributed to that third year. Peak LAI for an entire *P. taeda* stand in Alabama was recorded between 11-14 years, after which LAI decreased due to increased mortality and competitive stress induced by limited resources (Sword et al., 2002). A myriad of factors within the southeastern United States have contributed to suboptimal levels of LAI in pine plantations. These factors include low nutrient and water availability in association with high temperatures and elevated ozone levels (Teskey et al., 1987; Vose and Allen, 1988; Colbert et al., 1990; Hennessey et al., 1992; Stow et al., 1992; Albaugh et al., 1998)

P. taeda stand level forest growth is determined by: (1) intercepted incident radiation, (2) photosynthetic efficiency, i.e. the amount of CO₂ fixed per absorbed photon, a ratio known as quantum yield, (3) the consumption of fixed carbon in respiration, and the allocation of fixed carbon to stemwood (Vose and Allen, 1988). Distinct physiological differences are found throughout the vertical and horizontal profile of the individual tree. The upper crown supports sun shoots which when compared to the lower canopy shade shoots have a higher LAI. However within the lower canopy there are a larger number of branches supporting more needle-bearing shoots than with the upper canopy, resulting in a higher overall LAI (Yu et al., 2003). The upper crown foliage exhibits higher net photosynthetic rates due to higher photosynthetic capacity, i.e. the rate of photosynthesis under optimal light, CO₂, temperature, and water conditions (related to the amount of photosynthetic 'machinery' of the leaf), and greater light interception when compared to the lower canopy foliage. In the light limited phase of net photosynthetic response to increasing light levels, a positive linear relationship exists up to 12.5% (250 μmol/m/s). Beyond 12.5% this relationship shows net photosynthesis increasing at a decreasing rate to 25% (500 μmol/m/s), then saturating beyond the 25% threshold (Gough et al., 2004).

Within C3 plants, approximately 75% of leaf nitrogen (N) is dedicated to the biochemical and physiological processes of photosynthesis (Field and Mooney, 1986; Zhang et al., 1997). N reallocation to sun foliage occurs within C3 plants in order to maximize carbon gain (Zhang et al., 1997). Specifically, under high irradiance N is redistributed from chlorophyll and thylakoid production and maintenance to the production of RuBP carboxylase (Ribulose – 1,5 – biphosphate), a chemical compound required in the Calvin cycle to reduce CO₂ to sugar (sucrose). This N shift also increases the electron transport capacity per unit of chlorophyll to maintain electron transport balance and RuBP carboxylase activity (Evans, 1989). Within low light foliage N is redistributed to increase chlorophyll production allowing for increased absorption efficiency of incident radiation (Zhang et al., 1997). Zhang et al (1997) found that *P. taeda* had increased stomatal conductance of CO₂ with increasing light intensity.

In Situ Leaf Area Index

LAI is a dimensionless quantity broadly defined as the amount of leaf area (m²) in a canopy per unit ground area (m²). Four common definitions of LAI are: (1) the total leaf area counting both sides of a leaf per unit ground area, (2) the one-sided leaf area (one-half the total LAI) disregarding leaf shape, (3) the projected leaf area (horizontal), and (4) the projected leaf area (inclined) (Barclay, 1998; Asner et al., 2003). Each definition was designed with respect to the different processes LAI was used to estimate such as vegetation growth, physiological activity, or light attenuation (Asner et al., 2003). It is important to identify the definition used when comparing LAI values from one study to another. For instance, the one-sided LAI definition may exceed horizontal projected LAI values by a factor of 1.28 (hemi-circular cylinders representing conifer needles).

In situ LAI measurement methodologies include three types: (1) direct, (2) semi-direct, and (3) indirect. The only direct measurement techniques available in vegetative systems are: (1) area harvest sampling where all leaf biomass is destructively harvested and measured and (2) the

collection of deciduous litterfall across an entire stand where every leaf is accounted for its contribution to the total leaf surface area. Whether a technique fits the profile of a semi-direct method is a matter of semantics. Technically, allometric regression equations developed from whole-tree destructive sampling would be defined as an indirect method. Here, one or more independent variables (i.e. tree diameter and/or height) are measured to estimate LAI for that particular tree. However, the origins of these estimates reside in the data collected from direct sampling of foliar biomass, therefore this technique has a direct and indirect component. This definition holds fast only when the regression equations are used to estimate LAI from the stand from which the relationships were developed. Application of an allometric regression estimate beyond the originating site places the technique within the “indirect” category. The collection of litterfall is also a semi-direct LAI estimation technique when spatial and temporal sampling schemes are employed to scale the data to the stand level. Indirect methods include contact methods (plumb lines and inclined point quadrats), and non-contact optical methods that measure light transmittance through a forest canopy under the assumption of randomly distributed foliage (LiCOR Plant Canopy Analyzer (PCA) (LiCOR, Lincoln, Neb, USA), hemispherical photographs, TRAC, Decagon Ceptometer). Semi-direct and indirect optical methods of assessing LAI have been shown to agree within 25-30% across a wide variety of ecosystems and cover types (Gower et al., 1999). The following is a review of semi-direct and indirect estimation techniques used to evaluate LAI.

Direct and Semi-Direct Measures of LAI.

Litterfall measurement of LAI is advantageous in deciduous systems that have a single litterfall season with adequate spatial and temporal sampling schemes (Neumann et al., 1989), but provides challenges in the measurement of conifer leaf area due to continuous litterfall and replacement (Chason et al., 1991). Needle fall is not directly related to either new growth or growth in the previous year, but rather on the average life span of the needles and the cumulative

climate conditions over the life span. Loblolly pine, for example, produces two to four growth cycles per year and retains foliage for 2 years (Schultz, 1997).

For forested ecosystems, leaf area estimates from allometric relationships are developed from a subsampling of trees destructively harvested within a range of diameters found within a specific forest type. Allometry is the relationship between the mass or area of a part or all of an organism and an independent variable. The development of allometric equations from destructive harvests yields the advantages of quantifying stem, branch, and foliage area separately. These equations also allow for the characterization of the vertical distribution of LAI along with the apportionment of LAI by each age-cohort of foliage, and do not require estimates of clumping factors (Chen et al., 1997). Destructive sampling involves the sampling of specific leaf area (SLA) which is defined as the ratio of fresh foliage surface area to unit dry foliage mass. SLA provides the coefficient required to convert foliage mass to leaf area (Landsberg and Gower, 1997) and has been positively correlated with percent leaf nitrogen concentration and maximum photosynthetic rate (Reich et al., 1995). Because SLA and foliage-to-branch mass decreases with height in the vertical profile of the canopy, sampling must be stratified to account for this variation (Gower et al., 1999). SLA also varies by age-cohort of foliage with a two-fold difference found between new and old foliage (Landsberg and Gower, 1997). Application of destructive harvests within forested systems, however, requires allometric relationships to be applied beyond the range of sampled trees, potentially introducing extrapolation error.

Semi-direct estimates based on tree allometry and litterfall are labor intensive and do not always provide accurate and unbiased LAI estimates (Chason et al., 1991; Cutini et al., 1998). Allometric relationships have been shown to be stand and site specific dependent upon season, age, stand density, tree crown size, and climatic differences (Gholz et al., 1976; Pearson et al., 1984; Mencuccini and Grace, 1995; Gower et al., 1997). Yet even stand and site specific regression equations are dependent on the validity of the underlying model and the quality and abundance of the data to which it is fitted (Gregoire et al., 1995). Allometric techniques relate

LAI to forest mensurational data such as sapwood, basal area, and crown closure (Hall et al., 2003; Snell and Brown, 1978; Buckley, 1999) and are influenced by environmental factors and therefore may not be transferable to other forests (Deblonde et al., 1994). These coefficients vary between sites and species, producing significant errors in LAI estimations. Non-site specific sapwood allometrics overestimated LAI when compared to optical estimates (Jonckheere et al., 2004; Law et al., 2001). Grier et al., (1984), found errors in biomass estimates from generalized equations range between -8% to +93% as compared to site-specific equations for five Douglas-fir (*Pseudotsuga menziesii*) stands.

Indirect Measures of LAI.

Semi-direct destructive sampling is regarded as the most accurate approach, yielding the closest approximation of “true” LAI. However, destructive sampling is time consuming and labor intensive, motivating the development of a more rapid *in situ* LAI estimation technique employing indirect optical methods. Optical methods measure canopy gap fraction and gap size distribution to estimate LAI in forested canopies. Issues that confound optical estimation of LAI include an unknown foliage angle distribution, errors introduced due to nonrandom spatial distribution of foliage elements, and the contribution of supporting woody material to radiation interception (Chen and Cihlar, 1995a). Chen (1996) noted that optical methods that address these issues (i.e. random vs. non-random canopy architecture) have the potential of providing better estimates of LAI when compared to destructive sampling techniques in coniferous forests.

Indirect Optical LAI Measurement Theory. Indirect optical methods involve ground-based measurement of gap fraction defined as the direct or diffuse light transmittance through the canopy to the forest floor. These optical methods apply the Beer-Lambert Law (Beer, 1853) taking into account that the total amount of radiation intercepted by a canopy layer is dependent on the incident irradiance, canopy structure and optical properties of the site (Jonckheere et al., 2005). The Beer-Lambert Law is expressed as:

$$P(\theta) = e^{-G(\theta, \alpha)L_e / \cos(\theta)} \quad (1)$$

where θ is the zenith angle of view, α is the leaf angle distribution, $P(\theta)$ is the gap fraction defined as the probability of light penetration through the foliage at θ , L_e is the effective leaf area index, and $G(\theta, \alpha)$ is the projection coefficient, a factor corresponding to the fraction of foliage projected on the plane normal to the zenith direction. Effective LAI (L_e), defined as the “effect” of non-random foliage spatial distribution on indirect measurements of LAI, can be derived indirectly from this radiation inversion model (i.e., light extinction model) based on the probability (P) of a light ray missing all foliage elements while passing through a canopy at some angle θ . Under the assumption that canopy foliage elements are distributed according to a Poisson process (i.e., randomly distributed) it is possible to derive expressions for the 95% confidence limits of gap fraction.

Both optical sensors used in this study, the Tracing Radiation and Architecture of Canopies (TRAC) and digital hemispherical photography (DHP), are capable of extracting gap fraction from forest canopies. However, TRAC requires continuous measurement between a zenith θ of 30°-60°, usually one-half day, to process a gap fraction figure. Hemispherical photography measures gap fraction instantaneously over a wide range of zenith angles. An estimate of the projection coefficient $G(\theta, \alpha)$ in the absence of known leaf angle distribution α , requires gap fraction measurements over the entire range of zenith angles. However, at 1 radian (57.3°) the projection coefficient $G(\theta, \alpha)$ approaches 0.5 based on the insensitivity of the leaf angle distribution at that angle (Wilson, 1963; Jones, 1992). The 1 radian criteria for $G(\theta, \alpha)$ of 0.5 has been shown over a wide variety of leaf and needle structures. Therefore, a gap fraction determined from hemispherical photography at 1 radian may assume a projection coefficient of 0.5, eliminating the prior requirement of solving for this parameter over multiple angles.

Under the assumption of random canopy foliage elements, effective LAI (L_e) can be retrieved with gap fraction measurements made from the indirect optical sensors with an assumed projection coefficient $P(\theta)$ of 0.5. In nature, however, canopies exhibit non-random spatial patterns. The spatial distribution of foliage elements is dictated by distinct canopy architecture including crowns, whorls, branches, shoots, and groups of trees (Chen et al., 1997). Therefore, in order to account for the non-random nature of foliage distribution within a forest stand, a correction factor, $\Omega(\theta)$, or total clumping index (Chen, 1996), is required to convert the randomly-assumed effective LAI (L_e) to a non-random LAI, defined as L_t . Thus, effective LAI (L_e) is decomposed into two components: true LAI (L_t) and total clumping index $\Omega(\theta)$:

$$L_e = L_t * \Omega(\theta) \quad (2)$$

Chen (1996) defines $\Omega(\theta)$ as:

$$\Omega(\theta) = \frac{\Omega_E}{\gamma_E} \quad (3)$$

where $\Omega(\theta)$ is the total clumping index based on the quotient of Ω_E/γ_E , where Ω_E is the element clumping index and γ_E is the needle-to-shoot area ratio, defined as one-half the needle area to one-half of the shoot silhouette area. The total clumping index is a parameter determined by the deviation of the spatial distribution of a vegetative canopy from a random case (LeBlanc, 2005). Ω_E quantifies the effect of foliage clumping at scales larger than the shoot, while γ_E represents the needle-to-shoot area ratio quantifying within shoot clumping (Fassnacht et al., 1994; Chen et al., 1997). The needle-to-shoot area ratio measurement is untenable with optical measuring devices due to the insensitivity of the sensors to resolve the small gaps found within conifer shoots; thus

this parameter is extracted with field and lab measurements. The element clumping index, Ω_E , is quantified by measurements made with TRAC and DHP. A regular pattern of foliage dispersion yields a total clumping index of greater than 1.0, a random foliage distribution yields a value of 1.0, while nonrandom foliage distributions, typically found in coniferous forests, produce values less than 1.0 (Gower et al., 1999; Nilson, 1971).

The total clumping index $\Omega(\theta)$ is assumed to be equal to unity (i.e. 1.0) with the LiCOR PCA optical sensor. However, the element clumping index Ω_E , a component necessary for solving for $\Omega(\theta)$, can be generated from gap size distribution data retrieved from the TRAC and DHP sensors and processed by the gap removal method (Chen and Cihlar, 1995b). LiCOR PCA measures gap fraction but does not account for gap size distribution, thus resulting in an underestimation of LAI, especially within coniferous forest stands where foliage is clumped at the shoot and canopy levels (Gower and Norman, 1991; Fassnacht et al., 1994; Kucharik et al., 1998). Documented underestimations of LAI within the conifer forest type assuming a random distribution of vegetation include: 38% (Smith et al., 1993), 35-40% (Gower and Norman, 1991), and 26.5% (Cutini et al., 1998). To solve for Ω_E , a gap accumulation curve is produced, where the gap fraction is accumulated from the largest to the smallest gap, then a gap removal method is used to quantify gaps resulting from non-randomness of canopy (Chen and Cihlar, 1995a). The element clumping effect, Ω_E , is then determined from the difference between measured gap fraction and gap fraction after removal of gaps resulting from non-randomness. Leblanc (2002) describes the calculation of Ω_E as:

$$\Omega_E = [\ln \{f_m(0, \theta)\} / \ln \{f_{mr}(0, \theta)\}] * [1 + F_m(0, \theta) - F_{mr}(0, \theta)] / [1 - F_m(0, \theta)], \quad (4)$$

where, $f_m(0)$ is the measured total canopy gap fraction measured as the transmittance of direct or diffuse radiation at the zenith angles of interest, $f_{mr}(0)$ is the gap fraction for a canopy with randomly positioned elements obtained through the processing of canopy gap size.

When assuming a non-random spatial distribution of canopy elements, L_e acquired in the coniferous forest type will be lower than actual LAI if not corrected for clumping at the shoot and the stand levels. Yet, L_e is affected not only by the canopy randomness assumption, but also by the proportion of non-photosynthetic to photosynthetic materials apparent within the field of view of the optical sensor. Both the TRAC and the DHP indirect optical sensors are incapable of differentiating green photosynthetic biomass from all above ground materials, thus making L_e a measurement of overall plant area. Therefore, a ratio of the non-photosynthetic to photosynthetic material, defined as the woody-to-total area ratio (α) is required to correct L_e . Here, α is a ratio of the projected area of the wood to the total projected area. Integrating the corrections for clumping and the proportion of woody material within a canopy, Chen et al. (1997) modifies the equation (i.e., modified Beer-Lambert light extinction model) to solve for true LAI as:

$$LAI = (1 - \alpha) * [L_e(\lambda_E / \Omega_E)], \quad (5)$$

where LAI is the leaf area index representing one-half of the total leaf area per unit ground surface area, α is the woody-to-total area ratio, L_e is the effective LAI under the random vegetation spatial distribution assumption, λ_E is the needle-to-shoot area ratio, and Ω_E is the element clumping index. In summary, the effective LAI (L_e), is estimated from hemispherical photography gap fraction measurements at 57.3° , the element clumping index, Ω_E , is calculated from gap size distributions determined from TRAC measurements, the woody-to-total area (α) and needle-to-shoot area ratios (γ_E) are calculated from a combination of field and lab methods.

Reported Distribution of Modified Beer-Lambert Law Inputs. Needle-to-shoot area ratios have ranged between 1.2 and 2.1 for spruce and pine (Smith et al., 1993; Stenberg et al., 1994; Chen and Cihlar, 1995a; Chen et al., 1997; Gower et al., 1999). Jack pine (*Pinus banksiana*) and black spruce (*Picea mariana*) occupied the lower end of the range of λ_E with values recorded at 1.30-1.40 and 1.20-1.40 respectively. Douglas-fir (*Pseudotsuga menziesii*) and Scots pine (*Pinus sylvestris*) have reported λ_E values of 1.77 and 1.75, with red pine (*Pinus resinosa*) displaying the upper end of the λ_E range (2.08). The Ω_E ranges reported by Hall et al. (2003) showed that the clumping indices were similar for all species with 0.69-1.00 for lodgepole pine (*Pinus contorta*), 0.64-0.99 for white spruce, 0.77-0.96 for mixed forest, and 0.69-1.00 for deciduous forests. Effective LAI, L_e , measured with hemispherical photography at 31 sites in the Boreal Ecosystem Atmosphere Study (BOREAS), found the mean of the standard deviations for both *P. banksiana* (0.29) and *P. mariana* (0.32). The woody-to-total area ratio values range between 5-35% according to Gower et al. (1999). Woody-to-total area ratio values reported by Gower et al. (1999) include: *P. mariana* (0.12-0.17), *P. banksiana* (0.03-0.05 young, 0.11-0.34 old), *P. resinosa* (0.07), *P. menziesii* (0.08), and oak-hickory (0.11).

Indirect Optical Instruments. Indirect *in situ* optical estimation methods of LAI rely on the measurement of gap fraction, i.e., the fraction of transmitted incident radiation through a plant canopy. These instruments are of two categories dependent on the type of incident radiation received at the sensor, either direct or diffuse. Examples of diffuse light sensors include the LiCOR PCA Plant Canopy Analyzer and hemispherical photography. Examples of direct light sensors, sensors that detect solar irradiance at known solar angles along an established transect (Fournier et al., 2003), include: the TRAC and the DEMON (CSIRO, Canberra, Australia). The instruments used in this study include the TRAC and DHP.

TRAC. The TRAC sunfleck profiling instrument consists of three quantum photosynthetically active radiation (PAR) (400-700 nm) sensors (LI-COR, Lincoln, NE, Model LI-190SB), two uplooking and one downlooking, mounted on a wand with a built-in data logger

(Leblanc et al., 2002). The instrument is hand-carried in direct sun conditions along a linear transect at a constant speed of 0.3 m/s. Typical transect lengths of 50 m to 100 m or greater are oriented close to perpendicular to the direction of the sun and are marked in fixed intervals, typically 10 m subdivisions. A user defined time stamp initiates the transect collection with each intermediate 10-m subdivision also marked by the user as he/she progresses along the transect. The instrument records the downwelling solar photosynthetic photon flux density (PPFD) from one of the uplooking sensors in units of $\mu\text{mol}/\text{m}^2/\text{s}$ at a sampling frequency of 32 Hz. The data logger records light-dark transitions as the direct solar beam is alternately transmitted and eclipsed by canopy elements.

This record of sunflecks and shadows is processed to yield a canopy gap size distribution, a necessary component in the calculation of the element clumping index (Ω_e). The element clumping index quantifies the effects of nonrandom spatial distribution of canopy elements. TRACWin software (Leblanc et al., 2002) processes the Ω_e from determining the deviation of the measured gap size distribution from that of randomly distributed foliage (Morisette et al., 2006). TRACWin also processes an LAI estimate based on retrieved effective LAI (L_e) from user-defined inputs of a species-specific woody-to-total area ratio (α) and needle-to-shoot area ratio (γ_E). However, Leblanc et al. (2002) recommends integrating L_e retrieved from either hemispherical photography or the LiCOR PCA due to the fact that the TRAC acquires this parameter at only one solar zenith angle θ at the time of data acquisition. The other two instruments are capable of capturing multiple gap fraction estimates over many solar zenith angles from one data collection.

TRAC data quality is influenced by solar zenith and azimuth. Optimal results are achieved with a solar zenith angle θ between 30 and 60 degrees. As θ approaches the horizon ($\theta > 60^\circ$), the relationship between LAI and light extinction becomes increasingly nonlinear. Similarly, best results are attained when TRAC sampling is conducted with a solar azimuth perpendicular to the

transect azimuth. Sky condition is also a significant factor for TRAC measurements. Clear blue sky with unobstructed sun is optimal. Overcast conditions are unsuitable; the methodology requires distinct sunflecks and shadows.

Digital Hemispherical Photography (DHP). Historically, the indirect optical method employing hemispherical photography has been used in studies of forest light transmission and canopy structure (Anderson, 1964; Becker, 1971; Ducrey, 1975). Later, this method has been used to estimate canopy vegetation indices, i.e. LAI (Bonhomme, 1970, 1983; Bonhomme et al., 1974; Rich, 1990). Photographs taken upwards from the forest floor with a 180° hemispherical (fisheye) lens produce circular images that record the size, shape, and location of gaps in the forest overstory. Photographs can be taken using a 35 mm film or digital camera. A properly classified fish-eye photograph provides a detailed map of sky visibility and obstructions (sky map) relative to the location where the photograph was taken. Various software programs, such as *Gap Light Analyzer (GLA)* (Simon Fraser University, Burnaby, British Columbia, Canada), *Hemiview* (Delta-T Devices, Cambridge, UK), and *WinSCANOPY* (Regent Instruments Inc., Canada) are available to process film or digital fish-eye camera images into a myriad of metrics that reveal information about the light regimes beneath the canopy and the productivity of the plant canopy. These programs rely on an accurate projection of a three-dimensional hemispherical coordinate system onto a two-dimensional surface. Accurate projection requires calibration information for the fisheye lens that is used and any spherical distortions associated with the lens. The calculation of canopy metrics depends on accurate measures of gap fraction as a function of zenith angle and azimuth. The digital image can be divided into zenith and azimuth “sky addresses” or sectors. Each sector can be described by a combined zenith angle and azimuth value. Within a given sector, gap fraction is calculated with values between zero (totally “obscured” sky) and one (totally “open” sky), and is defined as the proportion of unobscured sky as seen from a position beneath the plant canopy (Delta-T Devices, 1998).

Hemispherical analysis relies on the basic assumptions that the canopy above the photograph is a single layer and that all and any leaves completely obscure incoming solar radiation. However, potential error may be introduced in the classification of sky and no sky regions due to unaccounted light transmission and reflection through and from the individual leaf. Canopy gaps existing in darker areas of the canopy may also be a result of the partial transmission of light through that portion of the canopy (Roxburgh and Kelly, 1995).

Satellite-Derived LAI

LAI has been estimated from remote sensing satellites using empirical relationships between ground estimated LAI and vegetation indices derived from primary spectral bands, especially the red and the near-infrared (NIR) wavelengths, taking advantage of the red-edge phenomenon existent within photosynthetically active vegetation. Other LAI products have been produced from a combination of spectral data integrated with radiative transfer modelling (MODIS LAI).

Vegetation Indices

Vegetation indices are defined as dimensionless, radiometric measures that function as indicators of relative abundance and activity of green vegetation (Jensen, 2000). The contrast between the visible and the NIR wavelengths forms a strong step in the electromagnetic spectrum of green vegetation that is often referred to as the “red edge”, located between 680 – 750 nm. All vegetation indices are predicated on this red edge feature exhibited by green vegetation. Leaf reflectance and transmittance properties are affected by leaf pigments, internal scattering, and leaf water content (Gates et al. 1965; Gausmann et al., 1969; Myers 1970; Peterson and Running, 1989; Jensen 2000). Healthy vegetation absorbs approximately 80% of the incoming solar radiation in the red and blue portions of the spectrum based on the presence of leaf pigments in the palisade mesophyll. However, scattering occurs in the NIR portion of the spectrum due to the

presence of spongy mesophyll. The effect of this morphological characteristic causes upwards of 76% scattering of incoming solar radiation in the 700-1200 nm region (Jensen, 2000).

Linear relationships between increasing vegetation and reflective correspondence do not occur over the entire range of possible values. This effect, an asymptotic increase of vegetation indices to increasing LAI, is termed saturation. The root of the LAI saturation problem with respect to satellite vegetation indices hinges on (1) leaf level differences (pigments, internal leaf structure, leaf orientation) (Baret and Guyot, 1991; Williams, 1991; Bouman, 1992; Yoder and Waring, 1994), (2) within tree crown differences (clumping and woody material contribution to total reflectance) (Williams, 1991; Huemmrich and Goward, 1997), and (3) differences in canopy level parameters such as tree height heterogeneity and the size and number of tree gaps (Cohen et al., 1990; Cohen and Spies, 1992; Leblon et al., 1996). The NDVI saturation issue with respect to increasing vegetation biomass is a function of the near flat response in the red reflectance and the significant positive increase in the NIR reflectance for LAI values exceeding 2.0 in moderate to high vegetative biomass areas (Gitelson, 2004).

Vegetation indices have been classified into three general categories: (1) intrinsic indices (Simple Ratio (SR) and the normalized difference vegetation index (NDVI)), (2) soil-line related indices (Perpendicular Vegetation Index (PVI), Weighted difference vegetation index (WDVI), Soil-adjusted vegetation index (SAVI), and the Modified-SAVI (MSAVI)), and (3) atmospheric-corrected indices (Atmospherically resistant vegetation index (ARVI) and Global environmental monitoring index (GEMI)). Intrinsic indices only involve spectral reflectance and relate very well to vegetation until saturation occurs at full canopy cover. These indices are extremely sensitive to soil optical properties and are a challenge to interpret when the soil is unknown. The effects of solar and viewing geometry, soil background, and atmospheric effects have confounded retrieved results from these equations (Rondeaux et al., 1996). NDVI is defined as:

$$\text{NDVI} = (\text{NIR} - \text{Red}) / (\text{NIR} + \text{Red}) \quad (6)$$

Soil-line related indices were developed to attempt to remove the effect of soil reflectance from canopy reflectance. Soil reflectance is affected by a combination of soil color, soil roughness, and soil water content. Soils tend to reflect highest when organic materials are composed of less decomposed substrates. Increased water in soils decreases soil reflectivity. In the blue channel soil reflectance is low ($\leq 10\%$) but increases monotonically with wavelength through the visible and NIR regions. Thus, a simple linear regression can be applied to describe the relationship between the red and the NIR wavelengths. This soil-line is defined as:

$$P(\lambda_2) = aP(\lambda_1) + b \quad (7)$$

where a and b are slope and intercept coefficients that are dependent on both wavelengths (λ) of soil reflectance P . SAVI was introduced as a hybrid between the intrinsic indices and the soil-line related indices. This index was created due to the fact that isovegetation lines are not parallel and do not converge at a single point, as exhibited by NDVI. The SAVI family of indices is derived from Huete's (1988) original formulation of the SAVI:

$$\text{SAVI} = (1 + L) * (\text{NIR} - \text{R}) / (\text{NIR} + \text{R} + L) \text{ with } L=0.5 \quad (8)$$

L is an adjusting factor, where Huete (1988) found that 0.5 to be the optimal adjustment factor in reducing soil noise over the full range of canopy covers. The Modified SAVI introduces a self-adjustable L so as to increase the SAVI vegetation sensitivity by increasing the dynamic range and further reducing the soil background effects (Qi et al., 1994).

$$\text{MSAVI} = (1 + L) * (\text{NIR} - \text{R}) / (\text{NIR} + \text{R} + L) \text{ with } L = 1 - 2a * \text{NDVI} * \text{WDVI} \text{ (Qi et al., 1994)} \quad (9)$$

where $\text{WDVI} = \text{NIR} - \text{R}$. Qi et al. (1994) noted that at higher vegetation covers L approaches zero, thus MSAVI behaves like NDVI. At low vegetation covers L approaches one and MSAVI

behaves like PVI or WdVI. MSAVI was documented as a very good predictor of vegetation cover in arid environments where vegetation did not exceed 25%. The Optimized SAVI does not require preliminary knowledge of the soil-line parameters. It has been documented that OSAVI is best utilized for agricultural crops.

$$\text{OSAVI} = (\text{NIR}-\text{R})/(\text{NIR} + \text{R} + \text{X}) \text{ where } \text{X}=0.16 \quad (10)$$

A range of X from 0.16 to 0.20 was found to give variations a little higher than SAVI for low vegetation cover (<50%), but still much better than NDVI, while having a very good behavior for vegetation covers greater than 50%.

Vegetation indices correlate with a range of biophysical factors: LAI, ground cover, leaf water content, chlorophyll content, fraction of light intercepted by the canopy, biomass, and productivity and are affected by soil brightness, atmospheric turbidity, solar angle, viewing angle, satellite instrument calibration, and instrument wavebands. However poor correlations have been reported between the normalized difference vegetation index (NDVI) and LAI with R^2 values ranging from 0.30 to 0.52 (Spanner et al., 1990a; Nemani et al., 1993; and Chen and Cihlar, 1996) (Table 1). Contributing to these poor correlations include a variety of influences, namely canopy closure, background materials (i.e. soil properties and moisture content), and understory contributions. The contribution of understory vegetation has been shown to dramatically increase the NIR reflectance from conifer stands (Nemani et al., 1993) thus affecting the overall response of NDVI. These poor correlations indicate inherent issues involved when using either the SR or NDVI when estimating LAI. McDonald et al., (1998), found that with crown closure (CC) up to 25% both indices showed little variation with coverage. CC of 25-65% revealed a constant increasing gradient of variability, while CC above 65% showed values of SR and NDVI were independent of changes in CC (i.e., saturation). Wulder et al. (1998) found that with increasing vertical stand complexity more leaf overlap resulted in higher LAI estimates. Thus stands with

varying vertical profiles could have similar LAI values due to similar horizontal expression (Wulder et al., 1998). Regarding coniferous forests in the United States, a negative relationship exists between red radiance and LAI and a weak, but slightly positive relationship is exhibited between NIR and LAI (Spanner et al., 1984; Running et al., 1986; Badhwar et al., 1986; Franklin, 1986; Peterson et al., 1987; Spanner et al., 1990a,b). As the basal area of a conifer stand is increased, the amount of green vegetation and the amount of shadow within the canopy also increased, thus causing a decrease in canopy reflectance in the visible wavelengths (i.e. red). An increased amount of green vegetation gave rise to an increased reflectance in the NIR that the effects of shadow may well have suppressed (Danson and Curran, 1993).

Table 1. Regression correlations for vegetation indices (NDVI and SR)

VI	Sensor	R ²	Forest Type	Citation
NDVI	TM	0.302-0.597	Temperate Coniferous	Spanner et al., 1990a
		0.32	Boreal Coniferous	Nemani et al., 1993
		0.74	Various	Turner et al., 1999
SR	TM	0.50-0.52	Boreal Coniferous	Chen and Cihlar, 1996
		0.122-0.554	Boreal Coniferous	Brown et al., 2002
		0.255-0.537	Temperate Coniferous	Spanner et al. 1990a
		0.59	Various	Turner et al., 1999
		0.53	Boreal Coniferous	Chen and Cihlar, 1996

A summary of VI responses to increased vegetative cover indicates that SR, NDVI, PVI, SAVI, TSAVI, and GEMI were significantly affected by changes in solar zenith angle, background reflectance, stand structure, and LAI. GEMI performed best at low covers where a decrease in the GEMI value corresponded to an increase in CC. The large dynamic ranges and small susceptibility to atmospheric perturbations with SAVI and TSAVI enabled both indices to perform better at higher covers. It was also observed that selection of an appropriate VI should be based on the local LAI range. In areas of low LAI, small changes in the red wavelength produced a larger proportional change in NDVI when compared to SR. In high LAI areas, a change in the

NIR will induce a larger proportional change in SR when compared to NDVI (Turner et al., 1999).

Influence of Understory

The confounding effect of understory vegetation to the overall estimates of either LAI or NDVI has been well documented in the literature (Franklin et al., 1997; Carlson and Ripley, 1997). Linear relationships between increasing vegetation and reflective correspondence do not occur over the entire range of possible values. As an example, effective LAI (L_e) values for boreal conifer stands varied by less than 5% from spring to summer, however the SR changed dramatically from spring to summer due to the growth of the understory (Chen, 1996). This is a result of the dramatic influence of hardwood understory to overall NIR reflectance from conifer forests. On average understory accounted for approximately 20% of the total LAI in both old growth ponderosa pine and young ponderosa pine regeneration (Law et al., 2001). At plots with natural regeneration of young trees, the understory accounted for 35-60% of the total LAI (Law et al., 2001). Understory can contribute 0-40% of the LAI of a forested stand (Peterson et al., 1987; Spanner et al., 1990a). The broadleaved component in the understory with a conifer overstory showed a large effect in the NIR, a moderate effect in the red and a little or no effect in the short-wave IR regions (Peterson and Running, 1989).

Other factors affect the NIR and red response within a forest stand. Spanner et al. (1990a) identified problems with the NIR/Red ratio such as canopy closure, understory contribution, and background materials. They found that the principal problem was that the near flat response of the NIR band occurred over a range of LAI values. Canopy cover was considered the most important variable in determining canopy reflectance, even with a variable understory component (Spanner et al., 1990a; Stenback and Congalton, 1990; Danson and Curran, 1993). The primary problem with the LANDSAT ETM⁺ scale is the variation in canopy closure and understory contribution that dramatically influences NIR reflectance from conifer forests (Nemani et al., 1993). Badhwar

et al., (1986) found that understory NIR reflectance dominated overall reflectance from open-canopied stands. In summary, canopy closure was identified to be the key spatial variable governing the scene brightness in conifer canopies, because it controls the fractions of understory vegetation visible to the sensor (Franklin, 1986; Spanner et al., 1990a). Thus, LAI values beyond 3, representing a more closed canopy, exhibited negligible NIR response from any broadleaved understory (Nemani et al., 1993).

MODIS MOD15A2 Description

The MODIS LAI/FPAR Collection 4 product (MOD15A2) is an 8-day composite projected into the Integerized Sinusoidal (ISIN) Projection and delivered in 1200 x 1200 km 5.8 Mb tiles in the Hierarchical Data Format (HDF). The HDF file naming convention lists the MODIS product, date of acquisition, global tile location (horizontal and vertical), collection number, and date and time of processing. An example for one MODIS LAI tile retrieved for Julian date 217 in 2002 was: MOD15A2.A2002217.h11v05.004.2003255163348.hdf. Here, the LAI tile with a horizontal and vertical location of 11 and 5 respectively was processed as a collection 4 product on Julian day 255 in 2003 at 4:33:48 pm. Four files are associated with each HDF tile: an LAI and FPAR file and two associated quality flag files (LAI and FPAR). The quality flag data described overall input quality, cloud conditions, and the algorithm used in the LAI retrieval process. Global coverage of the MOD15A2 product consisted of 36 tiles along the east-west axis and 18 tiles along the north-south axis. Thirteen tiles covered the lower 48 states in the US. Collections, defined as processed MODIS LAI retrievals from the latest algorithm improvements, began in February 2000 through February 2001 with the production of Collection 1. Collection 2 was produced as an internal science test and was not released to the public. Collection 3 ran from November 2000 to December 2002, and Collection 4 has been processed since February 2000 to the present (Tan et al., 2005).

MODIS LAI output is determined via two separate pathways: the main and the back-up algorithm. The main and back-up algorithms ingest a six biome-specific classification map at 1 km (MOD12Q1), a 1 km atmospherically corrected MODIS spectral reflectance product (MODAGAGG), and ancillary data (MOD15 Ancillary Radiative Transfer Coefficient Lookup Tables (LUTs), backup algorithm LUTs and output variable properties). The six biome types used to generate Collection 4 LAI data include: 1) grasses and cereal crops; 2) shrubs; 3) broadleaf crops; 4) savannas; 5) evergreen broadleaf forests; and 6) deciduous broadleaf forests. Biome-specific lookup tables (LUTs) containing the most probable LAI values are developed from iterative runs of a three-dimensional canopy radiative transfer (RT) model. In the case of the main algorithm, possible solutions (i.e. retrievals) are cases where the differences between the RT modeled and MODIS observed reflectances are within the uncertainty of the observed reflectances (Huemmrich et al., 2005). Dimensionless uncertainty assigned to the red and NIR MODIS bands are estimated at 20% and 5% respectively (Myneni et al., 2003). Thus, a 1-km MODIS cell is assigned the mean of the retrieved LAI distribution.

The radiation regime within a forest canopy is the integrated outcome of photon scattering by leaves, stems, and soils. In summary, the RT model solves for the inverse problem of three-dimensional vegetation canopies: given mean spectral and angular signatures of canopy-leaving radiance averaged over the three-dimensional canopy radiation field, find the desired vegetation parameters (i.e., LAI) (Knyazikhin et al., 1998). The RT model is dependent upon the parameterization of canopy architecture at the tree level (leaf normal orientation, stem-trunk-branch area fractions, leaf and crown size) and the stand level (trunk distribution, topography) with integration of spectral reflectance and transmittance patterns of vegetation elements. LAI retrieval success is predicated on the reflectance magnitude of the red and the NIR input bands. A low red or a high NIR reflectance usually results in a higher probability of a retrieval failure. Thus, a retrieval success only occurs when a MODIS pixel falls within the specified spectral and angular space of the LUT. In the case of main algorithm retrieval failure, a back-up technique is

invoked where LAI is determined from empirical relationships with vegetation indices (i.e., NDVI) for each of the six biomes. This secondary method is used when sufficient high-quality data are not available for a given compositing period. Data degradation over this eight-day cycle may be due to cloud cover or sensor system malfunctions.

Refinement of the Collection 4 algorithm was based on the integration of uncertainties for the biome data, input surface reflectance, and the radiative transfer model used to build the LUTs (Yang et al., 2005). Specifically, the algorithm was optimized to better simulate features of the MODIS reflectances for herbaceous vegetation (Biomes 1-4). Improved cloud screening and compositing algorithms were gained from atmospheric correction of MODIS surface reflectances and the biome map changed from AVHRR-based to MODIS-based. Regarding Collection 5, similar improvements to the algorithm have been implemented to improve woody vegetation LAI retrievals (Biomes 5-6). Collection 5 is scheduled to begin processing in April 2006 with an estimated completion date of early fall 2006.

Collection 5 changes include the addition of two biome classes, evergreen needle leaf forests and deciduous needle leaf forests, to the original 6-biome class MODIS product. LUTs were recalculated based on changes to parameters in the RT model (Shabanov et al., 2000). The LUTs for the woody vegetation biomes were significantly changed resulting in a decrease of LAI overestimation and improving the rate of best quality retrievals. The most significant parameter change within the evergreen needle leaf biome was the application of the photon recollision probability to the measured unit of the shoot rather than of the individual needle (Rautianen and Stenberg, 2005). Thus, a photon has a higher probability of colliding with multiple needles, thereby reducing the photon exitance from the canopy. This results in a significant reduction in the NIR wavelength received at sensor, thus reducing the overall LAI value. Only minor changes were made to the herbaceous vegetation class, as retrievals were optimized in Collection 4. Biome dependent uncertainties were introduced for Collection 5. Herbaceous vegetation was

assigned algorithm uncertainties of 20% and 5% for red and NIR wavelengths. Woody vegetation uncertainties were 30% for red wavelength and 15% for NIR.

Elements of Uncertainty

The critical examination of error sources was lacking in many published articles involving geospatial applications. Output products from these applications were commonly presented without associated estimates of error or uncertainty (Abbaspour et al., 2003). In the literature the terms error and uncertainty were used interchangeably; however, a clear distinction existed between the two. Error implied a quantitative measurement denoting the known difference between reality and the observation of that reality. Uncertainty, on the other hand, conveyed a limited knowledge regarding this deviation between the observation and the reality (Huevelink, 1998; Abbaspour et al., 2003). In the geospatial domain, uncertainty signified a knowledge deficiency regarding some true value located at some point with specified coordinates (Hunter and Goodchild, 1997).

The elements of uncertainty include: (1) inherent natural variability, (2) measurement error (systematic and random) and (3) sampling error. Natural variability includes structured and unstructured features. Structured features are regular cyclic transitions of some attributes in space and time. *P. taeda* for example exhibits a needle phenology of accretion and abscission that begins at bud burst in a pine shoot in mid-summer and progresses for 27 months until the last needle drops from that initial flush of needles. Thus, a cyclic low of leaf biomass was found in early spring with a maximum leaf biomass occurring in September. In contrast, unstructured features occur unexpectedly and their position and magnitude cannot be predicted. Leaf biomass, evaluated over a certain area, will vary due to tree stocking, mortality, nutrient and water deficiencies, and increased competition. Systematic measurement error, maybe manifested in a positive or negative shift (i.e. bias) from the true value, thereby resulting in a displaced mean value resulting in low accuracy but high precision (precision is a measure of reproducibility under

repeated measurements). Examples of this type of error include an imperfection in the instrument measuring the attribute or an imperfection in the measurement method. Indirect *in situ* optical methods typically underestimate LAI values measured with destructive harvests. In contrast, random measurement error produces observations distributed about the mean, creating a higher accuracy but typically a lower precision. Random measurement error can be reduced through repeated observations of the entity being measured.

Uncertainty analysis focuses on the way errors propagate through spatial analysis. Error propagation is defined as the magnitude of an error in output U given errors in inputs a_i (Aerts et al., 2003):

$$U = g(a_1, a_2, \dots, a_m) \tag{11}$$

where U is the output and g is the model operating on m inputs a_i ($i = 1, \dots, m$). Propagation often occurs in an additive fashion. Cascading errors are the selective combination of erroneous, imprecise, and inaccurate information into new data layers and may be additive or multiplicative, thus proving very difficult to predict.

A number of methods have been developed to track the propagation of error through a system. Two well-used methods have been contrasted in the literature: (1) the Monte Carlo Method, and (2) the Taylor Method. The Monte Carlo method repeatedly computes the result of $g(a_1, a_2, \dots, a_m)$ with randomly sampled input values (a_i) from a joint distribution. The Taylor Method approximates g by a linear function only if the Taylor series is truncated at second order, greatly simplifying the error analysis, but at the expense of introducing an approximation error (Huevelink, 1998). Both methods of tracking error propagation are valuable if the magnitudes of contributions of each individual input into a geospatial process are able to be identified (Huevelink, 1998).

CHAPTER III

SITE DESCRIPTIONS AND SAMPLING

The near-lab study site for the US EPA Office of Research and Development is the Albemarle-Pamlico Basin (APB), located in central-to-northern North Carolina and southern Virginia. The APB has a drainage area of 738,735 km² and includes three physiographic provinces: mountain, piedmont and coastal plain, ranging in elevation from 1280 m to sea level. The APB sub-basins include the Albemarle-Chowan, Roanoke, Pamlico, and Neuse River basins; all draining into the second largest estuarine system within the continental United States. The 1992 landcover estimates from the Multi-Resolution Land Characteristics Consortium (MRLC) dataset disclose that the APB consists primarily of forests (50%), agriculture (27%) and wetlands (17%). The forest component is distributed as follows: deciduous (48%), conifer (33%) and mixed (19%) (Vogelmann et al., 1998).

Five sites were chosen in the Albemarle-Pamlico Basin (APB) to: (1) evaluate the TRAC-DHP indirect optical *in situ* LAI estimation method (2 sites), (2) validate 1-km MODIS MOD15A2 cell (1 site), and to study the effects of hardwood understory on the spectral reflectance captured by the IKONOS multi-spectral sensor (2 sites) (Figure 1). The Appomattox site was chosen for MODIS MOD15A2 validation purposes. The two sites for validating *in situ* indirect optical measurements were located in south-central Virginia (Brunswick) and south-central North Carolina (SETRES); both sites part of forest nutritional study directed by the North Carolina State Forest Nutritional Cooperative (NCSFNC). Hardwood understory spectral reflectance was evaluated on two sites; one in northeastern North Carolina (Hertford) and the other in central Virginia (Appomattox). One additional site in Raleigh, NC (Schenck Forest) was

selected to measure TRAC (Ω_F) and DHP (L_e) variability. Table 2 summarizes the site locations and measurements.

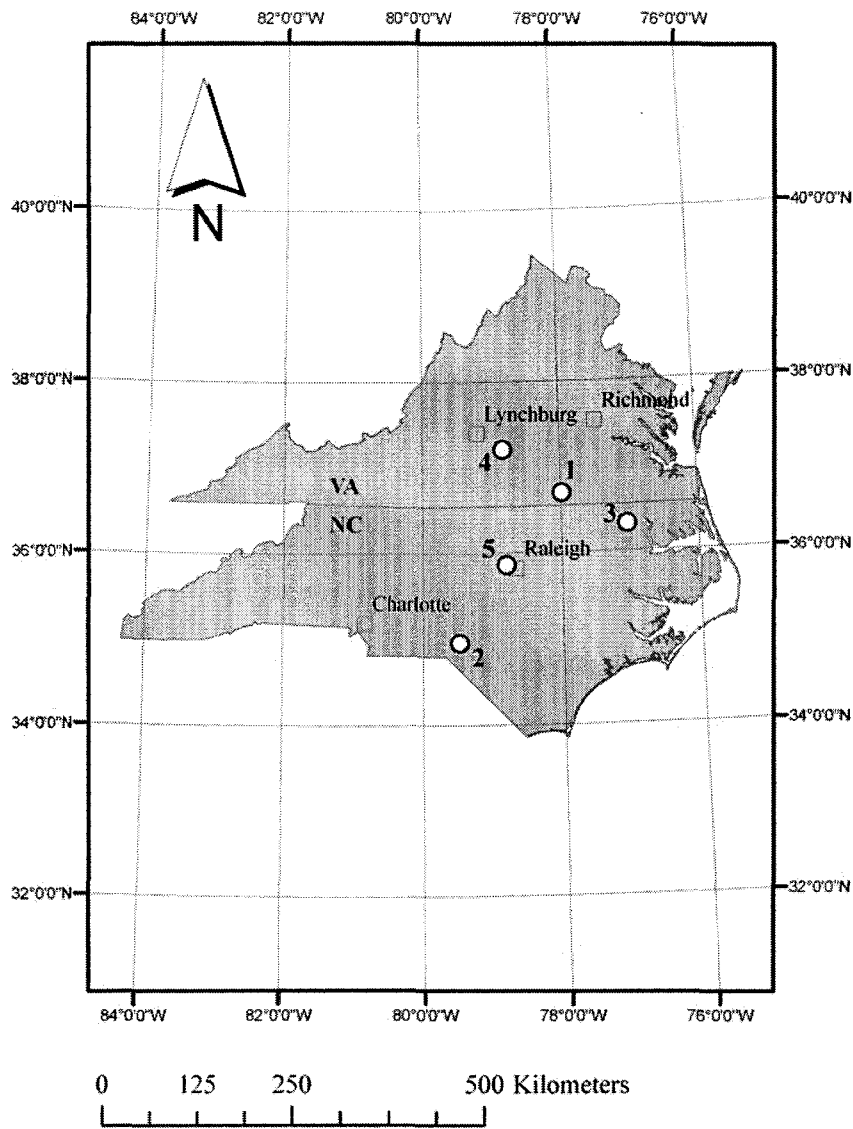


Figure 1. LAI validation site map: (1) Brunswick, (2) SETRES, (3) Hertford, (4) Appomattox, (5) Schenck.

Table 2. Five LAI research sites in APB with associated types and dates of measurements along with data analyzed from study in Oregon (For Type – Forest Type; IS – In Situ [CHPT IV]; U – Understory [CHPT V]; P – Propagation [CHPT VI]; NV – Natural Variation; MEW – Mean Element Width; SZA – Solar Zenith Angle; Con – Conifer; TH-Con – Thinned Conifer; Dec – Deciduous)

	For Type	Parameter	IS	U	P	Variation
SETRES	Con	Ω_E	X			NV (8/8/2003)
	Con	γ_E	X			NV (9/8/2003, 9/12/2003)
	Con	α	X			NV
	Con	L_e	X			NV (8/12/2003)
BRUNSWICK	Con	Ω_E	X			NV (9/16/2003)
	Con	γ_E	X			NV (9/16/2003)
	Con	α	X			NV
	Con	L_e	X			NV (7/30/2003)
HERT	Con	Ω_E		X		NV (7/27/2002; 8/5/2002)
	Con	L_e		X		NV (7/27/2002; 8/5/2002)
APPOMATTOX	Con	Ω_E		X	X	NV (U- 5/23/2002; 7/30/2002; 8/6/2002, P- 7/30/2002) MEW (P- 3/6/2002)
	Con	L_e		X	X	NV (U- 5/23/2002; 7/30/2002; 8/6/2002, P- 7/30/2002)
	TH-Con	Ω_E			X	NV (5/23/2002)
	TH-Con	L_e			X	NV (5/23/2002)
	Dec	Ω_E			X	NV (5/23/2002)
	Dec	α			X	NV
	Dec	L_e			X	NV (5/23/2002)
SCHENCK	Con	Ω_E			X	Atmospheric (8/5-11/2004), Inter/ Intra-operator (8/11/2004), SZA (8/11/2004)
		L_e			X	Light Regime (8/11/2003)
OREGON	Con	L_e			X	Inter-operator

CHAPTER IV

LOBLOLLY PINE (*Pinus taeda* L.) LAI ANALYSIS INTEGRATING TWO INDIRECT OPTICAL INSTRUMENTS: THE TRACING RADIATION AND ARCHITECTURE OF CANOPIES (TRAC) AND DIGITAL HEMISPHERICAL PHOTOGRAPHY (DHP)

Abstract

The assessment of satellite derived leaf area index (LAI) products requires appropriate ground-based measurements for validation purposes. With the NASA launch of Terra (1999) and Aqua (2001), 1 km 8-day composited retrievals of LAI have been produced for six classified biomes worldwide. The evergreen needle leaf biome has been examined at numerous validation sites, yet no research has investigated the dominant commercial species in the southeastern United States: loblolly pine (*Pinus taeda*). The aim of this research is to evaluate an *in situ* optical LAI estimation technique combining measurements from the Tracing Radiation and Architecture of Canopies (TRAC) optical sensor and digital hemispherical photography (DHP) in southeastern United States *P. taeda* forests. Stand level LAI estimated from allometric regression equations developed from whole-tree harvest data were compared to TRAC-DHP optical LAI estimates at one site located in the North Carolina Sandhills Region. In order to test the portability of these regression equations between stands, stand level LAI was estimated at another site in the southeastern Virginia piedmont region using allometric relationships determined at the North Carolina site. Within shoot clumping, or the needle-to-shoot area ratio (γ_E), was estimated at 1.21 and fell within the range of other previously reported values for coniferous species (1.2 – 2.1). Woody-to-total area ratios (α) on both sites (0.25 and 0.31, respectively) also fell within the range

of other published results (0.11-0.34). Overall, the indirect optical TRAC-DHP method of determining LAI was comparable with LAI estimates derived from allometric equations from whole-tree harvests on the site from which the equations were developed (North Carolina). Here, the TRAC-DHP yielded a value 11% below the value retrieved from stand level whole-tree harvest allometric equations. Alternatively, we concluded that these equations were not transferable from the originating site to the other site, based on a disagreement of 57% between the two estimates. Allometric equation transfer from one site to another is difficult due to a number of possible confounding issues including: (1) differences in specific leaf area, (2) gross differences in branch and shoot morphology and (3) stand differences with respect to mid-rotation decline.

Introduction

The advent of remotely sensed data from satellite platforms has enabled the examination of vegetative spatial distributions over regional and global scales. This assessment of ecosystem condition through the synoptic monitoring of terrestrial vegetation extent, biomass, and seasonal dynamics has begun to answer questions related to carbon sequestration and the expansion of greenhouse gases, biogenic emissions and the inputs into air quality, and other significant environmental issues. One input of interest, leaf area index (LAI) defined here as one-half the total green leaf area per unit ground surface area (Chen and Black, 1992a), has been used for the quantification of surface photosynthesis, evapotranspiration, and annual net primary production used in the calculation of terrestrial energy, carbon, water cycle processes, and biogeochemistry of vegetation. LAI has been identified as the variable of greatest importance for quantifying energy and mass exchange by plant canopies over landscapes (Running et al., 1986) and has been shown to explain 80% - 90% of the variation in the aboveground net primary production for forests in the United States (Gholz, 1982; Gower et al., 1992; Fassnacht and Gower, 1997).

The significance of LAI as source data for process-based ecological models has been well documented. Running and Coughlan (1988) ranked LAI as the most important attribute of vegetation structure for characterizing forest canopies over large areas at broad spatial scales using satellite remote sensing data. The leaf surface area has been identified as the main surface of exchange between the plant canopy and the atmosphere and has been related to canopy interception, transpiration, net photosynthesis, gas, water, carbon, and energy exchange, net primary productivity (NPP), biomass, rainfall interception, and dry deposition (Aber, 2001; Gholz, 1982; Pierce and Running, 1988; Gower and Norman, 1991; Hall et al., 2003; Chason et al., 1991). Gower et al. (1999) notes that most ecosystem process models that simulate carbon and hydrogen cycles require LAI as an input variable. By controlling terrestrial mass and energy fluxes, vegetation plays a vital role in global climate change. Interest in tracking LAI phenology includes the role forests play in the sequestration of carbon from carbon emissions (Johnsen et al., 2001), and the formation of tropospheric ozone from biogenic emissions of volatile organic compounds (BVOC) naturally released into the atmosphere (Geron et al., 1994).

The development of appropriate ground-based sampling strategies is critical to the accurate specification of uncertainties in LAI products derived from remotely sensed data (Tian et al., 2002). Errors produced in ground-derived measures of LAI accumulate in either an additive or multiplicative fashion. Issues of concern regarding *in situ* measurements of LAI for remote sensing validation include positional accuracy, spatial scale, and field sampling intensity (Hall et al., 2003). With the launch of the Moderate Resolution Imaging Spectrometer (MODIS) sensor aboard the Terra (1999) and Aqua (2002) EOS-AM spacecrafts, LAI and the fraction of photosynthetically active radiation (fPAR) have been estimated since early 2000 from the spectral and angular properties captured by the this sensor. The MOD15A2 LAI product is a 1 km global data product composited over an 8-day period. This product is derived from a three-dimensional radiative transfer model that is driven by an atmosphere corrected surface reflectance product (MOD09), a land cover product (MOD12) and ancillary information on surface characteristics.

The assessment and validation of this product (MOD15A2) in the evergreen needle leaf biome, one of six biomes delineated in the MOD12 land cover product, is required in the southeastern region of the United States.

One step in the process of MOD15A2 validation is assessing the accuracy and precision of the LAI field estimate. The aim of this paper is to evaluate an *in situ* optical LAI estimation technique combining the Tracing Radiation and Architecture of Canopies (TRAC) optical sensor and digital hemispherical photography (DHP) in southeastern U.S. loblolly pine (*Pinus taeda*) forests. Stand level LAI estimated from allometric regression equations developed from whole-tree harvest data were compared to TRAC-DHP optical LAI estimates at one site located in the North Carolina Sandhills Region. In order to test the portability of these regression equations between stands, stand level LAI was estimated at another site in the southeastern Virginia piedmont region using allometric relationships determined at the North Carolina site. The significance of accurate estimates of southern pine forest biomass (i.e. LAI) is important in accounting for local and regional carbon sequestration, atmospheric deposition, and biogenic emissions. The southern region accounts for 24% of the land area in the United States, of which 58% is forested. Of this forested land, 20% is owned by forest industry (Johnsen et al., 2001). In particular, the area of commercial forestlands in *P. taeda* has increased 15.3% in 29 years (1960-1989) (Schultz, 1997). Since *P. taeda* is a major component in understanding air quality and carbon sink/sources, understanding seasonal and annual fluctuations of LAI is important.

In Situ Measurement of LAI

LAI is a dimensionless quantity broadly defined as the amount of leaf area (m^2) in a canopy per unit ground area (m^2). Four common definitions of LAI are: (1) the total leaf area counting both sides of a leaf per unit ground area, (2) the one-sided leaf area (one-half the total LAI) disregarding leaf shape, (3) the projected leaf area (horizontal), and (4) the projected leaf area

(inclined) (Barclay, 1998; Asner et al., 2003). Each definition was designed with respect to the different processes LAI was used to estimate such as vegetation growth, physiological activity, or light attenuation (Asner et al., 2003). It is important to identify the definition used when comparing LAI values from one study to another. For instance, the one-sided LAI definition may exceed horizontal projected LAI values by a factor of 1.28 (hemi-circular cylinders representing conifer needles).

In situ LAI measurement methodologies include three types: (1) direct, (2) semi-direct, and (3) indirect. The only direct measurement techniques available in vegetative systems are: (1) area harvest sampling where all leaf biomass is destructively harvested and measured and (2) the collection of deciduous litterfall across an entire stand where every leaf is accounted for its contribution to the total leaf surface area. Whether a technique fits the profile of a semi-direct method is a matter of semantics. Technically, allometric regression equations developed from whole-tree destructive sampling would be defined as an indirect method. Here, one or more independent variables (i.e. tree diameter and/or height) are measured to estimate LAI for that particular tree. However, the origins of these estimates reside in the data collected from direct sampling of foliar biomass, therefore this technique has a direct and indirect component. This definition holds fast only when the regression equations are used to estimate LAI from the stand where the relationships were developed. Application of an allometric regression estimate beyond the originating site places the technique within the “indirect” category. The collection of litterfall is also a semi-direct LAI estimation technique when spatial and temporal sampling schemes are employed to scale the data to the stand level. Indirect methods include contact methods (plumb lines and inclined point quadrats), and non-contact optical methods that measure light transmittance through a forest canopy under the assumption of randomly distributed foliage (LiCOR Plant Canopy Analyzer (PCA) (LiCOR, Lincoln, Neb, USA), hemispherical photographs, TRAC, Decagon Ceptometer). Semi-direct and indirect optical methods of assessing LAI have been shown to agree within 25-30% across a wide variety of ecosystems and cover

types (Gower et al., 1999). The following is a review of semi-direct and indirect estimation techniques used to evaluate LAI.

Direct and Semi-Direct Measures of LAI.

Litterfall measurement of LAI is advantageous in deciduous systems that have a single litterfall season with adequate spatial and temporal sampling schemes (Neumann et al., 1989), but provides challenges in the measurement of conifer leaf area due to continuous litterfall and replacement (Chason et al., 1991). Needle fall is not directly related to either new growth or growth in the previous year, but rather on the average life span of the needles and the cumulative climate conditions over the life span. Loblolly pine, for example, produces two to four growth cycles per year and retains foliage for 2 years (Schultz, 1997).

For forested ecosystems, leaf area estimates from allometric relationships are developed from a subsampling of trees destructively harvested within a range of diameters found within a specific forest type. Allometry is the relationship between the mass or area of a part or all of an organism and an independent variable. The development of allometric equations from destructive harvests yields the advantages of quantifying stem, branch, and foliage area separately. These equations also allow for the characterization of the vertical distribution of LAI along with the apportionment of LAI by each age-cohort of foliage, and do not require estimates of clumping factors (Chen et al., 1997). Destructive sampling involves the sampling of specific leaf area (SLA) which is defined as the ratio of fresh foliage surface area to unit dry foliage mass. SLA provides the coefficient required to convert foliage mass to leaf area (Landsberg and Gower, 1997) and has been positively correlated with percent leaf nitrogen concentration and maximum photosynthetic rate (Reich et al., 1995). Because SLA and foliage-to-branch mass decreases with height in the vertical profile of the canopy, sampling must be stratified to account for this variation (Gower et al. 1999). SLA also varies by age-cohort of foliage with a two-fold difference found between new and old foliage (Landsberg and Gower, 1997). Application of destructive

harvests within forested systems, however, requires allometric relationships to be applied beyond the range of sampled trees, potentially introducing extrapolation error.

Semi-direct estimates based on tree allometry and litterfall are labor intensive and do not always provide accurate and unbiased LAI estimates (Chason et al., 1991; Cutini et al., 1998). Allometric relationships have been shown to be stand and site specific dependent upon season, age, stand density, tree crown size, and climatic differences (Gholz et al., 1976; Pearson et al., 1984; Mencuccini and Grace, 1995; Gower et al., 1997). Yet even stand and site specific regression equations are dependent on the validity of the underlying model and the quality and abundance of the data to which it is fitted (Gregoire et al., 1995). Allometric techniques relate LAI to forest mensurational data such as sapwood, basal area, and crown closure (Hall et al., 2003; Snell and Brown, 1978; Buckley, 1999) and are influenced by environmental factors and therefore may not be transferable to other forests (Deblonde et al., 1994). These coefficients vary between sites and species, producing significant errors in LAI estimations. Non-site specific sapwood allometrics overestimated LAI when compared to optical estimates (Jonckheere et al., 2004; Law et al., 2001). Grier et al. (1984), found errors in biomass estimates from generalized equations range between -8% to +93% as compared to site-specific equations for five Douglas-fir (*Pseudotsuga menziesii*) stands.

Indirect Measures of LAI.

Semi-direct destructive sampling is regarded as the most accurate approach, yielding the closest approximation of “true” LAI. However, destructive sampling is time consuming and labor intensive, motivating the development of a more rapid *in situ* LAI estimation technique employing indirect optical methods. Optical methods measure canopy gap fraction and gap size distribution to estimate LAI in forested canopies. Issues that confound optical estimation of LAI include an unknown foliage angle distribution, errors introduced due to nonrandom spatial distribution of foliage elements, and the contribution of supporting woody material to radiation

interception (Chen and Cihlar, 1995a). Chen (1996) noted that optical methods that address these issues (i.e. random vs. non-random canopy architecture) have the potential of providing better estimates of LAI when compared to destructive sampling techniques in coniferous forests.

Indirect Optical LAI Measurement Theory

Indirect optical methods involve ground-based measurement of gap fraction defined as the direct or diffuse light transmittance through the canopy to the forest floor. These optical methods apply the Beer-Lambert Law (Beer, 1853) taking into account that the total amount of radiation intercepted by a canopy layer is dependent on the incident irradiance, canopy structure and optical properties of the site (Jonckheere et al., 2005). The Beer-Lambert Law is expressed as:

$$P(\theta) = e^{-G(\theta,\alpha)L_e / \cos(\theta)} \quad (1)$$

where θ is the zenith angle of view, α is the leaf angle distribution, $P(\theta)$ is the gap fraction defined as the probability of light penetration through the foliage at θ , L_e is the effective leaf area index, and $G(\theta,\alpha)$ is the projection coefficient, a factor corresponding to the fraction of foliage projected on the plane normal to the zenith direction. Effective LAI (L_e), defined as the “effect” of non-random foliage spatial distribution on indirect measurements of LAI, can be derived indirectly from this radiation inversion model (i.e., light extinction model) based on the probability (P) of a light ray missing all foliage elements while passing through a canopy at some angle θ . Under the assumption that canopy foliage elements are distributed according to a Poisson process (i.e., randomly distributed) it is possible to derive expressions for the 95% confidence limits of gap fraction.

Both optical sensors used in this study, TRAC and hemispherical photography, are capable of extracting gap fraction from forest canopies. However, TRAC requires continuous measurement

between a zenith θ of 30° - 60° , usually one-half day, to process a gap fraction figure.

Hemispherical photography measures gap fraction instantaneously over a wide range of zenith angles. An estimate of the projection coefficient $G(\theta, \alpha)$ in the absence of known leaf angle distribution α , requires gap fraction measurements over the entire range of zenith angles.

However, at 1 radian (57.3°) the projection coefficient $G(\theta, \alpha)$ approaches 0.5 based on the insensitivity of the leaf angle distribution at that angle (Wilson, 1963; Jones, 1992). The 1 radian criterion for $G(\theta, \alpha)$ of 0.5 has been shown over a wide variety of leaf and needle structures.

Therefore, a gap fraction determined from hemispherical photography at 1 radian may assume a projection coefficient of 0.5, eliminating the prior requirement of solving for this parameter over multiple angles.

Under the assumption of random canopy foliage elements, effective LAI (L_e) can be retrieved with gap fraction measurements made from the indirect optical sensors with an assumed projection coefficient $P(\theta)$ of 0.5. In nature, however, canopies exhibit non-random spatial patterns. The spatial distribution of foliage elements is dictated by distinct canopy architecture including crowns, whorls, branches, shoots, and groups of trees (Chen et al., 1997). Therefore, in order to account for the non-random nature of foliage distribution within a forest stand, a correction factor, $\Omega(\theta)$, or total clumping index (Chen, 1996), is required to convert the randomly-assumed effective LAI (L_e) to a non-random LAI, defined as L_t . Thus, effective LAI (L_e) is decomposed into two components: true LAI (L_t) and total clumping index $\Omega(\theta)$:

$$L_e = L_t * \Omega(\theta) \quad (2)$$

Chen (1996) defines $\Omega(\theta)$ as:

$$\Omega(\theta) = \frac{\Omega_E}{\gamma_E} \quad (3)$$

where $\Omega(\theta)$ is the total clumping index based on the quotient of Ω_E/γ_E , where Ω_E is the element clumping index and γ_E is the needle-to-shoot area ratio, defined as one-half the needle area to one-half of the shoot silhouette area. The total clumping index is a parameter determined by the deviation of the spatial distribution of a vegetative canopy from a random case (LeBlanc, 2005). Ω_E quantifies the effect of foliage clumping at scales larger than the shoot, while γ_E represents the needle-to-shoot area ratio quantifying within shoot clumping (Fassnacht et al., 1994; Chen et al., 1997). The needle-to-shoot area ratio measurement is untenable with optical measuring devices due to the insensitivity of the sensors to resolve the small gaps found within conifer shoots; thus this parameter is extracted with field and lab measurements. The element clumping index, Ω_E , is quantified by measurements made with TRAC and DHP. A regular pattern of foliage dispersion yields a total clumping index of greater than 1.0, a random foliage distribution yields a value of 1.0, while nonrandom foliage distributions, typically found in coniferous forests, produce values less than 1.0 (Gower et al., 1999; Nilson, 1971).

The total clumping index $\Omega(\theta)$ is assumed to be equal to unity (i.e. 1.0) with the LiCOR PCA optical sensor. However, the element clumping index Ω_E , a component necessary for solving for $\Omega(\theta)$, can be generated from gap size distribution data retrieved from the TRAC and DHP sensors and processed by the gap removal method (Chen and Cihlar, 1995b). LiCOR PCA measures gap fraction but does not account for gap size distribution, thus resulting in an underestimation of LAI, especially within coniferous forest stands where foliage is clumped at the shoot and canopy levels (Gower and Norman, 1991; Fassnacht et al., 1994; Kucharik et al., 1998). Documented

underestimations of LAI within the conifer forest type assuming a random distribution of vegetation include: 38% (Smith et al., 1993), 35-40% (Gower and Norman, 1991), and 26.5% (Cutini et al., 1998). To solve for Ω_E , a gap accumulation curve is produced, where the gap fraction is accumulated from the largest to the smallest gap, then a gap removal method is used to quantify gaps resulting from non-randomness of canopy (Chen and Cihlar, 1995a). The element clumping effect, Ω_E , is then determined from the difference between measured gap fraction and gap fraction after removal of gaps resulting from non-randomness. Leblanc (2002) describes the calculation of Ω_E as:

$$\Omega_E = (\ln[f_m(0, \theta)] / \ln[f_{mr}(0, \theta)]) * ([1 + F_m(0, \theta) - F_{mr}(0, \theta)] / (1 - F_m(0, \theta))), \quad (4)$$

where, $f_m(0)$ is the measured total canopy gap fraction measured as the transmittance of direct or diffuse radiation at the zenith angles of interest, $f_{mr}(0)$ is the gap fraction for a canopy with randomly positioned elements obtained through the processing of canopy gap size.

When assuming a non-random spatial distribution of canopy elements, L_e acquired in the coniferous forest type will be lower than actual LAI if not corrected for clumping at the shoot and the stand levels. Yet, L_e is affected not only by the canopy randomness assumption, but also by the proportion of non-photosynthetic to photosynthetic materials apparent within the field of view of the optical sensor. All indirect optical sensors are incapable of differentiating green photosynthetic biomass from all other above ground materials, thus making L_e a measurement of overall plant area. Therefore, a ratio of the non-photosynthetic to photosynthetic material, defined as the woody-to-total area ratio (α) is required to correct L_e . Here, α is a ratio of the projected area of the wood to the total projected area. Integrating the corrections for clumping and the proportion of woody material within a canopy, Chen et al. (1997) modifies the equation (i.e., modified Beer-Lambert light extinction model) to solve for true LAI as:

$$\text{LAI} = (1 - \alpha) * [L_e(\lambda_E/\Omega_E)], \quad (5)$$

where LAI is the leaf area index representing one-half of the total leaf area per unit ground surface area, α is the woody-to-total area ratio, L_e is the effective LAI under the random vegetation spatial distribution assumption, λ_E is the needle-to-shoot area ratio, and Ω_E is the element clumping index. In summary, the effective LAI (L_e), is estimated from hemispherical photography gap fraction measurements at 57.3°; the element clumping index, Ω_E , is calculated from gap size distributions determined from TRAC measurements; the woody-to-total area (α) and needle-to-shoot area ratios (γ_E) are calculated from a combination of field and lab methods.

Reported Distribution of Modified Beer-Lambert Law Inputs

Needle-to-shoot area ratios have ranged between 1.2 and 2.1 for spruce and pine (Smith et al., 1993; Stenberg et al., 1994; Chen and Cihlar, 1995a; Chen et al., 1997, Gower et al., 1999). Jack pine (*Pinus banksiana*) and black spruce (*Picea mariana*) occupied the lower end of the range of λ_E with values recorded at 1.30-1.40 and 1.20-1.40 respectively. Douglas-fir (*Pseudotsuga menziesii*) and Scots pine (*Pinus sylvestris*) have reported λ_E values of 1.77 and 1.75, with red pine (*Pinus resinosa*) displaying the upper end of the λ_E range (2.08). The Ω_E ranges reported by Hall et al. (2003) showed that the clumping indices were similar for all species with 0.69-1.00 for lodgepole pine (*Pinus contorta*), 0.64-0.99 for white spruce, 0.77-0.96 for mixed forest, and 0.69-1.00 for deciduous forests. Effective LAI, L_e , measured with hemispherical photography at 31 sites in the Boreal Ecosystem Atmosphere Study (BOREAS), found a mean standard deviation of 0.29 and 0.32 for both *P. banksiana* and *P. mariana*, respectively. The woody-to-total area ratio values range between 5-35% according to Gower et al. (1999). Woody-to-total area ratio values reported by Gower et al. (1999) include: *P. mariana* (0.12-0.17), *P. banksiana* (0.03-0.05 young, 0.11-0.34 old), *P. resinosa* (0.07), *P. menziesii* (0.08), and oak-hickory (0.11).

Indirect Optical Instruments

Indirect *in situ* optical estimation methods of LAI rely on the measurement of gap fraction, which is the fraction of transmitted incident radiation through a plant canopy. These instruments comprise two categories dependent on the type of incident radiation received at the sensor, either direct or diffuse. Examples of diffuse light sensors include the LiCOR PCA Plant Canopy Analyzer and hemispherical photography. Examples of direct light sensors, sensors that detect solar irradiance at known solar angles along an established transect (Fournier et al., 2003), include the TRAC and the DEMON (CSIRO, Canberra, Australia). The instruments used in this study include the TRAC and DHP and are described in the following sections.

TRAC. The TRAC sunfleck profiling instrument consists of three quantum photosynthetically active radiation (PAR) (400-700 nm) sensors (LI-COR, Lincoln, NE, Model LI-190SB), two uplooking and one downlooking, mounted on a wand with a built-in data logger (Leblanc et al., 2002). The instrument is hand-carried in direct sun conditions along a linear transect at a constant speed of 0.3 m/s. Typical transect lengths of 50 m to 100 m or greater are oriented close to perpendicular to the direction of the sun and are marked in fixed intervals, typically 10 m subdivisions. A user defined time stamp initiates the transect collection with each intermediate 10-m subdivision also marked by the user progressing along the transect. The instrument records the downwelling solar photosynthetic photon flux density (PPFD) from one of the uplooking sensors in units of $\mu\text{mol}/\text{m}^2/\text{s}$ at a sampling frequency of 32 H_z . The data logger records light-dark transitions as the direct solar beam is alternately transmitted and eclipsed by canopy elements.

This record of sunflecks and shadows is processed to yield a canopy gap size distribution, a necessary component in the calculation of the element clumping index (Ω_e). The element clumping index quantifies the effects of nonrandom spatial distribution of canopy elements. TRACWin software (Leblanc et al., 2002) processes the Ω_e by determining the deviation of the measured gap size distribution from that of randomly distributed foliage (Morissette et al., 2006).

TRACWin also processes an LAI estimate based on retrieved effective LAI (L_e) from user-defined inputs of a species-specific woody-to-total area ratio (α) and needle-to-shoot area ratio (γ_E). However, Leblanc et al. (2002) recommends integrating L_e retrieved from either hemispherical photography or the LiCOR PCA because the TRAC acquires this parameter at only one solar zenith angle θ at the time of data acquisition. The other two instruments are capable of capturing multiple gap fraction estimates over many solar zenith angles from one data collection.

TRAC data quality is influenced by solar zenith and azimuth. Optimal results are achieved with a solar zenith angle θ between 30 and 60 degrees. As θ approaches the horizon ($\theta > 60$ degrees), the relationship between LAI and light extinction becomes increasingly nonlinear. Similarly, best results are attained when TRAC sampling is conducted with a solar azimuth perpendicular to the transect azimuth. Sky condition is also a significant factor for TRAC measurements. Clear blue sky with unobstructed sun is optimal. Overcast conditions are unsuitable; the methodology requires distinct sunflecks and shadows.

Digital Hemispherical Photography (DHP). Historically, the indirect optical method employing hemispherical photography has been used in studies of forest light transmission and canopy structure (Anderson, 1964; Becker, 1971; Ducrey, 1975). Later, this method has been used to estimate canopy vegetation indices, i.e. LAI (Bonhomme, 1970, 1983; Bonhomme et al. 1974; Rich, 1990). Photographs taken upwards from the forest floor with a 180° hemispherical (fisheye) lens produce circular images that record the size, shape, and location of gaps in the forest overstory. Photographs can be taken using 35 mm film or digital camera. A properly classified fish-eye photograph provides a detailed map of sky visibility and obstructions (sky map) relative to the location where the photograph was taken. Various software programs, such as *Gap Light Analyzer (GLA)* (Simon Fraser University, Burnaby, British Columbia, Canada), *Hemiview* (Delta-T Devices, Cambridge, UK), and *WinSCANOPY* (Regent Instruments Inc., Canada) are available to process film or digital fish-eye camera images into a myriad of metrics

that reveal information about the light regimes beneath the canopy and the productivity of the plant canopy. These programs rely on an accurate projection of a three-dimensional hemispherical coordinate system onto a two-dimensional surface. Accurate projection requires calibration information for the fisheye lens used and any spherical distortions associated with the lens. The calculation of canopy metrics depends on accurate measures of gap fraction as a function of zenith angle and azimuth. The digital image can be divided into zenith and azimuth “sky addresses” or sectors. Each sector can be described by a combined zenith angle and azimuth value. Within a given sector, gap fraction is calculated with values between zero (totally “obscured” sky) and one (totally “open” sky), and is defined as the proportion of unobscured sky as seen from a position beneath the plant canopy (Delta-T Devices, 1998).

Hemispherical analysis relies on the basic assumptions that the canopy above the photograph is a single layer and that all and any leaves completely obscure incoming solar radiation. However, potential error may be introduced in the classification of sky and no sky regions due to unaccounted light transmission and reflection through and from the individual leaf. Canopy gaps existing in darker areas of the canopy may also be a result of the partial transmission of light through that portion of the canopy (Roxburgh and Kelly, 1995).

Methods

Site Description

Two sites, located in Virginia and North Carolina, were chosen for evaluating the TRAC-DHP approach for estimating LAI (SETRES) and testing the portability of allometric equations between sites (Brunswick) (Figure 2). Both sites are part of a *P. taeda* long-term nutritional study established by the North Carolina State Forest Nutritional Cooperative (NCSFNC). One site, the Southeast Tree Research and Education Site (SETRES), is located in the Sandhills of Scotland

County, North Carolina (34.917°N, 79.500°W) and exists on a flat, infertile, excessively drained, sandy, siliceous, thermic Psammentic Hapludult soil from the Wakulla series (Soil Survey Division 2001). Annual precipitation averages 1210 mm (30 year average), but extended droughts are possible during the growing season. Average annual temperature is 17°C (30 year average). The site was planted with *P.taeda* on a 2 x 3m spacing in 1985 (Albaugh et al., 1998). In 1992 a long-term fertilization and irrigation experiment was established (Murthy and Dougherty, 1997; Dougherty et al., 1998). Site index (m at 25 years) was 16 for this site.

The other NCSFNC site, located in Brunswick County in south central Virginia (36.681°N, 77.994°), was planted with *P.taeda* in 1993. This site is located in the eastern portion of the piedmont, near the fall-line separating the piedmont and the coastal plain. Soils characterizing this area are primarily Ultisols, in particular the Appling and Cecil soil types. These soils are very deep, well-drained, and moderately permeable, and are described as fine, kaolinitic, thermic Typic Kanhapludults (Soil Survey Division 2001). Elevation is approximately 90 meters above sea level. Annual precipitation averages 1107 mm (57 year average) with recorded average annual temperatures of 8°C (min) and 21.3°C (max). Ten treatments were established at this site by the NCSFNC to identify the optimal rates and frequencies of nutrient application for high rates of production in forest plantations. Site index (m at 25 years) was 16.8 for this site.

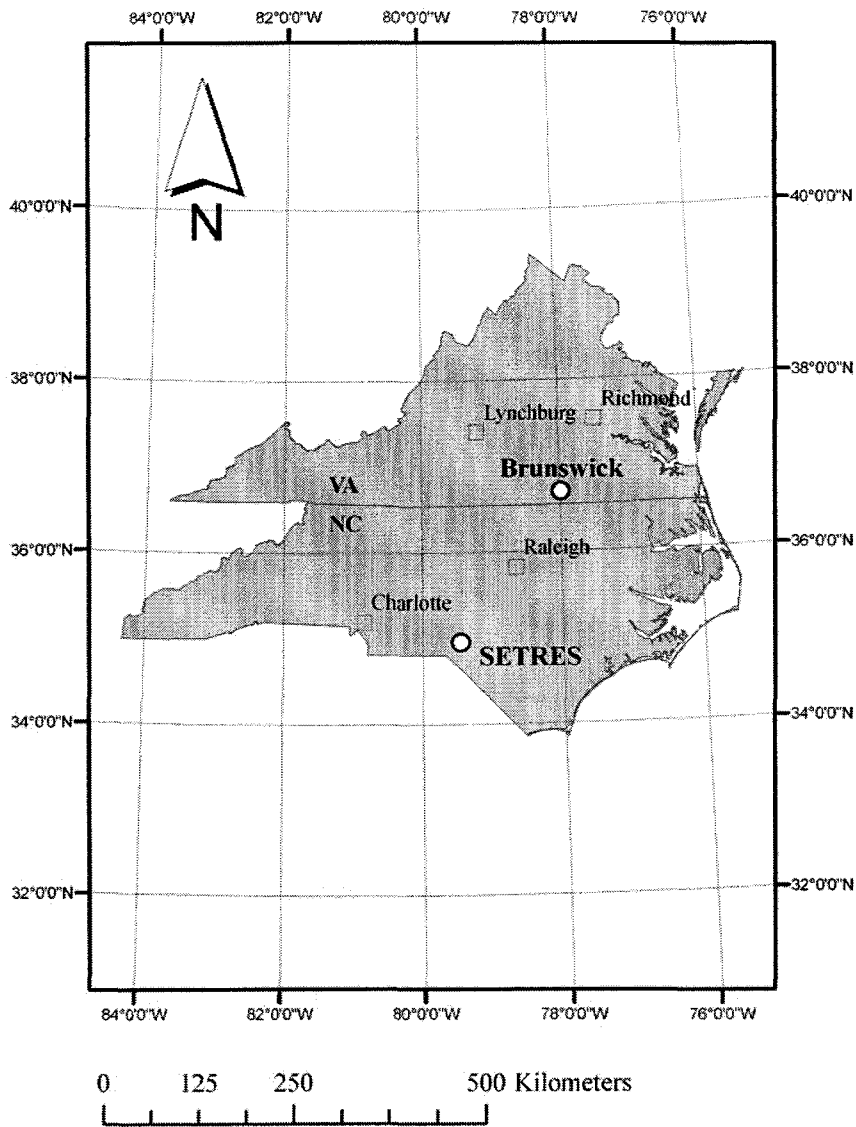


Figure 2. Location map of two sampling sites in North Carolina (SETRES) and Virginia (Brunswick)

At SETRES (NC), two plots were located in non-treatment areas with real-time differential GPS (OMNISTAR) with a ± 1 m horizontal accuracy. TRAC measurements were made only on plot 1 (S1P) (34.9024°N, 79.4862°W), whereas DHP measurements were made on both plots, S1P and S2P (34.9011°N, 79.4886°W). Measurements of forest structural attributes were made on

three plots at SIP using a 10 m radius fixed-area sampling method. All trees within this 10 m radius were tallied for species type, diameter at breast height (dbh) 1.37 m above tree base, and tree height (m). *P. taeda* stocking for both plots averaged 1770 trees/hectare with a mean dbh of 14.5 cm. The average height of the dominant-codominant crown class was 12.3 m ($\sigma \pm 1.3$). Less than 3% of the SETRES site comprised suppressed (less than 7.6 cm dbh) longleaf pine (*Pinus palustris*). Canopy closure, defined as the percent obstruction of the sky by canopy elements, was estimated at 77.5% using a GRS Densitometer (www.BenMeadows.com). Deciduous hardwood understory was present with all stems less than 5 cm dbh (Table 3).

The other site in Virginia (i.e. “Brunswick” site) was also located in a non-treatment area with real-time differential GPS (OMNISTAR). Biometric measurements were made on three point samples using a 10-basal-area-factor prism. This site had 1556 trees/ha with an average height and dbh of 11.2 m and 9.9 cm, respectively. Canopy closure was similar to the SETRES site with a recorded value of 82.4% (Table 3).

Table 3. Forest biometric summary for both sites (biometric measurements from both fixed plot [SETRES] and point plot [Brunswick] sampling methods)

Parameter	SETRES	Brunswick
Date Planted	1985	1992
Mean Height (m)	12.3	11.2
Mean DBH (cm)	14.5	9.9
Canopy Closure (%)	77.5	82.4
Stocking (Trees per Ha)	1770	1556
Site Index (m at 25 years)	16	16.8

Plot centers were located at both sites and three 100 m transects were laid out along the following azimuths: 45°, 180°, and 225°, with all three transects intersecting at the plot center or 50 m mark of each transect (Figure 3). Each 100 m transect was marked every 10 m with flagging for TRAC measurement time marks. TRAC measurements were made along transects closest to perpendicular to the solar azimuth at sampling time between the solar zenith angles of 30° and

60°. DHP measurements were located along each transect at the 10 m, 50 m, and 90 m mark and were made during diffuse light conditions (dawn or dusk).

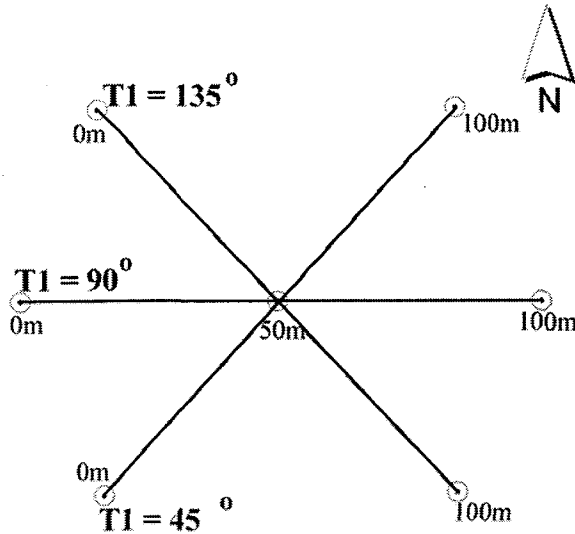


Figure 3. Plot design for SETRES and Brunswick Sites

Optical TRAC-DHP and Field Measurements

The following section presents the methods employed to extract the parameters from equation [5]. In summary, the effective LAI, L_e , is estimated from hemispherical photography gap fraction measurements; the element clumping index, Ω_E , is calculated from gap size distributions determined from TRAC measurements; the woody-to-total area and needle-to-shoot area ratios are calculated from a combination of field and lab methods.

TRAC Measurements. TRAC measurements were made at the SETRES site on August 8, 2003 between 11:15 am and 4:43 pm. Meteorological information obtained from the KSOP Moore County Airport weather station (35.237°N, 79.391°W) for that date and time period showed a relative humidity of 59 - 62%, a temperature of 84° - 86°C, visibility of 11.3 kilometers,

and cloud conditions ranging from few-to-scattered for level 1 clouds at an altitude of 1097 m - 1189 m and broken-to-few for level 2 clouds at an altitude of 1372 - 1463 m.

Four TRAC runs were made along transect 2 (45° azimuth) between 11:16 am and 12:08 pm. The solar zenith angle ranged from 34.76° to 26.1° and the solar azimuth changed from 116.9° to 135.1° during this time interval. The PPFD was measured at a minimum/maximum of 1150 $\mu\text{mol}/\text{m}^2/\text{s}$ and 1684 $\mu\text{mol}/\text{m}^2/\text{s}$ respectively, with magnitudes coinciding with increasing cloud cover (i.e., lower PPFD with increased crown cover). Transect 3 (90° azimuth) was run twice between 2:03 pm and 2:14 pm at a solar azimuth and solar zenith angle of 21.9° and 206.7°, respectively. PPFD was measured at 1772 $\mu\text{mol}/\text{m}^2/\text{s}$. The last TRAC measurements were made on transect 1 (135° azimuth) between 3:08 pm and 4:43 pm. Ranges for the solar zenith angle and the solar azimuth were 30.8°-48.9° and 236.2°- 258.9°, respectively. PPFD was measured at a minimum/maximum of 1082 $\mu\text{mol}/\text{m}^2/\text{s}$ and 1452 $\mu\text{mol}/\text{m}^2/\text{s}$ respectively.

The Brunswick site was sampled on September 16, 2003, with TRAC measurements made between 11:42 am and 12:21 pm. Atmospheric conditions were optimal for TRAC, with skies devoid of clouds and visibility at 8 km. Mid-day temperatures reached 25.7°C with a 42% relative humidity. Transect 2 (45° azimuth) was run twice with TRAC, with the solar azimuth ranging between 145.1° and 158° and the solar azimuth varying between 39.3° and 36.1°. Transect 1 (135° azimuth) was run once with TRAC at a solar azimuth of 149.8° and a solar zenith of 37.9°.

DHP Measurements. DHP measurements were made with a Nikon CoolPix 995 digital camera with a Nikon FC-E8 fish-eye converter in diffuse light conditions at both sites. An image size of 1600 x 1200 pixels was selected at an automatic exposure. The camera was mounted on a tripod and leveled over each stake at a height of 1.4 m. The camera was leveled through the combination of two bubble levelers, one on the tripod and one mounted on the lens cap. Proper leveling of the instrument ensured that the “true” horizon of the photograph was captured. The camera was oriented to true north in order to compare metrics derived from other canopy gap

instruments (i.e., TRAC, densitometer, etc.). The operator would select a delayed exposure (i.e., 3-10 seconds) to offset any vibration incurred when depressing the shutter.

At the SETRES site, on August 12, 2003, 19 DHPs were imaged on each plot, each image taken every 20 m along all three transects. Seven DHPs were taken on August 30, 2003 at the Brunswick site. DHP locations were established at the 0 m, 50 m, and 100 m mark of each of the three transects. The effective LAI (L_e) was determined from the processing of the DHPs using GLA software.

After downloading the images, a GLA configuration file was created for both sites. A configuration file contains information regarding image orientation, projection distortion and lens calibration, site location coordinates, length of growing season, sky-region brightness, and atmospheric conditions. GLA requires that each image be registered with respect to the location of due north on the image and the image circular area. This image registration process required that the FC-E8 fish-eye lens be recalibrated due to an actual field of view of 185° , not 180° . The image radius was reduced accordingly so that the 90° zenith angle represented the true horizon. After the image was registered, an analyst-derived threshold value was determined between sky (white pixels) and no-sky (black pixels). The GLA software outputs L_e values at the 4th ring (0° - 60° degrees) and the 5th ring (0° - 75°). In order to assume a projection coefficient of 0.5, L_e should be solved from a gap fraction determined at 57.3° . This can be accomplished in GLA where gap fraction data are returned for the following zenith values: 5.6° , 16.9° , 28.1° , 39.4° , 50.6° , 61.9° , 73.1° , and 84.4° . The gap fraction at 57.3° then can be determined by plotting gap fraction values against the corresponding zenith angle. Solving for L_e from the Beer-Lambert equation results in:

$$L_e = \ln P(\theta) [-2\cos(\theta)] \quad (6)$$

where $P(\theta)$ is the gap fraction at zenith angle θ .

Needle-to-Shoot Area Ratio (λ_E). Needle-to-shoot area ratios, defined as one-half the needle area (A_n) to one-half of the shoot silhouette area (A_s), were measured from samples taken from two sites, Brunswick and SETRES (Figure 2). The needle-to-shoot area ratio was obtained through laboratory analysis of shoot samples following the methodology of Chen and Black (1992a, b) and Fassnacht et al. (1994). Three trees in the dominant canopy crown class were randomly selected from both the SETRES (2 trees) and the Brunswick (1 tree) sites. Within each tree, four shoot samples were taken from the lower, middle, and upper sections of each crown. Shoots were defined as the combination of the prior and current year needle growth. Therefore, one sampled tree yielded 12 shoot samples. Samples were hydrated and cooled in order to retain leaf moisture, then transported back to the lab for analysis.

In the lab, images of discrete shoot projections used to derive one-half total shoot area (A_s) were captured using an apparatus designed to facilitate multiple angle imaging (Fassnacht et al. 1994). Chen (1996) defined A_s , as:

$$A_s = 2 * \frac{A_p(\theta, \phi) \cos(15^\circ) + A_p(\theta, \phi) \cos(45^\circ) + A_p(\theta, \phi) \cos(75^\circ)}{\cos(15^\circ) + \cos(45^\circ) + \cos(75^\circ)} \quad (7)$$

where θ is defined as the camera incident angle (i.e., the camera angle from vertical) between the surface on which the shoot main axis rests (i.e., light table) and the camera direction, and ϕ is the azimuth angle of the shoot main axis with respect to any reference azimuth angle. Digital images were taken at 15°, 45°, and 75° with a SONY DSC S85 CyberShot camera at 72 dots per inch (dpi) then processed for shoot silhouette area (cm²) with Image Tool 3.00 software, developed by the University of Texas Health Science in San Antonio (<http://ddsdx.uthscsa.edu/dig/itdesc.html>).

After processing the shoots for A_s , one-half the needle area per shoot, A_n , was estimated using the following formula:

$$A_n = \frac{x\sqrt{VnL}}{2} \quad (8)$$

where x is the loblolly shape factor, V is the volume of needles displaced (cm^3), n is the number of needles on a shoot, and L is the average length of the needles (cm). Needles within each shoot were first counted to solve for n . In solving for V , the volume displacement method was implemented. This method is based on the principle that 1 ml of displaced water translates to 1 cm^3 . For this technique, the entire shoot including the stem was immersed in an Erlenmeyer flask, without touching the bottom or the sides of the container. The displaced water volume was measured due to equal water exertion on all sides of the flask. The displaced volume of the needles was then determined by removing the needles, then measuring the displaced volume of the stem. Subtracting the needles and stem displaced volume from the displaced volume of the stem only resulted in the needle displacement volume. After finding V , 15 needles were randomly selected from each shoot and measured (cm) to give L . The loblolly shape factor is a dimensionless unit of measure, defined as the ratio of the perimeter (cm) of a needle cross-section to the square root of the cross-sectional area:

$$\text{Shape Factor} = \frac{\text{Perimeter}(cm)}{\sqrt{\text{Area}(cm^2)}} \quad \text{provided by M. Coyea (unpublished data, 1993) (9)}$$

Duke University Nicholas School of the Environment provided four digital cross-sectional loblolly slides sampled from the bottom and the top of two trees from the Duke FACE Site. Area and perimeter measurements were made using Image Tool 3.00 software (<http://ddsdx.uthscsa.edu/dig/itdesc.html>).

Woody-to-Total Area Ratio (α). The woody-to-total area ratio accounts for the percentage of woody material contributing to the calculation of gap fraction. The woody-to-total area ratio was

determined through a combined analysis approach isolating and retrieving the surface area measurement of the main stem area with ImageTool 3.00, then analyzing the main canopy with Leica Imagine 8.6 software using an unsupervised clustering algorithm, the Iterative Self-Organizing Data Analysis Technique (ISODATA) (Tou and Gonzales, 1974). Five trees were selected from both sites for analysis. Selection criteria included relative isolation of the tree of interest, thus reducing vegetation overlap with neighboring canopies. Images were taken with a Sony Digital Cyber-Shot DSC-S85 at 96 dots per inch resolution. Images were brought into ImageTool, calibrated, then the areas of both the main stem and the canopy were computed through on-screen digitization. The main canopy image was clipped and imported as a TIFF image into Leica Imagine 8.6 software and the ISODATA clustering algorithm was employed to separate green vegetation from the sky. This algorithm uses a minimum spectral distance to assign a cluster for each candidate pixel (ERDAS Imagine Field Guide, 4th Edition). Arbitrary cluster means are specified at the initiation of the process, then multiple iterations shift the cluster means in the data. Initial parameters using one standard deviation, 99% convergence, 20 classes, and a maximum of 10 iterations were imputed into the algorithm. In choosing plus and minus one standard deviation from the mean, a total of 33% of the variation was initially assigned to classes 1 and 20. Due to the large amount of variation ascribed to these two classes, the ISODATA algorithm splits and merges these classes over all the iterations. The percent of green vegetation identified from the ISODATA analysis was simply multiplied to the upper crown area computed earlier, to return a percent needle area.

Reference Stand-Level LAI: SETRES and Brunswick

Evaluation of the TRAC-DHP indirect optical technique for estimating stand level LAI required a comparison to an assumed “truth” baseline. The NCFNC provided reference estimated stand-level LAI for both the SETRES (Julian Day [JD] = 224) site and the Brunswick (JD = 229) site from a point-in-time estimation technique developed by Sampson et al. (2003). In a perfect

scenario, reference stand-level LAI would be obtained by a complete harvest and measurement of every needle at the time of the indirect optical measurements. This would provide the most accurate approach of evaluating the TRAC-DHP method for estimating LAI. Practically, however, this methodology is not feasible. Therefore, an alternate means is required to extract stand-level LAI from destructive harvest data acquired at different periods of time from the indirect optical measurements. A summary of the Sampson method is as follows: (1) Acquire three years of January stand-level foliage biomass (g/ha) from age and treatment specific whole tree regression equations, (2) Convert January stand-level foliage biomass (g/ha) to January stand-level LAI from year-specific January estimates of specific leaf area (cm^2/g) (SLA), (3) Determine stand-level LAI at the time period of interest by applying relative corrections for needle accretion and abscission.

Stand-level foliage biomass (g/ha) was estimated on both sites for three years of data corresponding to the current year (2003) and the two preceding years (2001-2002) for the month of January. Forest biometric measurements (dbh and height) were made for every tree by NCFNC at both the Brunswick (4 control plots) and SETRES sites (4 control plots) (January 2001-2003). January stand-level foliage biomass was estimated with the above mentioned biometric measurements from age and treatment specific whole tree regression equations developed at the SETRES location only following the methods presented in Albaugh et al. (1998) and (2004). These site and plot specific regression equations were based on destructive harvests from multiple years (1992, 1994, 1996, 1998, 2003) and included tree diameter and height as independent variables (Albaugh et al., 2005). After estimating three years of January stand-level foliage biomass (g/ha), an SLA conversion was applied to each year to yield a January stand-level LAI estimate. To arrive at stand-level LAI for the SETRES (JD = 224) and Brunswick (JD = 229) sites, modeled needle accretion and abscission was applied to each years stand-level LAI (2001-2003). A detailed description of Sampson et al. (2003) methodology is found in appendix A.

Results

Element Clumping Index (Ω_E) and Effective LAI (L_e)

Element clumping index (Ω_E) measured at SETRES plot S1P was averaged over five TRAC runs of 100 m over all three transects (n=5). The mean value found for Ω_E was 0.89 ($\sigma \pm 0.03$) with a Ω_E range of 0.08. As a comparison, ten 60 m TRAC runs resulted in a mean Ω_E of 0.87 ($\sigma \pm 0.03$) with a Ω_E range of 0.11. Only the Ω_E values from the 100 m TRAC runs were used in the LAI calculations used to compare with LAI values from destructive harvests. Element clumping index (Ω_E) measured at Brunswick was averaged over two TRAC runs of 100 m on the 45° transect. Inappropriate direct sun quality due to periodic cloud obstruction was the limiting factor in the choice of processing only two runs. The mean value found for Ω_E was 0.94.

Effective LAI (L_e) was measured with DHP at the SETRES site on both plots, S1P and S2P (n = 20/plot). These 20 L_e values per plot were averaged to return a mean L_e of 1.96 ($\sigma \pm 0.28$) and 1.97 ($\sigma \pm 0.29$), respectively. Ranges of L_e for the two plots were 0.97 (S1P) and 1.07 (S2P). Mean L_e measured at Brunswick was 2.26 ($\sigma \pm 0.30$) with a range of 1.17 (n=8).

Needle-to-Shoot Area Ratio (γ_E)

The *P. taeda* shape factor, defined as the ratio of the perimeter (cm) to the area (cm²) of a needle cross section (Eq. 2), had a mean value of 4.143 ($\sigma \pm 0.07$) with a range of 0.15. This value, in conjunction with the other field measured parameters for γ_E calculation (Eq. 9), yielded a needle area on 34 shoot samples across three plots, two at SETRES (S1P, S2P) and one at Brunswick (S1P). The one-half shoot area (A_s) had a mean value of 845.2 (cm²) across all three plots, ranging from a mean minimum of 706.9 (cm²) to a mean maximum of 976.44 (cm²) (Tables 4-6). The one-half shoot needle area (A_n) had a mean value of 745.7 (cm²) across all three plots, ranging from a mean minimum of 543.04 (cm²) to a mean maximum of 1000.41 (cm²) (Tables 4-

6). Thus, the resulting needle-to-shoot area ratio (γ_E) had a mean value of 1.21 ($\sigma \pm 0.18$) across all three plots, ranging from a mean minimum of 1.00 to a mean maximum of 1.32 (Tables 4-6).

Table 4. Needle-to-Shoot area ratio (γ_E) measurements on SETRES S1P.

Site	Plot	CP	S#	A_n	A_s	γ_E
SETRES	S1P	B	1	664.5	712.0	0.93
SETRES	S1P	B	2	638.6	757.6	0.84
SETRES	S1P	B	3	690.8	751.7	0.92
SETRES	S1P	B	4	589.4	546.5	1.08
SETRES	S1P	M	1	625.2	500.4	1.25
SETRES	S1P	M	2	690.5	1048.1	0.66
SETRES	S1P	M	3	1256.0	1038.2	1.21
SETRES	S1P	M	4	561.4	602.6	0.93
SETRES	S1P	T	1	839.8	460.5	1.82
SETRES	S1P	T	2	1858.7	727.5	2.55
SETRES	S1P	T	3	961.8	484.4	1.99
MEAN				852.3	693.6	1.29
SD				390.7	204.6	0.58

$A_n = \frac{1}{2}$ shoot needle area (cm^2), $A_s = \frac{1}{2}$ projected shoot area (cm^2), $\gamma_E =$ needle-to-shoot area ratio, CP is crown position (T = Top, M = Middle, B = Bottom), S# is sample number.

Table 5. Needle-to-Shoot area ratio (γ_E) measurements on SETRES S2P.

Site	Plot	CP	S#	A_n	A_s	γ_E
SETRES	S2P	B	1	521.3	465.0	1.12
SETRES	S2P	B	2	330.8	350.5	0.94
SETRES	S2P	B	3	1193.0	731.0	1.63
SETRES	S2P	B	4	426.7	595.7	0.72
SETRES	S2P	M	1	816.1	586.3	1.39
SETRES	S2P	M	2	667.6	620.5	1.08
SETRES	S2P	M	3	689.3	694.5	0.99
SETRES	S2P	M	4	526.0	571.3	0.92
SETRES	S2P	T	1	818.4	391.4	2.09
SETRES	S2P	T	2	1078.9	654.0	1.65
SETRES	S2P	T	3	462.2	291.6	1.58
SETRES	S2P	T	4	952.7	564.7	1.69
MEAN				706.9	543.0	1.291.32
SD				271.0	138.8	0.580.41

$A_n = \frac{1}{2}$ shoot needle area (cm^2), $A_s = \frac{1}{2}$ projected shoot area (cm^2), $\gamma_E =$ needle-to-shoot area ratio, CP is crown position (T = Top, M = Middle, B = Bottom), S# is sample number.

Table 6. Needle-to-Shoot area ratio (γ_E) measurements on SETRES S2P.

Site	Plot	CP	S#	A_n	A_s	γ_E
BRUNSWICK	S1P	B	1	1064.2	928.3	1.15
BRUNSWICK	S1P	B	2	758.0	535.2	1.42
BRUNSWICK	S1P	B	3	1006.3	119.2	0.90
BRUNSWICK	S1P	B	4	787.7	885.8	0.89
BRUNSWICK	S1P	M	1	595.5	745.6	0.80
BRUNSWICK	S1P	M	2	661.5	841.9	0.79
BRUNSWICK	S1P	M	3	1360.5	2070.6	0.66
BRUNSWICK	S1P	T	1	781.3	789.0	0.99
BRUNSWICK	S1P	T	2	424.5	473.5	0.90
BRUNSWICK	S1P	T	3	1837.1	1306.4	1.41
BRUNSWICK	S1P	T	4	1464.3	1309.1	1.12
MEAN					1000.4	1.00
SD					446.7	0.25

A_n = $\frac{1}{2}$ shoot needle area (cm^2), A_s = $\frac{1}{2}$ projected shoot area (cm^2), γ_E = needle-to-shoot area ratio, CP is crown position (T = Top, M = Middle, B = Bottom), S# is sample number.

Across all three plots, mean γ_E varied by crown position with the top portion of the canopy exhibiting the largest value ($\gamma_E = 1.617$) (Table 7). The variability attributed to these measurements was significant (Table 8). A linear mixed effects model run in S-PLUS 2000 showed that crown position was significant with respect to γ_E controlling for the random tree effect (df = 2, f-value = 12.99, p = 0.001). Finally, there was insufficient evidence to reject the null hypothesis that the γ_E means by site were not significantly different ($\alpha = 0.05$) based on an Analysis of Variance (ANOVA) test (Table 8).

Table 7. Needle-to-Shoot area ratio (γ_E) measurements across three plots, crown position

Statistics	All	Top	Middle	Bottom
Mean	1.21	1.62	0.97	1.05
SE	0.08	0.15	0.07	0.08
Median	1.08	1.65	0.93	0.94
SD	0.45	0.50	0.24	0.26
Variance	0.20	0.25	0.06	0.07
Kurtosis	1.23	-0.24	-0.86	1.40
Skewness	1.21	0.23	0.34	1.27
Range	1.90	1.66	0.74	0.92
Min	0.66	0.90	0.66	0.72
Max	2.56	2.56	1.39	1.63
n	34	11	11	12

Table 8. ANOVA ($\alpha = 0.05$) for (γ_E) three plots

Source of Variation	SS	df	MS	F	P-Value	F crit
Between Groups	0.6906	2	0.3453	1.8129	0.1801	3.3048
Within Groups	5.9040	31	0.1905			
Total	6.5946	33				

Woody-to-Total Area Ratio (α)

A mean woody-to-total area ratio (α) value of 0.25 ($\sigma \pm 0.095$) was observed for five dominant *P. taeda* trees sampled at three locations; SETRES (2), Brunswick (2), and Appomattox (1). The average α exhibited at SETRES ($\alpha = 0.31$) was larger than the average value found at Brunswick ($\alpha = 0.24$) and Appomattox ($\alpha = 0.15$). The small crown branches contributed only 3.9% of the SETRES α and 2.8% of the Brunswick α .

TRAC-DHP derived LAI

TRAC-DHP derived LAI is one-half the total green leaf area per unit ground surface area, or hemi-surface area (HSA) (Chen and Black, 1992a). In contrast, LAI derived from the NCSFNC destructive harvests is the projected area of leaves including individual leaf inclinations. To permit direct comparison, a conversion factor was applied to transform HSA LAI to projected LAI. The projected area of a multi-sided needle is generally smaller than the HSA. The conversion factor was calculated through the analysis of the four cross-sectional loblolly slides provided by the Duke University Nicholas School of the Environment. Four main projection axes were measured using ImageTool 3.0 for each of the four needle cross sections (Figure 4). For each of the four projection axis, a ratio of the length of the projection axis to half the perimeter was measured and averaged to yield one conversion factor. The conversion factor determined from this method was 0.42 ($\sigma \pm 0.02$).

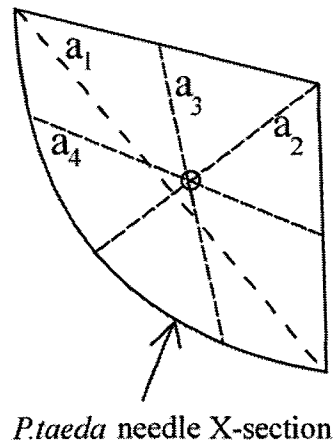


Figure 4. Main axis measured to determine HSA-to-Projected conversion factor.

Parameter inputs required for LAI retrieval from the modified Beer-Lambert light extinction model (equation 5) include the needle-to-shoot area ratio (γ_E), the element clumping index (Ω_E), the effective leaf area index (L_e), and the woody-to-total area ratio (α) (Table 9). HSA LAI calculated and converted to projected LAI were 1.06 (SETRES S1P and SETRES S2P) and 1.28 (Brunswick S1P) (Table 9).

Table 9. Parameter inputs for TRAC-DHP integration calculation of LAI

Site	Plot	γ_E	Ω_E	L_e	α	LAI (HSA)	LAI (Projected)
SETRES	S1P	1.21	0.899	1.965	0.31	1.82	1.06
SETRES	S2P	1.21	0.899	1.975	0.31	1.83	1.06
Brunswick	S1P	1.21	0.935	2.243	0.24	2.21	1.28

γ_E and α were measured in the field and analyzed in the lab; Ω_E (TRAC) and L_e (DHP); HSA Conversion Factor = 0.42

Allometric Reference Stand-Level LAI

The SETRES site exhibited the lower of the two estimates of LAI for 2003 with a mean value of 1.19 ($\sigma \pm 0.17$) and with a 0.41 range (Figure 5). In comparison, the Brunswick site showed a

mean LAI value of 2.28 (SD = 0.52) with a 1.36 range (Figure 6). To synchronize TRAC-DHP LAI measurements with LAI estimates from allometric regression equations, Julian day (JD) 229 and 224 were evaluated for the Brunswick and SETRES sites respectively. Mean LAI over the four plots at both sites was 1.20 ($\sigma \pm 0.18$) and 3.01 ($\sigma \pm 0.18$) for SETRES and Brunswick (Table 10, Figure 7).

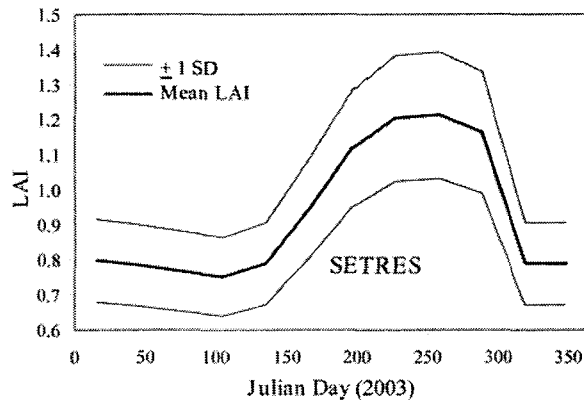


Figure 5. Seasonal LAI derived from allometric equations derived from destructive harvest data from SETRES for the SETRES site (2003).

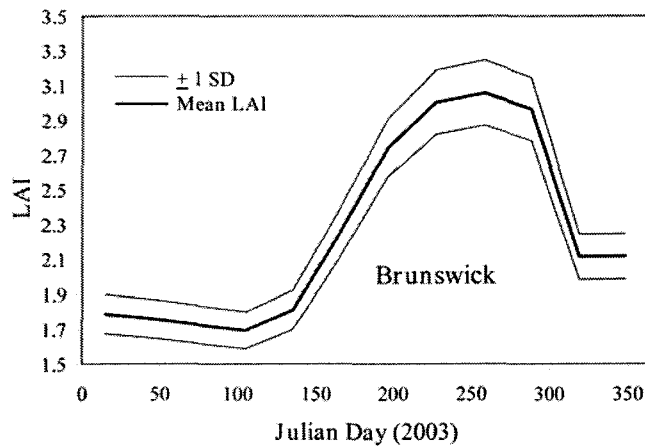


Figure 6. Seasonal LAI estimated using the SETRES allometric equations for the Brunswick site (2003)

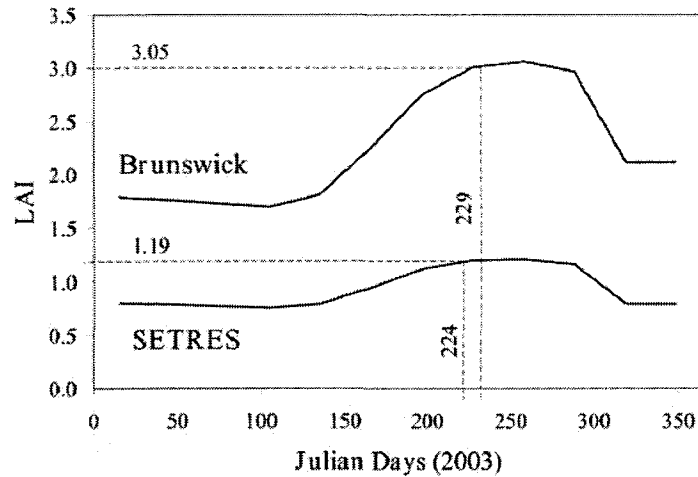


Figure 7. Mean seasonal LAI derived from allometric equations derived from destructive harvest data from SETRES for two sites: SETRES and Brunswick (2003)

Table 10. Control plot LAI estimated from allometric equations derived from destructive harvest data at SETRES for both sites: SETRES and Brunswick (2003).

Location	Plot	Year	Julian Day	LAI
SETRES	1	2003	224	1.28
SETRES	2	2003	224	1.35
SETRES	3	2003	224	0.94
SETRES	4	2003	224	1.22
SETRES	AVE			1.20
Location	Plot	Year	Julian Day	LAI
Brunswick	1	2003	229	2.82
Brunswick	2	2003	229	2.88
Brunswick	3	2003	229	3.12
Brunswick	4	2003	229	3.20
Brunswick	AVE			3.01

Comparison of LAI Estimates

The TRAC-DHP indirect optical approach to estimating LAI performed well when LAI values were compared to values from the destructive harvest data on the site (SETRES) where the allometric equations were developed (Table 11). Optical LAI estimates for both plots were 11% under the values reported from the destructive harvest derived LAI (1.06 LAI TRAC-DHP: 1.20 LAI Destructive Harvest). In contrast, the Brunswick site showed little agreement between the

two estimation techniques (1.28 LAI TRAC-DHP: 3.01 LAI Allometric), with TRAC-DHP underestimating LAI by 2.3x when compared to the allometric LAI (Table 11).

Table 11. TRAC-DHP: Allometric (ALLO) LAI comparison

Site	Plot	TRAC-DHP LAI	ALLO LAI	Difference (LAI)	% Difference LAI
SETRES	S1P	1.06	1.20	0.14	11
SETRES	S2P	1.06	1.20	0.13	11
Brunswick	S1P	1.28	3.01	1.73	57

Discussion

To date, no attempt has been made to quantify input measurements into the TRAC-DHP optical integrated technique to estimate LAI in *P. taeda* forest stands. A good correlation was found between LAI derived from this technique and LAI retrieved from the site on which allometric regression equations were developed (SETRES). However, as will be explained later, the transferability of these equations beyond the site for which they were developed yields compromising results.

As reported, an 11% underestimation of LAI via the TRAC-DHP method was observed at the SETRES site. Good correspondence can be attributed to reasonable estimates of the input parameters in equation [5]: woody-to-total area ratio (α), needle-to-shoot area ratio (γ_E), element clumping index (Ω_E), and effective LAI (L_e). The woody-to-total area ratio estimates at SETRES ($\alpha = 0.31$) and Brunswick ($\alpha = 0.24$) were within the range of conifer (α , 0.03 – 0.34) reported values from Gower et al. (1999). Also, the trend of younger pine incurring a smaller proportion of woody area when compared to older pine is evident in these values, where the Brunswick site α (stand age in 2003 = 11 years) was smaller than the SETRES site α (stand age in 2003 = 18 years). The needle-to-shoot area ratio ($\gamma_E = 1.21$) was also within reason with other reported values from the literature. Gower et al. (1999) reported a range of γ_E values from 1.2 (*P. banksiana*) to 2.08 (*P. resinosa*). Also, the calculated shape factor for *P. taeda* (4.14) was

comparable to published values from Chen (1996): *P. banksiana* (4.00), and *P. mariana* (4.10). The element clumping index measured on both sites exhibited a narrower range than that was found with *P. banksiana* in Canadian boreal ecotone (Chen, 1996). *P. banksiana* ranged 0.18 Ω_E units (approximate) over the 30°- 45° SZA compared to a 0.10 Ω_E over the same 15° SZA range from this study. Atmospheric conditions limited the time period for acquiring the Ω_E . Typical weather conditions at both sites included high relative humidity with increasing cloud cover throughout the day. Finally, the effective LAI acquired from DHP analysis resulted in a narrow range of variability within each plot at both sites ($\sigma \pm 0.28 L_E - \pm 0.30 L_E$)

The question arises as to why discrepancies exist between the two LAI estimation techniques on the one site (Brunswick) and not on the other (SETRES). The most significant issue regards the portability of site-specific allometric equations. The canopy architecture for *P. taeda* exhibits significant variation due to indeterminate growth (multiple flushes) and high plasticity, i.e. developmental patterns, in foliage accretion and abscission in response to site fertility and drought (Dougherty et al., 1995; Herbert and Jack, 1998; Vose, 1988; Vose and Allen, 1988; Sampson et al., 2003). Due to site to site variation in *P. taeda*, allometric equations estimating foliage biomass developed at the SETRES site may not apply to the Brunswick site due to stand structure variability and site fertility (Smolander et al., 1996; Sampson and Allen, 1995; Vose and Allen, 1988). Both stands exhibit similar site characteristics in stocking, crown closure, and site index. It is evident from biometric measurements and a higher site index that the Brunswick site is more productive ($\pm 5\%$) than the SETRES site based on the expected height growth attained at a stand age of 25 years. However, productivity comparisons based on differential LAI production show the Brunswick site 2.3x more productive than the SETRES site. The parameter inputs of relative accretion and abscission of *P. taeda* needles may differ between the two sites, however to observe an impact on LAI productivity on each site would require a large difference in average retention duration. Also, further confounding matters, SLA measurements have been known to vary by species, leaf age, position in the canopy, and nutrition (Lambers and Poorter, 1992).

An examination of LiCOR PCA measurements made on the control plots at the Brunswick site during the period of maximum LAI (September 2003) revealed an effective LAI (L_e) value similar to the values retrieved from the DHP. L_e values were 3.1 (LiCOR PCA) and 2.3 (DHP), a 25% difference between the two measurements. Le Dantec et al. (2000) compared DHP L_e to LiCOR PCA L_e and found a similar difference between the two techniques, with the DHP 15% lower in estimating L_e than the LiCOR PCA. This shows that the DHP estimates are not compromised and show reliable estimates of this parameter. The SETRES site showed a similar comparison between measured L_e from both instruments with a 6% underestimation with the DHP. These results indicate that monthly LAI generated from whole tree regression equations are assumed to be accurate on the site where parameter inputs were measured.

Conclusions

The process of validating optically-derived LAI from ground measurements requires the assumption of a comparative data layer of higher accuracy as “real truth”, in this case LAI derived from allometric equations developed from whole tree harvests. However, as has been reported in prior work, both methods incur sampling and non-sampling error. The TRAC-DHP integrated approach to optical LAI estimation has proved reliable on the SETRES site where the allometric equations for LAI estimation derived from whole-tree harvests were developed. TRAC-DHP indirect estimated LAI was significantly smaller than the allometrically-derived LAI estimated at the Brunswick site primarily due to the lack of Brunswick-specific allometric equations. Due to the documented variability existing within the *P. taeda* crown characteristics, added measurements of the needle-to-shoot area ratio (γ_E) and the woody-to-total area ratio (α) across multiple sites and ages would provide site-specific parameter inputs for equation [5].

CHAPTER V

NDVI CHANGE DETECTION ANALYSIS OF IKONOS 4 M IMAGERY IN THE EVALUATION OF LEAF AREA INDEX (LAI) DIFFERENCES ON TWO LOBLOLLY PINE (*Pinus taeda*) STANDS FOLLOWING COMPLETE UNDERSTORY REMOVAL

Abstract

The confounding effect of understory vegetation contributions to satellite derived estimates of leaf area index (LAI) was investigated on two loblolly pine (*Pinus taeda*) forest stands located in the southeastern United States. Previous studies have shown that understory can account for 0-40% of the total LAI values as estimated from satellite sensors. The vegetation index (VI), the normalized difference vegetation index (NDVI), has been correlated in many studies with *in situ*-derived estimates of LAI. In addition to canopy closure and soil background effects, one other primary factor affecting this VI is the influence of the understory on the near-infrared (NIR) and red spectral response. In order to separate NDVI contributions of the dominant-codominant crown class from that of the understory, two *P. taeda* 1 ha plots centered in planted stands of ages 19 and 23 years with similar crown closures (70%) were analyzed for *in situ* LAI and NDVI differences following a complete understory removal at the peak period of LAI. Understory vegetation was removed from both stands via mechanical harvest and herbicide application in late July and early August 2002. IKONOS data was acquired both prior and subsequent to understory removal and were evaluated for NDVI response. Total vegetative biomass removed under the canopies was estimated using the Tracing Radiation and Architecture of Canopies (TRAC) instrument combined with digital hemispherical photography (DHP). Results indicate that significant NDVI differences were detected between the two dates of pre- and post harvest

IKONOS imagery; however this image differencing was problematic due to the large period of time between pre- and post harvest imagery dates (approximately 3 months) and the difference (pre- and post harvest) of acquisition azimuths. Within image NDVI change between the harvested and non-harvested areas for the post harvest IKONOS imagery for both sites resulted in an NDVI decrease of 1.8% for the Hertford, NC site and a 5% decrease at the Appomattox, VA site. Corresponding *in situ* LAI estimates showed a decrease of 17.6% (Hertford) and 9.9% (Appomattox) between the harvested and non-harvested areas.

Introduction

Assessment of forest stand-level biomass has been required for the parameterization of many process-based ecological models. Specifically, the leaf surface area has been identified as the main surface of exchange between the plant canopy and the atmosphere and has been related to canopy interception, transpiration, net photosynthesis, gas, water, carbon, and energy exchange, net primary productivity (NPP), biomass, rainfall interception, and dry deposition (Aber, 2001; Gholz, 1982; Pierce and Running, 1988; Gower and Norman, 1991; Hall et al., 2003; Chason et al., 1991). Leaf surface area has been quantified in the ratio of leaf area to ground surface area, a ratio termed the leaf area index (LAI). LAI has been defined here as one-half the total green leaf area per unit ground surface area (Chen and Black, 1992b). LAI has been estimated from remote sensing satellites using empirical relationships between ground estimated LAI and vegetation indices derived from primary spectral bands, especially the red and the near-infrared (NIR) wavelengths, taking advantage of the red-edge phenomenon existent within photosynthetically active vegetation. However, separating the spectral signal from multi-layered forest canopies especially those with a significant presence of understory has proven difficult in the assessment of LAI in those forest stands. This research investigated the confounding effect of understory contributions to satellite derived estimates of LAI on two loblolly pine (*Pinus taeda*) plantations (ages 19 and 23 years) located in North Carolina and Virginia, USA. Understory vegetation was

removed from 1 hectare (ha) plots (100 m x 100 m) within both stands via mechanical harvest and herbicide application in late July and early August 2002. IKONOS multi-spectral imagery was collected both prior and subsequent to understory removal and was evaluated for change in vegetative index (VI) response in the harvested and non-harvested areas. Total vegetative biomass (LAI) removed under the canopies was estimated using an integrated optical LAI estimation technique combining measurements from the Tracing Radiation and Architecture of Canopies (TRAC – 3rd Wave Engineering, Ontario, Canada) instrument with digital hemispherical photography (DHP).

Literature Review

Vegetation Indices

Vegetation indices are defined as dimensionless, radiometric measures that function as indicators of relative abundance and activity of green vegetation (Jensen, 2000). The contrast between the visible and the NIR wavelengths forms a strong step in the electromagnetic spectrum of green vegetation that is often referred to as the “red edge”, located between 680 – 750 nm. All vegetation indices are predicated on this red edge feature exhibited by green vegetation. Leaf reflectance and transmittance properties are affected by leaf pigments, internal scattering, and leaf water content (Gates et al., 1965; Gausmann et al., 1969; Myers, 1970; Peterson and Running, 1989; Jensen, 2000). Healthy vegetation absorbs approximately 80% of incoming solar radiation in the red and blue portions of the spectrum based on the presence of leaf pigments in the palisade mesophyll. However, scattering occurs in the NIR portion of the spectrum due to the presence of spongy mesophyll. The effect of this morphological characteristic causes upwards of 76% scattering of incoming solar radiation in the 700-1200 nm region (Jensen, 2000).

Linear relationships between increasing vegetation and reflective correspondence do not occur over the entire range of possible values. This effect, an asymptotic increase of vegetation

indices with increasing LAI, is termed saturation. The root of the LAI saturation problem with respect to satellite vegetation indices hinges on (1) leaf level differences (pigments, internal leaf structure, leaf orientation) (Baret and Guyot, 1991; Williams, 1991; Bouman, 1992; Yoder and Waring, 1994), (2) within tree crown differences (clumping and woody material contribution to total reflectance) (Williams, 1991; Huemmrich and Goward, 1997), and (3) differences in canopy level parameters such as tree height heterogeneity and the size and number of tree gaps (Cohen et al., 1990; Cohen and Spies, 1992; Leblon et al., 1996). The NDVI saturation issue with respect to increasing vegetation biomass is a function of the near flat response in the red reflectance and the significant positive increase in the NIR reflectance for LAI values exceeding 2.0 in moderate to high vegetative biomass areas (Gitelson 2004).

Vegetation indices have been classified into three general categories: (1) intrinsic indices (Simple Ratio (SR) and the normalized difference vegetation index (NDVI)), (2) soil-line related indices (Perpendicular Vegetation Index (PVI), Weighted difference vegetation index (WDVI), Soil-adjusted vegetation index (SAVI), and the Modified-SAVI (MSAVI)), and (3) atmospheric-corrected indices (Atmospherically resistant vegetation index (ARVI) and Global environmental monitoring index (GEMI)). Intrinsic indices involve only spectral reflectance and relate very well to vegetation until saturation occurs at full canopy cover. These indices are extremely sensitive to soil optical properties and are a challenge to interpret when the soil is unknown. The effects of solar and viewing geometry, soil background, and atmospheric effects have confounded retrieved results from these equations (Rondeaux et al., 1996).

Vegetation indices correlate with a range of biophysical factors: LAI, ground cover, leaf water content, chlorophyll content, fraction of light intercepted by the canopy, biomass, and productivity and are affected by soil brightness, atmospheric turbidity, solar angle, viewing angle, satellite instrument calibration, and instrument wavebands. However poor correlations have been reported between the normalized difference vegetation index (NDVI) and LAI with R^2 values ranging from 0.30 to 0.52 (Spanner et al., 1990a; Nemani et al., 1993; and Chen and Cihlar, 1996)

(Table 12). Contributing to these poor correlations include a variety of influences, namely canopy closure, background materials (i.e. soil properties and moisture content), and understory contributions. The contribution of understory vegetation has been shown to dramatically increase the NIR reflectance from conifer stands (Nemani et al., 1993) thus affecting the overall response of NDVI. These poor correlations indicate inherent issues involved when using either the SR or NDVI when estimating LAI. McDonald et al. (1998), found that with crown closure (CC) up to 25% both indices showed little variation with coverage. CC of 25-65% revealed a constant increasing gradient of variability, while CC above 65% showed values of SR and NDVI were independent of changes in CC (i.e., saturation). Wulder et al. (1998) found that with increasing vertical stand complexity more leaf overlap resulted in higher LAI estimates. Thus stands with varying vertical profiles could have similar LAI values due to similar horizontal expression (Wulder et al., 1998). Regarding coniferous forests in the United States, a negative relationship was found between red radiance and LAI and a weak, but slightly positive relationship was exhibited between NIR and LAI (Spanner et al., 1984; Running et al., 1986; Badhwar et al., 1986; Franklin, 1986; Peterson et al., 1987; Spanner et al., 1990a,b). As the basal area of a conifer stand increased, the amount of green vegetation and the amount of shadow within the canopy also increased, thus causing a decrease in canopy reflectance in the visible wavelengths (i.e. red). An increased amount of green vegetation gave rise to an increased reflectance in the NIR that the effects of shadow may well have suppressed (Danson and Curran, 1993).

Table 12. Regression correlations for vegetation indices (NDVI and SR)

VI	Sensor	R ²	Forest Type	Citation
NDVI	TM	0.302-0.597	Temperate Coniferous	Spanner et al., 1990a
		0.32	Boreal Coniferous	Nemani et al., 1993
		0.74	Various	Turner et al., 1999
SR	TM	0.50-0.52	Boreal Coniferous	Chen and Cihlar, 1996
		0.122-0.554	Boreal Coniferous	Brown et al., 2000
		0.255-0.537	Temperate Coniferous	Spanner et al. 1990a
		0.59	Various	Turner et al., 1999
		0.53	Boreal Coniferous	Chen and Cihlar, 1996

A summary of VI responses to increased vegetative cover indicates that SR, NDVI, PVI, SAVI, TSAVI, and GEMI were significantly affected by changes in solar zenith angle, background reflectance, stand structure, and LAI. GEMI performed best at low covers where a decrease in the GEMI value corresponded to an increase in CC. The large dynamic ranges and small susceptibility to atmospheric perturbations with SAVI and TSAVI enabled both indices to perform better at higher covers. It was also observed that selection of an appropriate VI should be based on the local LAI range. In areas of low LAI, small changes in the red wavelength produced a larger proportional change in NDVI when compared to SR. In high LAI areas, a change in the NIR will induce a larger proportional change in SR when compared to NDVI (Turner et al., 1999).

Influence of Understory

The confounding effect of understory vegetation to the overall estimates of either LAI or NDVI has been documented in the literature (Franklin et al., 1997; Carlson and Ripley, 1997). Linear relationships between increasing vegetation and reflective correspondence do not occur over the entire range of possible values. As an example, effective LAI (L_e) values for boreal conifer stands varied by less than 5% from spring to summer, however the SR changed dramatically from spring to summer due to the growth of the understory (Chen, 1996). This is a result of the dramatic influence of hardwood understory to overall NIR reflectance from conifer forests. On average understory accounted for approximately 20% of the total LAI in both old growth ponderosa pine and young ponderosa pine regeneration (Law et al., 2001). At plots with natural regeneration of young trees, the understory accounted for 35-60% of the total LAI (Law et al., 2001). Understory can contribute 0-40% of the LAI of a forested stand (Peterson et al., 1987; Spanner et al., 1990a). The broadleaved component in the understory with a conifer overstory showed a large effect in the NIR, a moderate effect in the red and a little or no effect in the short-wave IR regions (Peterson and Running, 1989).

Other factors affect the NIR and red response within a forest stand. Spanner et al. (1990a) identified problems with the NIR/Red ratio such as canopy closure, understory contribution, and background materials. They found that the principal problem was that the near flat response of the NIR band occurred over a range of LAI values. Canopy cover was considered the most important variable in determining canopy reflectance, even with a variable understory component (Spanner et al., 1990a; Stenback and Congalton, 1990; Danson and Curran, 1993). The primary problem with the LANDSAT ETM⁺ scale is the variation in canopy closure and understory contribution that dramatically influences NIR reflectance from conifer forests (Nemani et al., 1993). Badhwar et al., (1986) found that understory NIR reflectance dominated overall reflectance from open-canopied stands. In summary, canopy closure was identified to be the key spatial variable governing the scene brightness in conifer canopies, because it controls the fractions of understory vegetation visible to the sensor (Franklin, 1986; Spanner et al., 1990a). Thus, LAI values beyond 3, representing a more closed canopy, exhibited negligible NIR response from any broadleaved understory (Nemani et al., 1993).

Methods

In situ broadleaf understory contributions to overall stand LAI were analyzed on two *P. taeda* 1 ha sites located in the Albemarle-Pamlico Basin. On these same two sites, a vegetation index change detection analysis was completed using 4-m multi-resolution IKONOS imagery. On both 1 ha sites, broadleaf understory and ground vegetation was removed via mechanical harvest and herbicide application in late July and early August 2002. IKONOS imagery was acquired pre- and post harvest through the NASA Data Buy Program for analysis (Morissette et al. 2003). LAI was measured pre- and post harvest *in situ* implementing the indirect optical estimation method integrating TRAC and DHP measurements. Pre- and post harvest pair-wise IKONOS images for each site were first georectified then normalized using the localized relative radiometric normalization technique in order to assess change between the two dates (Elvidge et al. 1995).

Pair-wise images were then clipped to include the 1 ha site plus the unaltered *P. taeda* stand immediately surrounding the site. Vegetation indices utilizing the red edge properties characteristic within photosynthetically active vegetation were utilized to create derivative bands for the assessment of LAI change. Comparisons between dates and within date were made employing low pass spatial filters at varying resolutions. An analysis of variance (ANOVA) was implemented to test for significant differences between dates pre- and post harvest. A within date ANOVA was applied to test for differences in the post harvest image between unaltered understory and the altered (removed) 1-ha area.

Site Descriptions

Two sites chosen for this research were located on commercial forestland managed for pulp and paper production in Virginia and North Carolina. The Virginia site (Appomattox) is located in Campbell County, Virginia (37.219°N, -78.879°W) approximately 15.5 km SSW of Appomattox, Virginia (Figure 8). This upper piedmont region ranges in elevation of 165-215 m above mean sea level. The MeadWestvaco Corporation, a supporter of the Sustainable Forestry Initiative, permitted sampling access to the US EPA for this *P. taeda* stand including a complete understory removal within the 1 hectare study area via mechanical harvest and herbicide application. Recorded annual precipitation (2002) was 1045 mm, with a mean temperature of 13.9°C. *P. taeda* was planted in 1983 with site conditions contributing to a 25-year site index value of 18.9. Site index is a relative measure of forest site quality based on the height (m) of the dominant and codominant trees in well-stocked, even-aged stands at a specific age.

Measurements of forest structural attributes (height [m] and diameter [cm]) were made at both sites within the 1 ha areas using a point sampling method (9 plots/ha) with a basal-area-factor of 10 for trees larger than 5 cm diameter at breast height (dbh). Three plots within both 1 ha area were sampled for understory components (stems less than 5 cm dbh) using a 4.57 m radius fixed area sampling method. Canopy closure, defined as the percent obstruction of the sky by canopy

elements, was estimated using a GRS Densitometer (www.BenMeadows.com). Stocking values, expressed as trees per hectare (TPH), were 1250 TPH for the dominant-codominant crown class and 3790 TPH for all trees comprising the understory (suppressed). Appomattox understory did not have one dominant species as found in the Hertford site understory, however all tree species were deciduous (Figure 9). The average diameter (dbh), measured 1.4 m above the base of the tree, was 21.6 cm. The average height of the dominant-codominant crown class was 15.9 m. This *P. taeda* stand supported a basal area (BA) per hectare of 36.7 m², with BA defined as the cross-sectional area of a tree at 1.4 m above the tree base per unit area. The crown closure was 71% for this forest type.

The Hertford site, located in Hertford County, North Carolina (36.383°N, -77.001°W), is approximately 5.8 km WSW of Winton, North Carolina (Figure 8). This coastal plain site is 8-10 m above mean sea level with a moderately well drained thermic Aquic Hapludult soil type (Craven fine sandy loam). Recorded mean temperature for July and August (2002) was 27°C with a mean maximum and minimum temperature of 31.8°C and 22.2°C, respectively. Relative humidity for these two months averaged 70.5%. *P. taeda* was planted in 1983 and thinned in 2003. In 2002, stocking values were 1740 TPH for the dominant-codominant canopy class and 2830 TPH for the suppressed canopy crown class. Understory was dominated (60%) by the broadleaf evergreen tree species *Ilex opaca* (American Holly) (Figure 10). The average height and diameter of this stand was 18.5 cm and 14.3 m, respectively. Measured basal area and crown closure was 37.3 m²/ha and 71%, respectively.

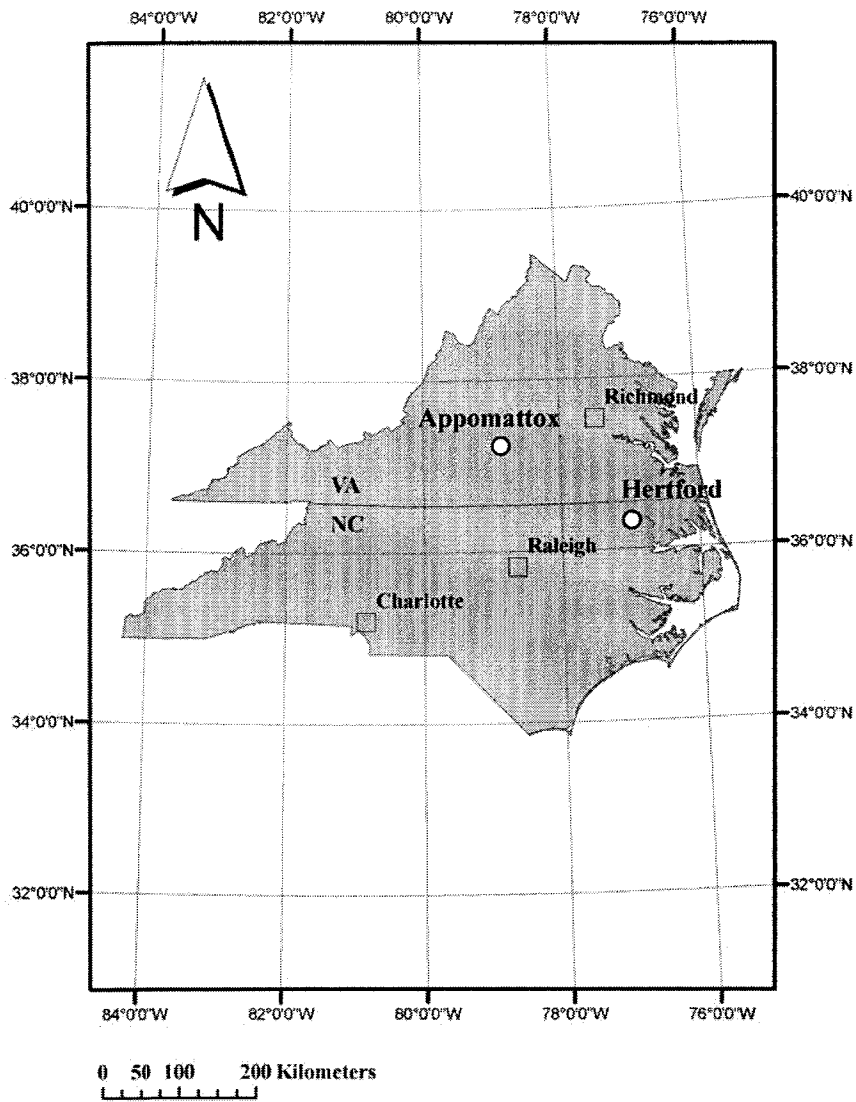


Figure 8. North Carolina and Virginia *P. taeda* site locations.

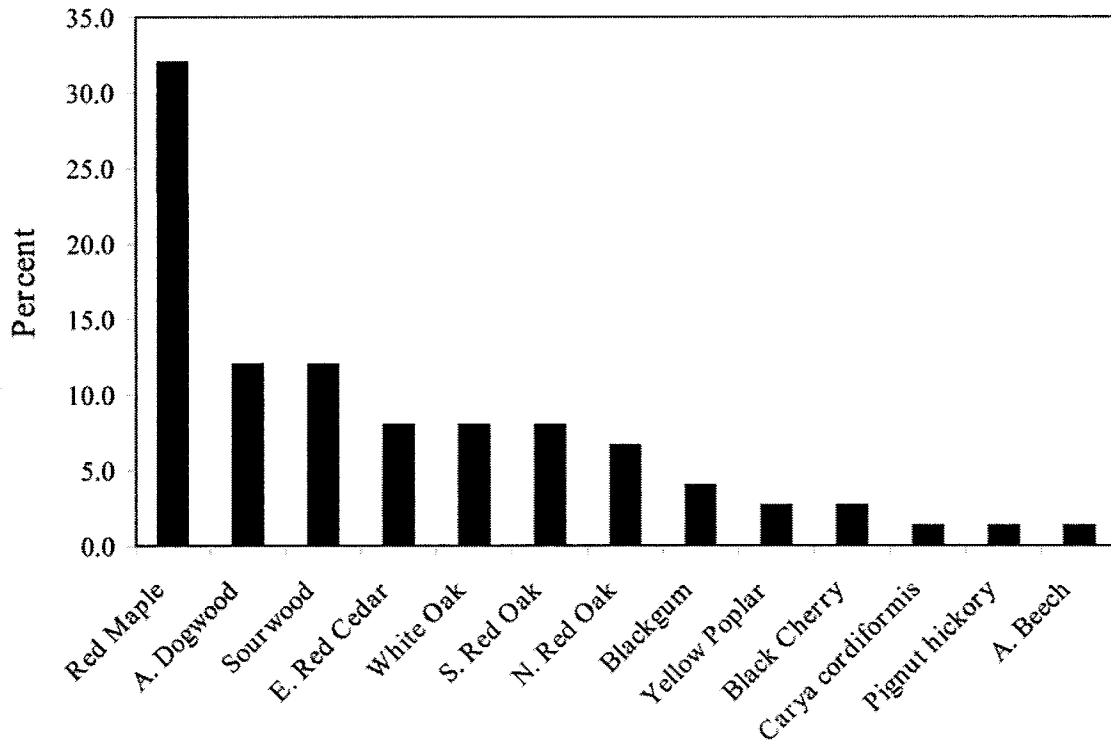


Figure 9. Distribution of understory (% Stems/ha) tree species sampled on the Appomattox site.

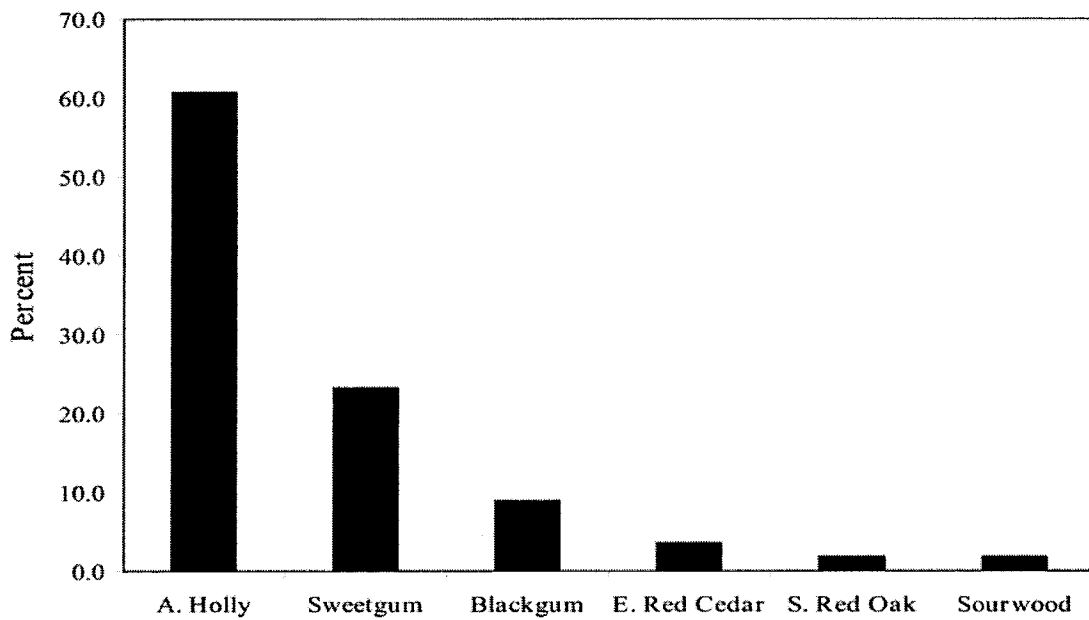


Figure 10. Distribution of understory (% Stems/ha) tree species sampled on the Hertford site.

Understory harvest and herbicide application

Understory removal was contracted for both sites to be completed between July 29 and August 9, 2002. Actual completion dates were July 30, 2002 (Hertford) and August 2, 2002 (Appomattox). The perimeter of both 100 x 100 m plots was flagged and a mechanical harvest was applied, effectively shredding all understory. To ensure elimination of all photosynthetically active vegetation in the understory, including forbs, herbs, and grasses, an herbicide treatment of 2 quarts/acre of Accord Concentrate (Dow AgroSciences) was applied to both plots (Figure 11).



Figure 11. Understory Harvest, Appomattox, VA (A) showing pre-harvest (B) and post harvest (C) conditions.

In situ LAI Measurements

Indirect optical estimation of LAI utilizing the TRAC-DHP method was completed on both sites prior to and immediately following understory removal. In addition to the pre- and post harvest LAI estimates, TRAC-DHP measurements were made throughout the 2002 season to assess LAI change over time. This indirect optical estimation method employs an equation (1) developed by Chen (1996) based on the Beer-Lambert (Beer, 1853) light extinction model taking into account that the total amount of radiation intercepted by a canopy layer is dependent on the incident irradiance, canopy structure and optical properties of the site (Jonckheere et al., 2005). This equation solves for true LAI and is defined:

$$\text{LAI} = (1 - \alpha) * [L_e(\lambda_E/\Omega_E)], \quad (1)$$

where LAI is the leaf area index representing one-half of the total leaf area per unit ground surface area, α is the woody-to-total area ratio, L_e is the effective LAI, λ_E is the needle-to-shoot area ratio, and Ω_E is the element clumping index. In summary, the effective LAI, L_e , is estimated from DHP gap fraction measurements; the element clumping index, Ω_E , is calculated from gap size distributions determined from TRAC measurements; the woody-to-total area and needle-to-shoot area ratios are calculated from a combination of field and lab methods.

The TRAC sunfleck-profiling instrument consists of three quantum photosynthetically active radiation (PAR) (400-700 nm) sensors (LI-COR, Lincoln, NE, Model LI-190SB), two uplooking and one downlooking, mounted on a wand with a built-in data logger (Leblanc et al., 2002). The instrument is hand-carried in direct sun conditions along a linear transect at a constant speed of 0.3 m/sec. Typical transect lengths of 50 m to 100 m or greater are oriented close to perpendicular to the direction of the sun and are marked in fixed intervals, typically 10 m subdivisions. A user defined time stamp initiates the transect collection with each intermediate 10 m subdivision also marked by the user progressing along the transect. The instrument records the downwelling solar

photosynthetic photon flux density (PPFD) from one of the uplooking sensors in units of $\mu\text{mol}/\text{m}^2/\text{s}$ at a sampling frequency of 32 Hz. The data logger records light-dark transitions as the direct solar beam is alternately transmitted and eclipsed by canopy elements. A 30°-60° zenith θ is recommended for TRAC measurements in order to process gap fraction. TRAC data are processed by TRACWin software (Leblanc, et al., 2002) to yield the element clumping index (Ω_e) from the deviation of the measured gap size distribution from that of randomly distributed foliage (Morisette et al 2006).

DHP measurements were made with a Nikon CoolPix 995 digital camera with a Nikon FC-E8 fish-eye converter in diffuse light conditions. An image size of 1600 x 1200 pixels was selected at an automatic exposure. The camera was mounted on a tripod and leveled over each stake at a height of 1.4 m. The camera was leveled through the combination of two bubble levelers, one on the tripod and one mounted on the lens cap. Proper leveling of the instrument ensured that the “true” horizon of the photograph was captured. The camera was oriented to true north in order to compare metrics derived from other canopy gap instruments (i.e., TRAC, densitometer, etc.). The operator would select a delayed exposure (i.e., 3-10 seconds) to offset any vibration incurred when depressing the shutter.

After downloading the images, a GLA configuration file was created for all sites. A configuration file contains information regarding image orientation, projection distortion and lens calibration, site location coordinates, length of growing season, sky-region brightness, and atmospheric conditions. GLA requires that each image be registered with respect to the location of due north on the image and the image circular area. This image registration process required that the FC-E8 fish-eye lens be recalibrated due to an actual field of view of 185°, not 180°. The image radius was reduced accordingly so that the 90° zenith angle represented the true horizon. After the image was registered, an analyst derived threshold value was determined between sky (white pixels) and no-sky (black pixels). The GLA software outputs L_e values at the 4th ring (0°-

60° degrees) and the 5th ring (0°-75°). In order to assume a projection coefficient of 0.5, L_e should be solved from a gap fraction determined at 57.3°. This can be accomplished in GLA where gap fraction data are returned for the following zenith values: 5.6°, 16.9°, 28.1°, 39.4°, 50.6°, 61.9°, 73.1°, and 84.4°. The gap fraction at 57.3° then can be determined by plotting gap fraction values against the corresponding zenith angle. Solving for L_e from the Beer-Lambert equation results in:

$$L_e = \ln P(\theta) [-2\cos(\theta)] \quad (2)$$

where $P(\theta)$ is the gap fraction at zenith angle θ .

Sample Design. The primary sampling unit was the quadrant, a 100 x 100 m grid with five 100 m east-west TRAC sampling transects, labeled line 1 (L1) through line 5 (L5). Interspersed among the TRAC transect were five DHP transects (lines A-E) (Figure 12). Quadrants were designed to approximate an LANDSAT ETM⁺ 3 x 3 pixels window. Quadrants on both sites were randomly selected within an area that allowed a 50 m minimum buffer to a road or any open areas. The TRAC transect L1_0 m position was located using real-time (satellite) differentially corrected GPS to a horizontal accuracy of ± 1.0 m. From this point, TRAC transects were staked every 10 m with pre-labeled 18 in plastic stakes. The stakes were used in TRAC measurements as walking-pace and distance markers. DHP transects were staked at the 10, 30, 50, 70, and 90 m positions located between the TRAC transects.

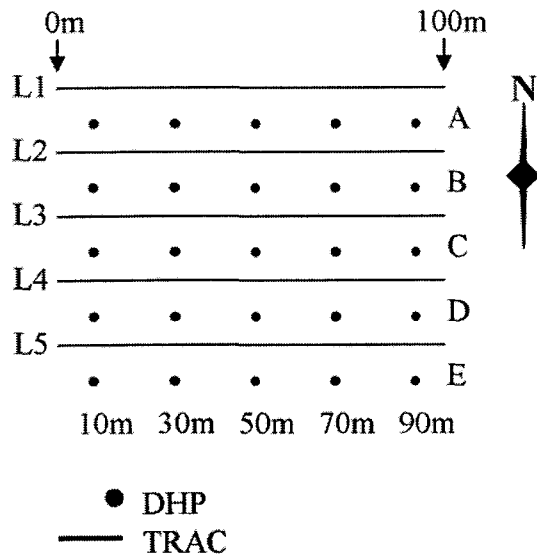


Figure 12. 100 x 100 m (1 ha) quadrant design.

IKONOS Image Processing

High resolution (4 m) 11-bit IKONOS image pairs corresponding to pre- and post understory harvest conditions were acquired from NASA's Scientific Data Purchase for both sites (Morisette et al., 2003). Pre-harvest Appomattox and Hertford images were obtained on May 24 and May 12, 2002, respectively, whereas post harvest images were acquired on August 3 (Appomattox) and August 13 (Hertford). Acquisition time occurred within a narrow morning window of 9:57 am – 10:32 am, with collection azimuth differing significantly between dates for both sites (Figures 13 and 14). Images were geometrically registered (georectified) to 1998 color infrared digital orthophotograph quarter-quadrangles (DOQQ) for both sites using Leica Imagine 8.6 software. Prior to the geometric registration, field ground control points were collected using ± 1 m real-time differentially corrected GPS (Omnistar) and compared to DOQQ locations of the same point. Offsets in the X and Y direction were assessed for DOQQ accuracy prior to assuming this data layer as the base for georectification.

After the georectification process was completed image analysis was conducted to test: (1) image-to-image NDVI change detection using relative radiometric normalization technique , (2)

within image NDVI change detection (Appomattox and Hertford post harvest images), (3) spatial averaging unit appropriate for the *P. taeda* forest type, and (4) differences between NDVI and four other vegetation indices. To test pre- and post harvest image-to-image NDVI change detection, the Appomattox image pair was subset to a 37.4 ha area centered about the 1 ha harvested area (Figure 15). A relative radiometric normalization using an automatic scattergram-controlled regression was applied to the Appomattox August 3 image in conjunction with the April 23 image (Elvidge et al., 1995). NDVI images were created from these normalized image pairs. The 37.4 ha image pairs were then clipped to a 4.0 ha area completely contained within the *P. taeda* forest type, again centered about the 1.0 ha harvested area. NDVI image subtraction was applied to both normalized images on an averaged 5 by 5 pixel (i.e., 5x5 window) basis. This 5x5 spatial averaging window was chosen based on the spatial distribution of the trees within the two stands at Hertford and Appomattox. Stocking values of 1250 TPH (Appomattox) translated into a nominal tree spacing of ± 3 m. Thus a 20 m x 20 m area (5x5 window) would theoretically contain 50 trees with the associated gaps, more than ample size to sample the variability within this crown type. NDVI change less than either positive or negative 0.01 was deemed as a “no-change” pixel. Descriptive statistics were generated for both the harvested and non-harvested areas between the two dates. To test within image NDVI change, both site-specific image pairs were subset to include both the 1 ha harvested area and the similar surrounding *P. taeda* forest stand type. Change and no change was evaluated on an averaged 5 by 5 pixel basis, employing an analysis of variance (ANOVA) to test for differences between the harvested and non-harvested areas. While this test could be considered as a pseudo-replicated analysis (Hurlbert, 1984), the goal was not to provide an overall test in a formal experimental design, but to explain the difference beyond the pixel-to-pixel variability. Spatial NDVI averaging window sizes of 3, 5, 7, and 9 pixels were evaluated on the Hertford post harvest image to test for optimal resolution

capturing *P. taeda* crown variability. Finally, percent change within the Hertford image was evaluated using the vegetation indices: tNDVI, $\sqrt{(NIR/Red)}$, NIR – Red, and SR.

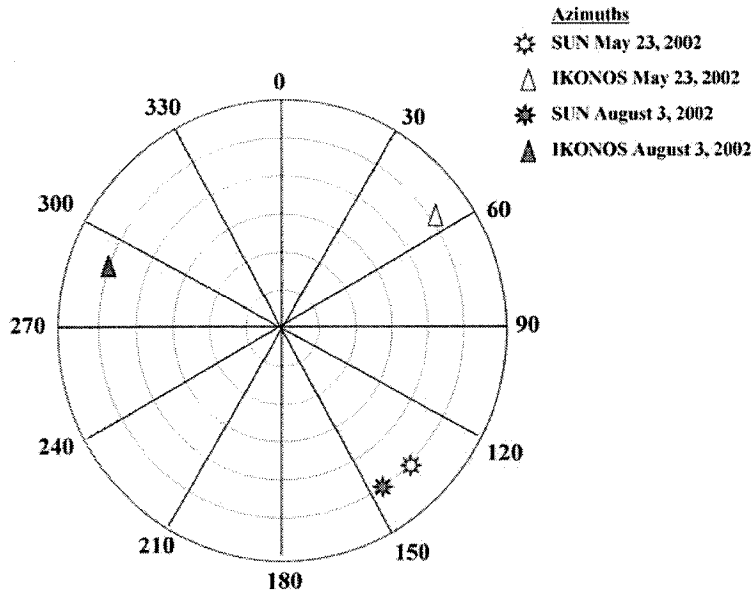


Figure 13. Sun and IKONOS collection azimuths from Appomattox image pairs.

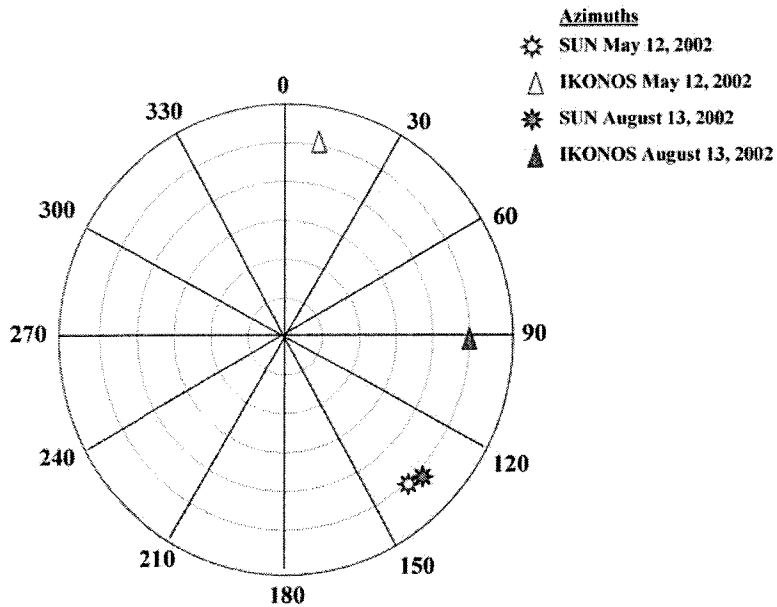


Figure 14. Sun and IKONOS collection azimuths from Hertford image pairs.

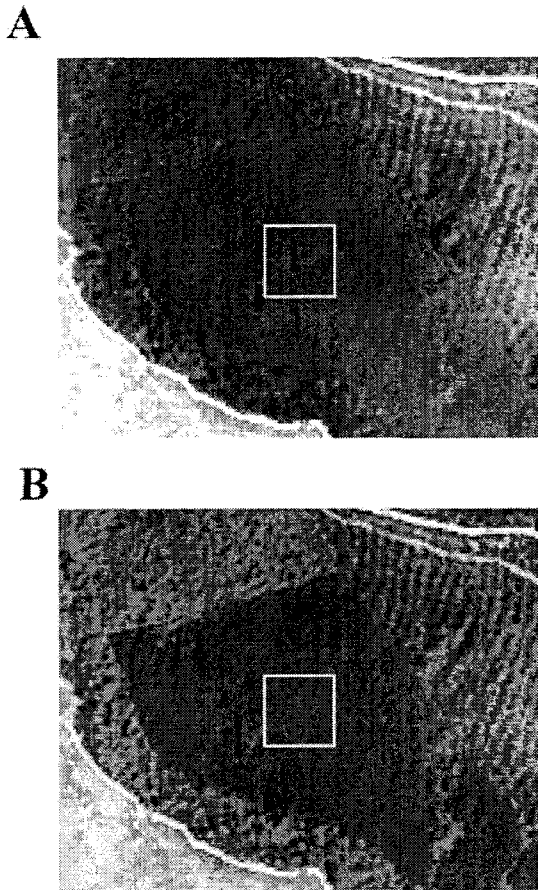


Figure 15. True color (A) and false color composites (B) subset (37.4 ha) of post harvest image (Appomattox) later normalized to pre-harvest image. Yellow bounding box is 100 x 100 m harvested area.

Results

In situ LAI Measurements

Collections of pre and post harvest TRAC measurements (Ω_E) on both sites were designed to acquire PPFD values between the optimal sampling period of $30^\circ - 60^\circ$ (zenith θ). However, due to limited atmospheric conditions (i.e. increased scattered clouds) or time-limited constraints due to the distance between sites, some TRAC measurements were made outside the preferred $30^\circ - 60^\circ$ range and therefore the time of day.

Appomattox. Pre harvest TRAC measurements were completed on July 30, 2002 between 9:13 am and 9:41 am. Solar zenith angles during the collection period ranged between 57.0° and 51.3° with solar azimuth values ranging from 91.1° to 95.6° for the same period. Atmospheric conditions were clear skies with a 16.1 km visibility. Relative humidity and temperature was 59% and 30.6°C, respectively. The five TRAC transects were run successively with PPFD values varying between 340 $\mu\text{mol}/\text{m}^2/\text{s}$ and 1013 $\mu\text{mol}/\text{m}^2/\text{s}$.

Post harvest TRAC measurements were completed on August 6, 2002 between 9:34 am and 9:54 am. Solar zenith angles during the collection period ranged between 53.8° and 49.9° with solar azimuth values ranging from 96.3° to 99.8° for the same period. Atmospheric conditions were broken clouds with a 16.1 km visibility. Relative humidity and temperature was 79% and 26.1°C, respectively. Due to the early morning TRAC collection, TRAC transects were run north-south rather than west-east. Only three 100 m transects were run beginning at L1_10, L1_50, and L1_90. The three TRAC transects were run successively with PPFD values varying between 401 $\mu\text{mol}/\text{m}^2/\text{s}$ and 668 $\mu\text{mol}/\text{m}^2/\text{s}$.

Pre and post harvest mean TRAC estimates of Ω_E were 0.885 ($\sigma = 0.049$) and 0.904 ($\sigma = 0.037$), respectively. Effective LAI (L_e) estimated from DHP measurements on July 29, 2002 (pre-harvest) was 2.251 ($\sigma = 0.280$). Post harvest DHP measurements made on August 6, 2002 showed a mean L_e value of 2.070 ($\sigma = 0.200$). The woody-to-total area ($\alpha = 0.25$) and the needle-to-shoot area ($\gamma_E = 1.21$) ratios were estimated from field and lab measurements from three and two independent *P. taeda* forest stands, respectively. Applying these input parameters into the modified Beer-Lambert light extinction model, LAI was calculated pre- and post harvest (July 30, 2002 = 2.31; August 6, 2002 = 2.08), a 9.9% reduction in LAI between the two dates.

Hertford. Pre harvest TRAC measurements were completed on July 27, 2002 between 11:38 am and 12:18 pm. Solar zenith angles during the collection period ranged between 27.2° and 21.1° with solar azimuth values ranging from 122.9° to 140.9° for the same period. Atmospheric conditions were mostly cloudy with an 8.0 km visibility. Relative humidity and temperature was

77% and 30.0°C, respectively. The five TRAC transects were run successively with PPFD values varying between 585 $\mu\text{mol}/\text{m}^2/\text{s}$ and 928 $\mu\text{mol}/\text{m}^2/\text{s}$.

Post harvest TRAC measurements were completed on August 5, 2002 between 12:59 pm and 1:26 pm. Solar zenith angles during the collection period ranged between 19.8° and 19.7° with solar azimuth values ranging from 169.4° to 188.6° for the same period. Atmospheric conditions were clear with a 16.1 km visibility. Relative humidity and temperature was 49% and 33.0°C, respectively. The five TRAC transects were run successively with PPFD values varying between 1345 $\mu\text{mol}/\text{m}^2/\text{s}$ and 1416 $\mu\text{mol}/\text{m}^2/\text{s}$.

Pre and post harvest mean TRAC estimates of Ω_E were 0.918 ($\sigma = 0.028$) and 0.893 ($\sigma = 0.029$), respectively. Effective LAI (L_e) estimated from DHP measurements on July 25, 2002 (pre-harvest) was 2.214 ($\sigma = 0.284$). Post harvest DHP measurements made on August 5, 2002 showed a mean L_e value of 1.776 ($\sigma = 0.102$). The woody-to-total area ($\alpha = 0.27$) and the needle-to-shoot area ($\gamma_E = 1.21$) ratios were estimated from field and lab measurements from three and two independent *P. taeda* forest stands, respectively. Applying these input parameters into the modified Beer-Lambert light extinction model, LAI was calculated pre- and post harvest (July 25, 2002 = 2.53; August 5, 2002 = 2.09), a 17.6% reduction in LAI between the two dates.

IKONOS Image Analysis

Georectification. Mean differences in geolocated GCPs compared to DOQQ points of the same location showed reasonable accuracy for both sites in the both the X and Y direction. The Appomattox site showed a mean deviation in the X and Y directions of 2.36 m and 2.13 m, respectively. The Hertford site showed a mean deviation in the X and Y directions of 2.07 m and 0.53 m, respectively. The georectification process for both sites (post harvest images) resulted in root mean square error (RMSE) within one-half pixel (i.e., approximately 2 m). RMSE was below one-half pixel for the Hertford site (RMSE = 0.27 m) and close to one-half pixel for the

Appomattox site (RMSE = 2.10 m). The pre-harvest images were registered to the corrected post harvest images for georectification.

Image-to-Image NDVI Change Detection. Testing image-to-image NDVI change at both sites was problematic in that the time between the two image dates (pre- and post harvest) was lengthy (94 days – Hertford; 73 days – Appomattox). Also, the nominal collection azimuths differed within the Appomattox image pairs (236.7°) and the Hertford image pairs (83.8°). Therefore, this method was applied only to the Appomattox image pair to see if any change could be detected.

Mean non-harvested NDVI for the May 23, 2002 image was 9.1% greater than the non-harvested NDVI for the post-harvest image (August 3, 2002) (Table 13). Within the 1 ha harvested area, a 14.3% decrease in NDVI was observed between the May 23, 2002 image and the August 3, 2003 image. ANOVA results indicate that there were significant differences between the non-harvest areas ($p = <0.0001$, $F = 3010.2$, $df = 1$) and between the harvested areas ($p = <0.0001$, $F = 1303.9$, $df = 1$) for both dates. Within the harvested region an NDVI image subtraction resulted in 81.2% of the area exhibiting a decrease in NDVI greater than 0.01. The remaining 18.8% of the harvested area indicated no change in NDVI. Within the non-harvested region 11.9% of the area showed an NDVI decrease (> 0.01), 8.5% resulted in an NDVI increase (> 0.01), and the rest area was unchanged. Actual field measured LAI change between dates resulted in a 14.4% net increase in LAI (May 23 LAI = 2.11; August 6 LAI = 2.47).

Table 13. Image-to-image NDVI analysis (5x5 averaged) of May 23 and August 3, 2002 images (Appomattox)

	Harvested (n =16)			Non-harvested (n = 60)		
	5/23/02	8/3/02	ANOVA	5/23/02	8/3/02	ANOVA
Mean	0.575	0.493		0.571	0.519	
σ	0.004	0.004		0.009	0.006	
p			< 0.001			< 0.001

Within Image NDVI Change Analysis. Significant differences were detected between the non-harvested and harvested regions within the post-harvest August 3, 2002 Appomattox NDVI

image ($p = <0.0001$, $F = 300.9$, $df = 1$) and the post-harvest August 13, 2002 Hertford NDVI image ($p = <0.0001$, $F = 30.3$, $df = 1$) (Figures 16 and 17). A 5.0% decrease in NDVI was detected within the harvested region of the Appomattox NDVI image (Non-harvest NDVI = 0.519; Harvest NDVI = 0.493), whereas only a 1.8% difference was detected between harvested and non-harvested regions within the August 13, 2002 Hertford NDVI image (Non-harvest NDVI = 0.433; Harvest NDVI = 0.425).

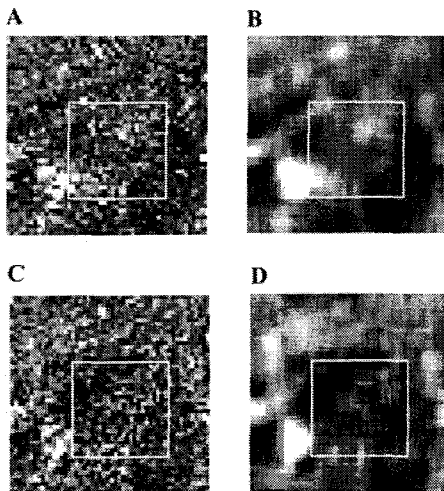


Figure 16. Appomattox May 23, 2002 NDVI (A) and 5x5 NDVI (B). Appomattox August 3, 2002 NDVI (C) and 5x5 NDVI (D).

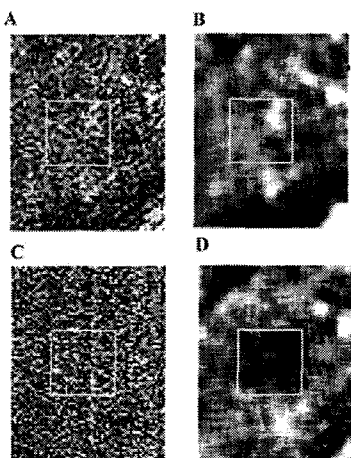


Figure 17. Hertford May 12, 2002 NDVI (A) and 5x5 NDVI (B). Hertford August 13, 2002 NDVI (C) and 5x5 NDVI (D).

Spatial averaging window size. The mean values between four spatial averaging window sizes (3x3, 5x5, 7x7, and 9x9) for both the harvested and the non-harvested regions were identical (Figure 18). All p-values indicated significant differences in the means for the two regions within each window size (< 0.001). Notice the random noise associated with image A in Figure 18. This is a result of the 4 m NDVI values occurring over canopy gap areas with no understory vegetation (darker pixels) and other 4 m NDVI values occurring over crown tops (light pixels). The spatial averaging in panels B-E (Figure 18) resolve NDVI decreases at the canopy level.

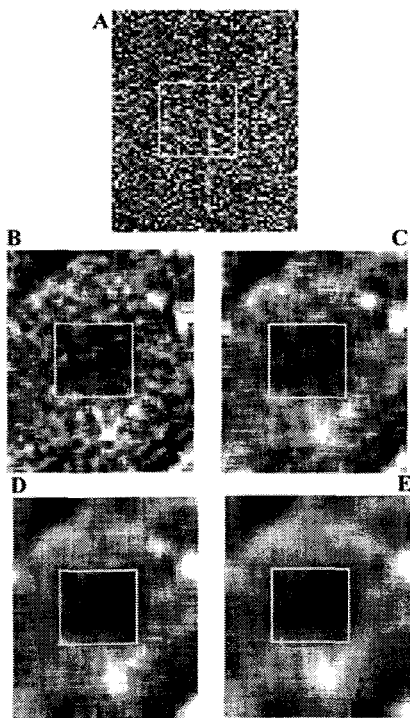


Figure 18. Comparison of various spatial averaging windows on Hertford August 13, 2002 NDVI image A) Raw NDVI, B) 3x3 NDVI, C) 5x5 NDVI, D) 7x7 NDVI, E) 9x9 NDVI

Other Vegetation Indices. Analysis of the four additional vegetation indices besides NDVI revealed that NDVI and NIR – Red resulted in the detection of the largest change across all four indices (Table 14). The vegetation index tNDVI was the least sensitive to detecting change.

Table 14. Vegetation indices differences evaluating biomass change detection for the August 13, 2002 Hertford IKONOS NDVI image.

	NDVI (Harvest:Non)	tNDVI (Harvest:Non)	$\sqrt{\text{NIR} / \text{Red}}$ (Harvest:Non)	NIR - Red (Harvest:Non)	NIR/Red (Harvest:Non)
Mean	0.425:0.433	0.963:0.966	1.580:1.591	401.4:408.8	0.426:0.434
σ	0.004:0.005	0.003:0.002	0.010:0.009	7.59:7.56	0.004:0.004
% Difference	1.80	0.33	0.73	1.80	1.72
p	<0.001	<0.001	<0.001	<0.001	<0.001

Discussion

The image-to-image NDVI change detection within the Appomattox site did show a larger decrease in NDVI within the 1 ha area than did the within-image NDVI decrease between the harvested and non-harvested areas. However, the image-to-image processing technique had some underlying issues in that the pre-harvest IKONOS acquisition was 2 ½ to 3 months prior to the post harvest acquisition. *P. taeda* incurs tremendous change over the growing season, with the addition of 2-3 needle flushes common within this species. Sampson et al. (2003) found that *P. taeda* LAI varied twofold inter-annually with a minimum LAI in March-April and a maximum in September. Also confounding the issue of detecting change in the spectral response between the two dates was the collection solar azimuth differences for the May and August IKONOS acquisitions. An acquisition azimuthal difference of 236.7° could affect shadowing and the amount of received reflection at the sensor in the NIR. *In situ* estimated LAI increased 14.4% from the May 2002 to August 2002 time period. However, the May 2002 NDVI for the non-harvested area was 9.1% greater than the same area within the August 2002 image. Possible explanations for this decrease in NDVI with a corresponding increase *in situ* measured LAI may result from higher NIR reflectivity and red absorption from planophile broadleaf foliage in the understory compared to erectophile foliage typical of conifer needles (Turner et al. 1999). Also, another possible explanation may be the relative visibility of the deciduous understory in the low LAI *P. taeda* conditions typical for the early-late spring period. Correcting for the 9.1% decrease

in NDVI from May 2002 to August 2002, the retrieved 14.3% reduction in the harvested region between the two dates was in actuality only a 5.2% reduction in NDVI. This figure compares closely with the within post harvest image NDVI reduction result between the harvested and non-harvested region of 5.0%. A direct comparison of empirically-derived LAI, i.e. the correlation of spectral data with *in situ* estimated LAI, and *in situ* LAI was not possible due to the narrow range of LAI values within this stand.

Harvested and non-harvested NDVI was compared for both sites within each corresponding August 2002 image. Significant differences between both regions (harvested versus non-harvested) were detected. However, within the harvested region, the Appomattox and Hertford sites behaved differently with respect to the percent reduction in NDVI and the *in situ* estimated reduction in LAI. The Appomattox site showed a larger decrease in NDVI than the Hertford site within the harvested areas (5% versus 1.8%), yet the Hertford site exhibited a greater reduction in LAI (17.6% versus 9.9%). One possible explanation for this result may be the large percentage of *Ilex opaca* (American Holly) existent within the understory (60%). This species is extremely shade tolerant, thus exhibits characteristics typical of this shade class: (1) increased photosynthetic and respiratory efficiency, (2) increased light use efficiency, and (3) increased leaf surface area. There is a visible difference between the leaf underside and top of leaf. The non-Lambertian surface (leaf and canopy) could produce significantly spectral differences dependent on the image acquisition angle. In addition to the *Ilex opaca* issue, returned reflectance to the sensor may further have been reduced by the larger presence of organic soils in this coastal plain site compared to the piedmont site (Appomattox).

A general comparison of empirically-derived LAI and *in situ* LAI was made possible for these two sites by utilizing an LAI-NDVI relationship determined from narrow band NIR (0.8 μm) and red (0.66 μm) wavelengths retrieved from the HyMap (Integrated Spectronics Pty Ltd., 1997) sensor (Flores, 2003). *In situ* estimated LAI on two *P. taeda* stands, located in the North Carolina Sandhills and Coastal Plain regions, were regressed against NDVI. The developed non-

linear regression equation was applied to both the Appomattox and Hertford sites to evaluate LAI reduction from satellite-derived NDVI:

$$Y = 0.0544e^{5.378X} \quad (3)$$

where Y is the dependent variable (LAI) and X is the independent variable (NDVI). Flores (2003) found this equation to be transferable across sites, stand structures, and seasons. Applying NDVI values for both sites into equation [12] resulted in a decrease in LAI within the 1 ha harvested region of 0.12 (Appomattox) and 0.023 (Hertford). Comparing the differences explained by the *in situ* estimated LAI and LAI derived from the empirical relationship with NDVI, approximately 56.3% of the understory component is unaccounted for when using NDVI on the Appomattox site. A larger component of understory LAI is unaccounted for on the Hertford site (98.9%), again possibly in response to the spectral characteristics exhibited by *Ilex opaca*. Use of equation [12] provides only a partial understanding of the highly variable spectral returns in the red and NIR wavelengths.

The 5x5 spatial averaging window was chosen to offset issues inherent within higher spatial resolution sensors; (1) the introduction of heterogeneity at a finer scale than that from which *in situ* LAI is measured and (2) the resolving of canopies at the individual tree level (Cohen et al., 1990; Turner et al., 1999). Regarding the comparison of the various VIs, NDVI detected the most change in biomass compared to the other four indices. Both sites had yet to reach the asymptotic point in the NDVI-LAI relationship; thus the relationship was described as linear. However, the SR vegetation index may be more useful in areas of higher biomass due to the linear relationship with LAI (Flores 2003).

Conclusions

Appomattox results showed that the percentage of removed understory detected by the IKONOS sensor was 4.7% when compared to an actual *in situ* LAI reduction of 9.9%. The Hertford results showed a larger percentage of understory LAI undetected by the IKONOS sensor (1.0%) when compared to the actual LAI reduction as measured *in situ* (17.6%). Possible reasons for these differences may be based upon underlying soil types (organic) and/or bi-directional reflectance distribution functions for the non-Lambertian *Ilex opaca* canopy. Off-nadir image acquisitions for both sites would inhibit view of understory conditions for both sites (solar elevation $\approx 65^\circ$).

CHAPTER VI

UNCERTAINTY ANALYSIS OF A FINE RESOLUTION LEAF AREA INDEX (LAI) SURFACE MAP FOR MODIS LAI VALIDATION IN SOUTHCENTRAL VIRGINIA

Abstract

This research assesses the uncertainty associated with the creation of a high spatial resolution (30 m) leaf area index (LAI) reference map used in the validation of the Moderate Resolution Imaging Spectroradiometer (MODIS) MOD15A2 LAI product. The MODIS LAI product has been produced and improved upon since 2000. Validation of this product in the southeastern United States needle-leaf biome is required for possible assimilation into ecological process-based models developed within the United States Environmental Protection Agency. Assessing the uncertainty inherent within the high resolution LAI reference map is necessary for validation of the 1 km² MODIS LAI product. This research addresses two major sources of uncertainty: (1) uncertainty associated with the indirect *in situ* optical measurements of LAI and (2) uncertainty in the process of classifying land cover. The indirect *in situ* optical estimation of leaf area index (LAI) utilized the integrated measurements from the Tracing Radiation and Architecture of Canopies analyzer (TRAC) and digital hemispherical photography (DHP). Land cover classification variability was investigated with respect to inter-operator differences in the classification of land cover from a 100 km² fine spatial resolution image (30 m). Variation from these two main sources of uncertainty was then incorporated into the calculation of LAI per land cover class for a 1 km² cell that corresponded to one MODIS MOD15A2 LAI cell. LAI values within this 1 km² fine resolution reference LAI surface map (RSM) were then aggregated to

produce one overall LAI value allowing for the comparison and validation of the MODIS LAI product.

Measurement uncertainty within the *in situ* indirect optical estimation method was quantified for four parameter inputs specified by the modified Beer-Lambert light extinction model: effective leaf area index (L_e), element clumping index (Ω_E), needle-to-shoot area ratio (γ_E), and the woody-to-total area ratio (α).

Land cover classification variability was examined on the basis of training site signature selection for six analyst-derived classifications of a 100 km² Landsat ETM⁺ image centered over a highly heterogeneous area in southcentral Virginia. These classifications were then degraded to coarser resolutions, assigning the dominant land cover to the new cell resolution. Analyst-to-analyst differences were noted at the varying scales as well as overall accuracy assessment results compared to a land cover map digitized from an August 3, 2002 Ikonos panchromatic image. Results indicated that highest accuracies for all six analysts occurred at the 450 m scale resolution (i.e. 20.25 ha), corresponding to a 364 m² (13.25 ha) average patch size for all land cover classes. This would suggest a 500 x 500 m (i.e. 1/2 km) MODIS LAI cell resolution would be more appropriate at capturing the regional patterns of LAI existent in the highly heterogeneous southeastern US landscape than would the current 1 km MODIS LAI product.

Upscaling, the process of establishing a site-specific relationship between *in situ* LAI and fine resolution satellite reflectance data, was ignored in this research due to the narrow range of possible LAI values found within the conifer component on the validation site. In summary, two levels of uncertainty, variability measured within *in situ* LAI measurements and land cover classification, were propagated to return a mean LAI value per land cover class with associated errors. These mean LAI values at the land cover level were then aggregated to 1 km², resulting in a single LAI value with associated uncertainty. This RSM LAI value was then compared to the MODIS LAI cell with associated variance. MODIS LAI was 2.5 times greater than the value of the reference data set.

Introduction

Leaf area index (LAI), defined here as one-half of the total leaf area per unit ground surface area (Chen, 1996), has been estimated at a global scale from spectral data processed from the Moderate Resolution Imaging Spectroradiometer (MODIS) sensor aboard two NASA EOS-AM spacecraft, Terra (launched in 1999) and Aqua (launched in 2002). The MOD15A2 LAI product is a 1 km global data product composited over an 8-day period and is derived from a three-dimensional radiative transfer model driven by an atmosphere corrected surface reflectance product (MOD09), a land cover product (MOD12) and ancillary information on surface characteristics. In 2002 the United States Environmental Protection Agency (US EPA) initiated validation research in the evergreen needle leaf biome, as defined in the MOD12 classification, in a regional study located in the southeastern United States. The validation effort was prompted by the potential use of MODIS LAI inputs into atmospheric deposition and biogenic emission models developed within the US EPA Office of Research and Development. The MODIS LAI validation process involves the creation of a high spatial resolution LAI surface map, which when scaled to the MOD15A2 resolution (1 km) allowed for comparison and analysis with the 1 km MODIS LAI product. Creation of this LAI surface map involved: (1) the collection of *in situ* LAI measurements via indirect optical measurements, (2) the correlation of land cover specific LAI estimates with spectral values retrieved from high resolution imagery (20 m - 30 m), and (3) the aggregation of these 30 m cells to 1 km spatial resolution, matching the resolution of the MODIS product and enabling a comparison of the two LAI values (Morisette et al., 2006). This research assessed the uncertainty associated with the creation of the high-resolution LAI reference map, specifically addressing uncertainty in the indirect *in situ* optical measurements of LAI and the uncertainty in the land cover classification process.

A number of global LAI products have been produced since the advent of the 21st century. The European Space Agency (ESA), The European Commission, and The French Space Agency (CESBIO/CNES) have processed data from a single sensor (CESBIO/CNES) and from the

integration of data from multiple sensors (ESA and European Commission) to produce multiple vegetation products (Table 15). Validation efforts for these LAI products have a similar structured design as the MODIS LAI validation process where field observed LAI measurements are upscaled, i.e., the process of associating field measurements with spectral values from high resolution imagery, then aggregated to the target LAI product resolution (Morisette et al., 2006). It has been noted, however, that unaccounted measurement uncertainty in generated reference LAI maps served no utility for validation analysis of these moderate resolution sensor products (Huang et al., 2005). Foody (2000) suggested that errors found in a remotely sensed reference data set may be of greater magnitude than that of the coarser spatial resolution map being assessed.

Agency	Program	Product	Sensors	Platform
European Space Agency (ESA)	GLOBCARBON	LAI, fAPAR ¹ , VGC ²	VEGETATION ATSR-2 ³ AATSR ⁴ MERIS ⁵	SPOT ⁶ 4 and 5 ERS ⁷ -2 Envisat Envisat
French Space Agency (CESBIO/CNES)	-	LAI, NDVI, fVC ⁸	POLDER ⁹ -2	ADEOS
European Commission	CYCLOPES ¹⁰	LAI, fAPAR	VEGETATION MERIS ¹¹ POLDER-2 AVHRR ¹² SEVERI ¹³	SPOT 4 and 5 Envisat ADEOS NOAA MSG ¹⁴
National Aeronautic Space Agency (NASA)	MODLAND	LAI, FPAR	MODIS	Terra, Aqua

Table 15. Global LAI products. ¹fAPAR - fraction of absorbed photosynthetically Active Radiation. ²VGC – Vegetation Growth Cycle, ³ATSR - Along Track Scanning Radiometer, ⁴AATSR - Advanced Along Track Radiometer, ⁵MERIS - Medium Resolution Imaging Spectrometer, ⁶SPOT - Satellite Pour l'Observation de la Terre, ⁷ERS – European Remote-Sensing Satellite, ⁸fVC – fraction of vegetation cover, ⁹POLDER - POLarization and Directionality of the Earth's Reflectances, ¹⁰CYCLOPES – Carbon Cycle and Change in Land Observational Products from an Ensemble of Satellites, ¹¹MERIS - Medium Resolution Imaging Spectrometer, ¹²AVHRR – Advanced Very-High Resolution Radiometer, ¹³SEVERI – Spinning Enhanced Visible and Infra Red Imager, ¹⁴MSG – Meteosat Second Generation

This research quantified selected elements of uncertainty within the indirect *in situ* optical estimation of LAI integrating the combined measurements from the Tracing Radiation and Architecture of Canopies (TRAC) and digital hemispherical photography (DHP), i.e. the TRAC-DHP method. Also investigated in this study is the effect of inter-operator differences in the classification of land cover from fine spatial resolution (cell resolution = 30 x 30 m) imagery. Variation from these two main sources of uncertainty was then incorporated into the calculation of LAI per land cover class for a 1 km² cell that corresponded to one MODIS MOD15A2 LAI cell. LAI values within this 1 km² fine resolution reference LAI surface map (RSM) were then aggregated to produce one overall LAI value which then allowed for the comparison and validation of the MODIS product.

Literature Review

The critical examination of error sources is lacking in many published articles involving geospatial applications. Output products from these applications are commonly presented without associated estimates of error or uncertainty (Abbaspour et al., 2003). In the literature the terms error and uncertainty are used interchangeably; however, a clear distinction exists between the two. Error implies a quantitative measurement denoting the known difference between reality and the observation of that reality. Uncertainty, on the other hand, conveys a limited knowledge regarding this deviation between the observation and the reality (Huevelink, 1998; Abbaspour et al., 2003). In the geospatial domain, uncertainty signifies a knowledge deficiency regarding some true value located at some point with specified coordinates (Hunter and Goodchild, 1997).

The elements of uncertainty include: (1) inherent natural variability, (2) measurement error (systematic and random) and (3) sampling error. Natural variability includes structured and unstructured features. Structured features are regular cyclic transitions of some attributes in space and time. Loblolly pine (*Pinus taeda*), for example exhibits a needle phenology of accretion and abscission that begins at bud burst in a pine shoot in mid-summer and progresses for 27 months until the last needle drops from that initial flush of needles. Thus, a cyclic low of leaf biomass was found in early spring with a maximum leaf biomass occurring in September (Sampson et al., 2003). In contrast, unstructured features occur unexpectedly and their position and magnitude cannot be predicted. Leaf biomass, evaluated over a certain area, will vary due to tree stocking, mortality, nutrient and water deficiencies, and increased competition. Systematic measurement error may be manifest in a positive or negative shift (i.e. bias) from the true value, resulting in a displaced mean value resulting in low accuracy but high precision (precision is a measure of reproducibility under repeated measurements). Examples of this type of error include an imperfection in the instrument measuring the attribute or an imperfection in the measurement method. Indirect *in situ* optical methods typically underestimate LAI values measured with destructive harvests. In contrast, random measurement error produces observations distributed

about the mean, creating a higher accuracy but typically a lower precision. Random measurement error can be reduced through repeated observations of the entity being measured.

Uncertainty analysis focuses on the way errors propagate through spatial analysis. Error propagation is defined as the magnitude of an error in output U given errors in inputs a_i (Aerts et al., 2003):

$$U = g(a_1, a_2, \dots, a_m) \quad (1)$$

where U is the output and g is the model operating on m inputs a_i ($i = 1, \dots, m$). Propagation often occurs in an additive fashion. Cascading errors are the selective combination of erroneous, imprecise, and inaccurate information into new data layers and may be additive or multiplicative, thus proving very difficult to predict.

A number of methods have been developed to track the propagation of error through a system. Two well-used methods have been contrasted in the literature: (1) the Monte Carlo Method, and (2) the Taylor Method. The Monte Carlo method repeatedly computes the result of $g(a_1, a_2, \dots, a_m)$ with randomly sampled input values (a_i) from a joint distribution. The Taylor Method approximates g by a linear function, greatly simplifying the error analysis, but at the expense of introducing an approximation error (Huevelink, 1998). Both methods of tracking error propagation are valuable if the magnitudes of contributions of each individual input into a geospatial process are able to be identified (Huevelink, 1998).

A schematic overview of the process of creating a 1 km² RSM is illustrated in four stages: (1) ground sampling, (2) correlation, (3) regression, and (4) aggregation (Figure 19). Uncertainty introduced into the RSM can originate from multiple sources including: (1) measurement error and natural variability from indirect *in situ* optical LAI estimates, (2) spatial scale differences between the ground sampling footprint and the resolution of the base image (Landsat ETM⁺), (3) base image (Landsat ETM⁺) input surface reflectance error, (4) land cover classification error in

determining proportions of varying LAND COVER types, and (5) spatial averaging error in the aggregation process. Registration differences also exist at the comparison stage but are not included in this research in the uncertainty associated with the creation of the RSM. Existing within each of these five basic elements of uncertainty in RSM creation are numerous sub-components of uncertainty. In this paper, error and natural variability associated with the indirect *in situ* optical estimation of LAI and LAND COVER classification variability measured between analysts was quantified and propagated over a 1 km² area coinciding with one MODIS LAI MOD15A2 pixel.

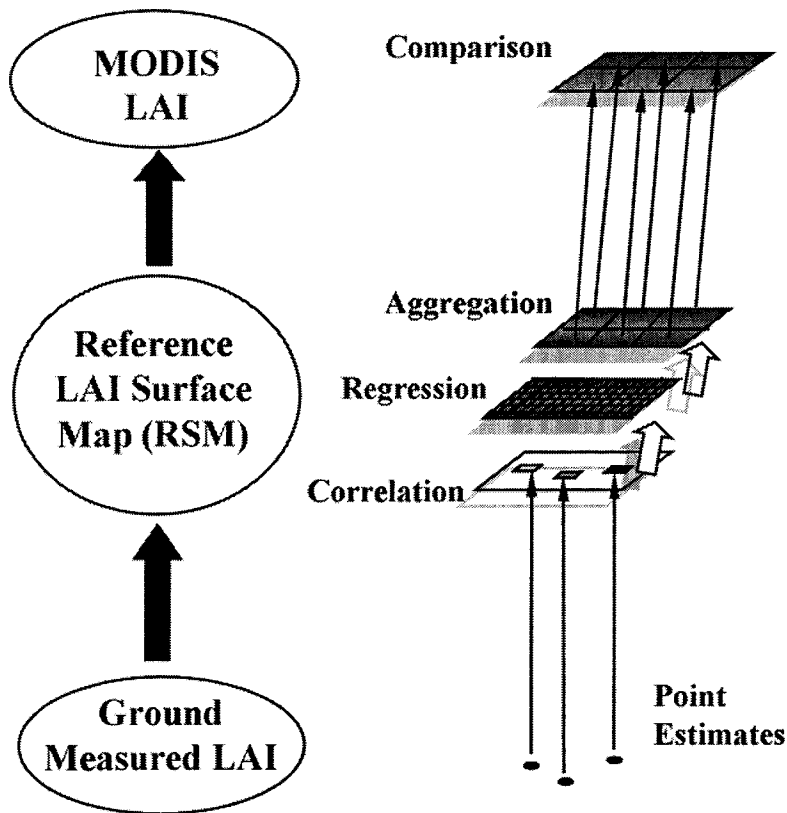


Figure 19. The MODIS MOD15A2 validation procedure.

Uncertainty: Indirect *in situ* optical LAI estimation methods

Potential error induction points along the process of RSM creation included the parameters quantified within the indirect *in situ* optical LAI estimation technique. These indirect methods for estimating LAI utilize a light extinction model developed by August Beer and Johann H. Lambert, the Beer-Lambert Law (Beer, 1853). This law takes into account that the total amount of radiation intercepted by a canopy layer is dependent on the incident irradiance, canopy structure and optical properties of the site (Jonckheere et al., 2005). The Beer-Lambert Law is based on the probability (P) of a light ray missing all foliage elements while passing through a canopy at some angle θ :

$$P(\theta) = e^{-G(\theta, \alpha)L_e / \cos(\theta)} \quad (2)$$

where θ is the zenith angle of view, α is the leaf angle distribution, $P(\theta)$ is the gap fraction defined as the probability of light penetration through foliage at θ , L_e is the effective leaf area index, and $G(\theta, \alpha)$ is the projection coefficient, a factor corresponding to the fraction of foliage projected on the plane normal to the zenith direction. This light extinction model operates under the assumption of randomly distributed canopy elements (i.e. stems, shoots, branches, etc.). In nature, however, this assumption is rarely met. Thus, correction factors have been formulated to quantify clumping (non-randomness) of canopy architecture at the shoot level, in the case of conifers, and at the stand level. The shoot has been deemed the basic element of photosynthetic light capture in conifers (Stenberg et al., 1995) and is defined as a collection of current and one year needle growth arranged in a complex geometric configuration. Shoot-level clumping is parameterized in the needle-to-shoot area ratio (γ_E) and is measured in the field and lab due to shoot architectural complexities and the inability of optical instruments to resolve within-shoot gaps. Clumping at scales larger than shoot (i.e. stand level) is estimated by the parameter (Ω_E),

defined as the element clumping index. Effective LAI (L_e), retrieved without correction for stand and shoot clumping, typically underestimates the amount of LAI within a particular stand. Another issue regarding indirect *in situ* optical LAI sensors is the inability to resolve leaf area from stem area. Thus retrieved L_e from these optical instruments is in reality a plant area index (PAI). The woody-to-total area ratio (α) correction is applied to isolate LAI from L_e . This parameter is measured in the field either through destructive sampling or through image classification techniques separating photosynthetic from non-photosynthetic material. In summary, the Beer-Lambert Law without corrections for clumping and the segregation of photosynthetic and non-photosynthetic elements of a forest stand merely returns an effective LAI, typically an underestimate of true LAI; particularly in coniferous forest stands where clumping is more pronounced than with deciduous forest stands. Chen et al. (1997) summarizes the inclusion of these correction parameters to the Beer-Lambert model by the equation (known as the modified Beer-Lambert light extinction model):

$$LAI = (1 - \alpha) * [L_e(\gamma_E/\Omega_E)], \quad (3)$$

where LAI is the leaf area index representing one-half of the total leaf area per unit ground surface area, with the other parameters previously described. In a study in the boreal ecotone, Chen (1996) reported a cumulative error of 25-35% across all four parameters (α , L_e , γ_E , Ω_E) implementing an indirect *in situ* optical LAI estimation method integrating LiCOR Plant Canopy Analyzer (PCA) (L_e) and TRAC measurements (Ω_E) (Deblonde et al., 1994; Leblanc et al., 2002). Variability attributed to each component was: L_e (3-5%), Ω_E (3-10%), γ_E (5-10%), and α (5-12%).

Uncertainty: Inter-analyst differences in Land Cover classification

A number of image processing considerations are required for the extraction of meaningful information from remotely sensed data (Jensen, 2000). These processes include image

acquisition, exploration (spectral pattern and histogram analysis), preprocessing (radiometric and geometric correction), classification (categorical definitions and classification approach), and accuracy assessment (sampling design). The quality of a classified image is determined by the cumulative error associated with these intermediate steps. Errors incurred along any point of this process may have an additive, multiplicative, or negating effect on the end classification. One important component associated with the supervised classification approach is the selection of training sites for extraction of spectral signatures emanated from specific cover types. High quality (pure) training site selection is vital in the classification process to train the classification algorithm for LAND COVER mapping extended over the entire image. The highest likelihood of pixel membership to a particular cover class is determined by the analysis of the multivariate statistical parameters derived from the representative training sites.

Classification error has been well documented throughout the literature assessing the accuracy through the contingency table or error matrix (Congalton and Green, 1999). The term ‘contingency’ refers to ‘an event which may or may not occur; that which is possible or probable (<http://www.dictionary.net>). Within the error matrix, accuracies and errors are described in a series of rows and columns comparing a classified map with a corresponding reference dataset. Correctly classified pixels are noted on the main diagonal while incorrectly classified pixels reside in the marginals (off-diagonal). Information generated from the error matrix includes: (1) an overall accuracy across all classes, (2) errors of inclusion (commission) and errors of exclusion (omission) per class, (3) and a kappa coefficient of agreement, a test of whether one data set is significantly different from another (Cohen, 1960; Bishop et al., 1975; Congalton et al., 1983). Another useful tool in the utilization of the error matrix is the Z-test, a test performed to determine if two independent kappa values from two classifications are significantly different from one another. The Z test statistic is defined as:

$$Z = |\hat{K}1 - \hat{K}2| / \sqrt{(\sigma^2 \hat{K}1 + \sigma^2 \hat{K}2)} \quad (4)$$

The \hat{K} statistic is asymptotically normally distributed due to the non-continuous (discrete) nature of remotely sensed data. The Z-test is based on the standard normal deviate where Z is standardized and normally distributed (Congalton and Green, 1999).

MODIS MOD15A2 Description. The MODIS LAI/FPAR Collection 4 product (MOD15A2) is an 8-day composite projected into the Integerized Sinusoidal (ISIN) Projection and delivered in 1200 x 1200 km 5.8 Mb tiles in the Hierarchical Data Format (HDF). The HDF file naming convention lists the MODIS product, date of acquisition, global tile location (horizontal and vertical), collection number, and date and time of processing. An example for one MODIS LAI tile retrieved for Julian date 217 in 2002 was:

MOD15A2.A2002217.h11v05.004.2003255163348.hdf. Here, the LAI tile with a horizontal and vertical location of 11 and 5 respectively was processed as a collection 4 product on Julian day 255 in 2003 at 4:33:48 pm. Four files are associated with each HDF tile: an LAI and FPAR file and two associated quality flag files (LAI and FPAR). The quality flag data described overall input quality, cloud conditions, and the algorithm used in the LAI retrieval process. Global coverage of the MOD15A2 product consisted of 36 tiles along the east-west axis and 18 tiles along the north-south axis. Thirteen tiles covered the lower 48 states in the US. Collections, defined as processed MODIS LAI retrievals from the latest algorithm improvements, began in February 2000 through February 2001 with the production of Collection 1. Collection 2 was produced as an internal science test and was not released to the public. Collection 3 ran from November 2000 to December 2002, and Collection 4 has been processed since February 2000 to the present (Tan et al., 2005).

MODIS LAI output is determined via two separate pathways: the main and the back-up algorithm. The main and back-up algorithms ingest a six biome-specific classification map at 1

km (MOD12Q1), a 1 km atmospherically corrected MODIS spectral reflectance product (MODAGAGG), and ancillary data (MOD15_ANC_RIx.hdf) containing radiative transfer coefficient lookup tables (LUTs), backup algorithm LUTs and output variable properties. The six biome types used to generate Collection 4 LAI data include: 1) grasses and cereal crops; 2) shrubs; 3) broadleaf crops; 4) savannas; 5) evergreen broadleaf forests; and 6) deciduous broadleaf forests. Biome-specific lookup tables (LUTs) containing the most probable LAI values are developed from iterative runs of a three-dimensional canopy radiative transfer (RT) model. In the case of the main algorithm, possible solutions (i.e. retrievals) are cases where the differences between the RT modeled and MODIS observed reflectances are within the uncertainty of the observed reflectances (Huemmrich et al., 2005). Dimensionless uncertainty assigned to the red and NIR MODIS bands are estimated at 20% and 5% respectively (Myneni et al., 2003). Thus, a 1-km MODIS cell is assigned the mean of the retrieved LAI distribution.

The radiation regime within a forest canopy is the integrated outcome of photon scattering by leaves, stems, and soils. In summary, the RT model solves for the inverse problem of three-dimensional vegetation canopies: given mean spectral and angular signatures of canopy-leaving radiance averaged over the three-dimensional canopy radiation field, find the desired vegetation parameters (i.e., LAI) (Knyazikhin et al., 1998). The RT model is dependent upon the parameterization of canopy architecture at the tree level (leaf normal orientation, stem-trunk-branch area fractions, leaf and crown size) and the stand level (trunk distribution, topography) with integration of spectral reflectance and transmittance patterns of vegetation elements. LAI retrieval success is predicated on the reflectance magnitude of the red and the NIR input bands. A low red or a high NIR reflectance usually results in a higher probability of a retrieval failure. Thus, a retrieval success only occurs when a MODIS pixel falls within the specified spectral and angular space of the LUT. In the case of main algorithm retrieval failure, a back-up technique is invoked where LAI is determined from empirical relationships with vegetation indices (i.e., NDVI) for each of the six biomes. This secondary method is used when insufficient high-quality

data are not available for a given compositing period. Data degradation over this eight-day cycle may be due to cloud cover or sensor system malfunctions.

Refinement of the Collection 4 algorithm was based on the integration of uncertainties for the biome data, input surface reflectance, and the radiative transfer model used to build the LUTs (Yang et al., 2005). Specifically, the algorithm was optimized to better simulate features of the MODIS reflectances for herbaceous vegetation (Biomes 1-4). Improved cloud screening and compositing algorithms were gained from atmospheric correction of MODIS surface reflectances and the biome map changed from AVHRR-based to MODIS-based. Regarding Collection 5, similar improvements to the algorithm have been implemented to improve woody vegetation LAI retrievals (Biomes 5-6). Collection 5 is scheduled to begin processing in April 2006 with an estimated completion date of early fall 2006.

Collection 5 changes include the addition of two biome classes, evergreen needle leaf forests and deciduous needle leaf forests, to the original 6-biome class MODIS product. LUTs were recalculated based on changes to parameters in the RT model (Shabanov et al., 2000). The LUTs for the woody vegetation biomes were significantly changed resulting in a decrease of LAI overestimation and improving the rate of best quality retrievals. The most significant parameter change within the evergreen needle leaf biome was the application of the photon recollision probability to the measured unit of the shoot rather than of the individual needle (Rautianen and Stenberg, 2005). Thus, a photon has a higher probability of colliding with multiple needles, thereby reducing the photon exitance from the canopy. This results in a significant reduction in the NIR wavelength received at sensor, thus reducing the overall LAI value. Only minor changes were made to the herbaceous vegetation class, as retrievals were optimized in Collection 4. Biome dependent uncertainties were introduced for Collection 5. Herbaceous vegetation was assigned algorithm uncertainties of 20% and 5% for red and NIR wavelengths. Woody vegetation uncertainties were 30% for red wavelength and 15% for NIR.

Methods

Uncertainty was assessed for elements within the process of creating a 1 km² RSM used in the validation of an August 5, 2002 (Julian Day 217) 1 km² MODIS MOD15A2 LAI pixel located at corner coordinates: UL = 687260.93, 4121691.56, LR = 688260.93, 4120691.59 (meters, datum NAD 83, zone 17, projection UTM) (Figure 20). First, measurement uncertainty and natural variability were estimated from the indirect *in situ* optical LAI estimation technique combining measurements from the TRAC optical sensor and DHP in *P. taeda* forest stands. Parameters assessed within the TRAC-DHP method included the element clumping index (Ω_E) derived from the TRAC instrument, the effective leaf area index (L_e) measured with DHP, the needle-to-shoot area index (γ_E) measured in the field and in the lab, and the woody-to-total area ratio (α) also measured in the field. Within the deciduous component, the only accounted uncertainty was the associated natural variability of TRAC-DHP derived LAI. With this information, uncertainty ranges were calculated for each land cover type found within the MODIS validation cell. Land cover types constrained to this analysis were defined as: LC 1 (Deciduous forest), LC 2 (Coniferous forest), LC 3 (Mixed forest), LC 4 (Water), and LC 5 (Other vegetation). Finally, inter-analyst classification variability based on training signature selection was assessed to determine the range of land cover proportions over the area of interest. Contributed variability from the indirect *in situ* optical measurements and the land cover classifications were combined to arrive at a mean LAI value with associated variance for the 1 km² reference LAI surface map (RSM). This 1 km² RSM was then compared to the retrieved LAI from the MOD15A2 product. There are three distinct methodologies presented in this paper addressing (1) the *in situ* optical measurement variances, (2) the classification variance between analysts, and (3) the scaling up process of (1) and (2) to MODIS spatial resolution scale (1 km²). Therefore, the methods section is partitioned to describe all three processes.

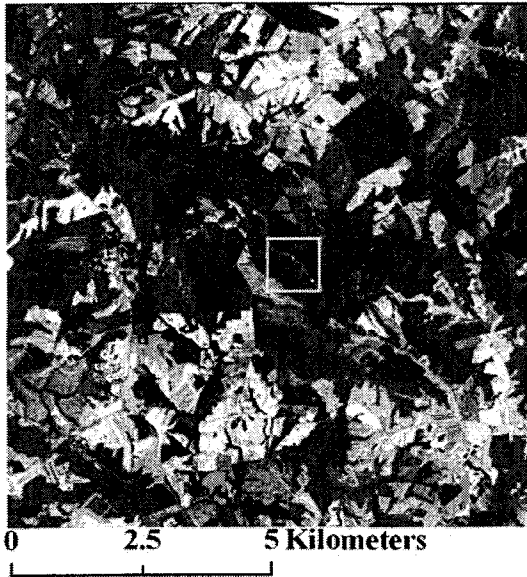


Figure 20. MOD15A2 LAI validation site (yellow square) constrained within a 100 km² Landsat ETM⁺ image, Appomattox, Virginia.

Process 1: TRAC-DHP *in situ* variability

Four primary sites, two in southcentral Virginia and two in the central and southern regions of North Carolina one in central North Carolina , were sampled for variance estimates associated with the TRAC-DHP method.

MODIS LAI validation and TRAC-DHP parameterization site; Appomattox, Virginia. The MODIS LAI validation site was located in Campbell County, Virginia (37.219°N, -78.879°W) approximately 15.5 km SSW of Appomattox, Virginia (Figure 20). This upper piedmont region has a range of elevation of 165-215 m above mean sea level. The area was a mixture of rural agricultural fields and managed and unmanaged forest stands. The MeadWestvaco Corporation, a supporter of the Sustainable Forestry Initiative, permitted sampling access to the US EPA for LAI research on 505 hectares in 2002. Annual precipitation (2002) recorded at Appomattox, Va. was 1045 mm, with an average temperature of 13.9°C. The dominant soil types for the forested area within this region were potentially highly erodible to highly erodible thermic Oxyaquic

Hapludults - thermic Typic Kanhapludults (Mattaponi-Cecil Complex), thermic Typic Hapludults (Tatum series), and the thermic Typic Hapludults – thermic Lithic Dystrupects (Tatum-Manteo Complex). These soils were moderately to somewhat excessively well-drained and were found on 2–15% slopes.

Two forest stand types dominated the forest composition on the MeadWestvaco tract: coniferous (thinned and unthinned) and deciduous. The primary tree species across the entire site was planted loblolly pine (*Pinus taeda*) with upland hardwood oak (*Quercus sp.*) comprising the deciduous component. Within the coniferous forest type, unthinned *P. taeda* planted in 1983 with a 25-year site index value of 18.9, reached economic maturity in 2003 and was subsequently harvested. Site index is a relative measure of forest site quality based on the height (m) of the dominant and codominant trees in well-stocked, even-aged stands at a specific age.

Measurements of forest structural attributes (height [m] and diameter [cm]) were made within a 1 ha area, where TRAC and DHP measurements were also made, using a point sampling method (9 plots/ha) with a basal-area-factor of 10 for trees larger than 5 cm diameter at breast height (dbh).

Three plots within the 1 ha area were sampled for understory components (stems less than 5 cm dbh) using a 4.57 m radius fixed area sampling method. Canopy closure, defined as the percent obstruction of the sky by canopy elements, was estimated using a GRS Densitometer

(www.BenMeadows.com). Stocking values, expressed as trees per hectare (TPH), were 1250

TPH for the dominant-codominant crown class and 3790 TPH for all trees comprising the

understory (suppressed). Four crown classes are recognized in most forested systems: (1)

dominant, (2) codominant, (3) intermediate, and (4) suppressed. Dominant trees extend above the general level of the crown cover and receive full light from above and partly from the side.

Codominant trees form the main canopy of the forest, receiving full light from above but little sunlight from the sides. Trees in the intermediate class are shorter than the dominant and

codominant classes, with crowns receiving little direct sunlight from above and no sunlight from the sides. Suppressed trees are below the heights of the previous three classes and receive no

direct sunlight at all (Avery and Burkhart, 1983). The average diameter (dbh), measured 1.4 m above the base of the tree, was 21.6 cm. The average height of the dominant-codominant crown class was 15.9 m. The conifer stand supported a basal area (BA) per hectare of 36.7 m², with BA defined as the cross-sectional area of a tree at 1.4 m above the tree base per unit area. The crown closure was 71% for this forest type.

The other *P. taeda* forest stand was planted in 1982 and thinned in early 2002. Prior to thinning, the site was stocked at 1400 TPH with a basal area per hectare of 28.9 m². The mechanical thinning operation reduced the basal area and trees per hectare to 11.5 m² and 313 TPH respectively, a 60.2% reduction in biomass (MeadWestvaco). The average height and dbh for this stand was 16.9 m and 23.2 cm, respectively. The 25-year site index (SI = 16.2) was lower than that found on the unthinned conifer site.

The deciduous component of the Appomattox validation site was primarily northern red oak (*Q. rubra*), white oak (*Q. alba*), and chestnut oak (*Q. prinus*). The average height and dbh was 21.3 m and 24.3 cm, respectively. Stocking at the dominant-codominant crown class was 1255 TPH, with a basal area of 22.9 m² per hectare.

TRAC-DHP parameterization sites; Brunswick (Va), SETRES (NC), and Schenck (NC). Two sites, located in Virginia and North Carolina, were part of a *P. taeda* long-term nutritional study established by the North Carolina State Forest Nutritional Cooperative (NCSFNC) (Figure 21). One site, the Southeast Tree Research and Education Site (SETRES), was located in the Sandhills of Scotland County, North Carolina (34.917°N, -79.50°W) and existed on a flat, infertile, excessively drained, sandy, siliceous, thermic Psammentic Hapludult soil from the Wakulla series (Soil Survey Division, 2001). Annual precipitation averaged 1210 mm (30 year average), but extended droughts were possible during the growing season. Average annual temperature was 17°C (30 year average). The site was planted with *P.taeda* on a 2 x 3 m spacing in 1985 (Albaugh et al., 1998). In 1992 a long-term fertilization and irrigation experiment was established (Murthy and Dougherty, 1997; Dougherty et al., 1998). Site index (m at 25 years) was 16 for this site.

The other NCSFNC site, located in Brunswick County in southcentral Virginia (36.681°N, -77.994°W), was planted with *P.taeda* in 1993. This site is located in the eastern portion of the piedmont, near the fall-line separating the piedmont and the coastal plain. Soils characterizing this area were primarily Ultisols, in particular the Appling and Cecil soil types. These soils were very deep, well-drained, and moderately permeable, and are described as fine, kaolinitic, thermic Typic Kanhapludults (Soil Survey Division, 2001). Elevation is approximately 90 meters above sea level. Annual precipitation averaged 1107 mm (57 year average) with recorded average annual temperatures of 8°C (min) and 21.3°C (max). Ten treatments were established at this site by the NCSFNC to identify the optimal rates and frequencies of nutrient application for high rates of production in forest plantations. Site index (m at 25 years) was 16.8 for this site.

The Schenck Forest site (35.8176°N, 78.7197°W) is located in western Raleigh, NC and managed by the North Carolina State University School of Forestry. This site is primarily even-aged *P. taeda* planted in 1938. Most of the TRAC and DHP variances were measured on this site.

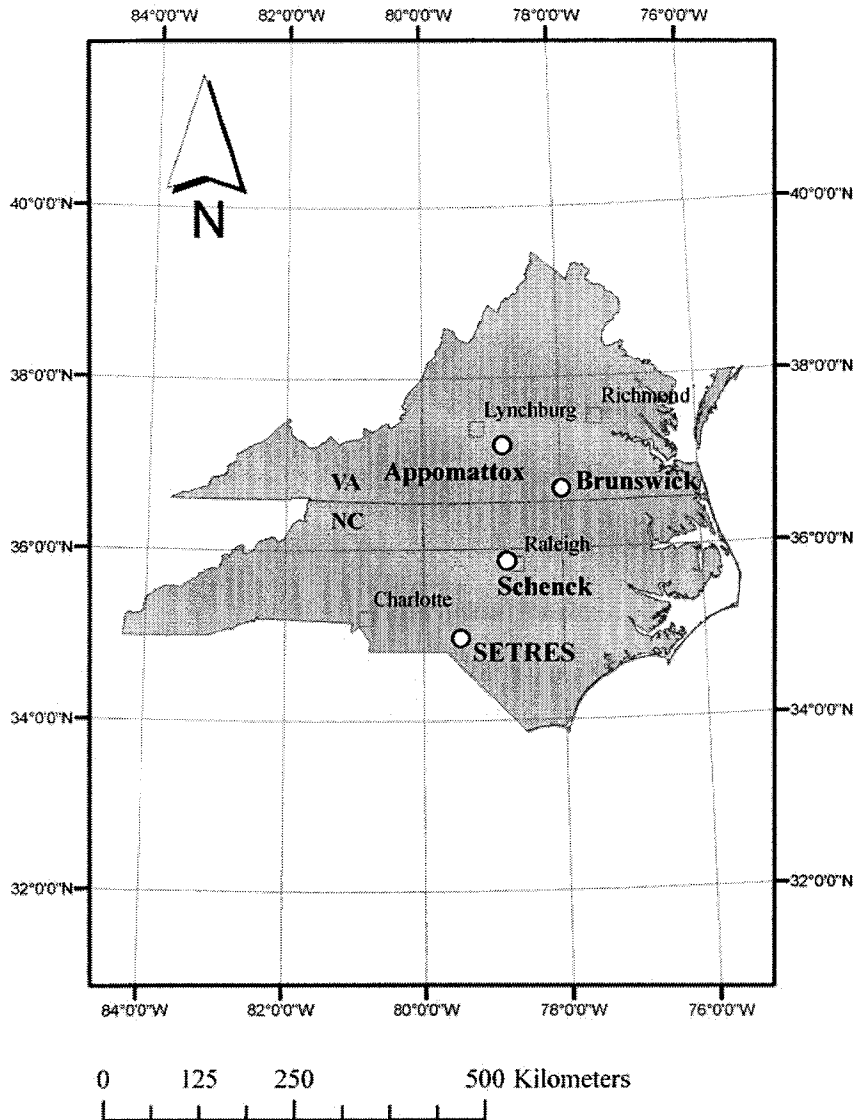


Figure 21. Location map of four sampling sites in North Carolina and Virginia

Forest attributes measured at the Brunswick and SETRES sites included basal area (m^2) per hectare, TPH, mean dbh, and height. Crown closure and understory cover estimates were also retrieved at the SETRES and Brunswick sites. *P taeda* stocking at the SETRES site averaged 1770 TPH with a 14.5 cm dbh. The average height of the dominant-codominant crown class was 12.3 m. Less than 3% of the SETRES site comprised suppressed (less than 7.6 cm dbh) longleaf

pine (*Pinus palustris*). Canopy closure was estimated at 77.5% for this forest type. Deciduous hardwood was present in the understory with all stems measuring less than 5 cm dbh (Table 16).

The Brunswick site had 1556 TPH with an average height and dbh of 11.2 m and 9.9 cm respectively. Canopy closure within this forest type was 82.4 % (Table 16).

Table 16. Forest biometric summary for all sites (UP – unthinned pine; TP – thinned pine; H – hardwood)

Parameter	SETRES	Brunswick	Appomattox UP	Appomattox TP	Appomattox H
Date Planted	1985	1992	1983	1982	1922
Mean Height (m)	12.3	11.2	15.9	16.9	21.3
Mean DBH (cm)	14.5	9.9	21.6	23.2	24.3
Canopy Closure (%)	77.5	82.4	71.0	-	-
Stocking (TPH)	1770	1556	1250	313	1255
Site Index (m at 25 years)	16	16.8	18.9	16.2	18.3

Optical Instrument Descriptions: TRAC and DHP. The TRAC sunfleck-profiling instrument consists of three quantum photosynthetically active radiation (PAR) (400-700 nm) sensors (LI-COR, Lincoln, NE, Model LI-190SB), two uplooking and one downlooking, mounted on a wand with a built-in data logger (Leblanc et al., 2002). The instrument is hand-carried in direct sun conditions along a linear transect at a constant speed of 0.3 m/sec. Typical transect lengths of 50 m to 100 m or greater are oriented close to perpendicular to the direction of the sun and are marked in fixed intervals, typically 10 m subdivisions. A user defined time stamp initiates the transect collection with each intermediate 10 m subdivision also marked by the user progressing along the transect. The instrument records the downwelling solar photosynthetic photon flux density (PPFD) from one of the uplooking sensors in units of $\mu\text{mol}/\text{m}^2/\text{s}$ at a sampling frequency of 32 Hz. The data logger records light-dark transitions as the direct solar beam is alternately transmitted and eclipsed by canopy elements. TRAC data are processed by TRACWin software (Leblanc et al., 2002) to yield the element clumping index (Ω_e) from the deviation of the measured gap size distribution from that of randomly distributed foliage (Morissette et al., 2006).

DHP measurements were made with a Nikon CoolPix 995 digital camera with a Nikon FC-E8 fish-eye converter in diffuse light conditions. An image size of 1600 x 1200 pixels was selected at an automatic exposure. The camera was mounted on a tripod and leveled over each stake at a height of 1.4 m. The camera was leveled through the combination of two bubble levelers, one on the tripod and one mounted on the lens cap. Proper leveling of the instrument ensured that the “true” horizon of the photograph was captured. The camera was oriented to true north in order to compare metrics derived from other canopy gap instruments (i.e., TRAC, densitometer, etc.). The operator would select a delayed exposure (i.e., 3-10 seconds) to offset any vibration incurred when depressing the shutter.

After downloading the images, a GLA configuration file was created for all sites. A configuration file contains information regarding image orientation, projection distortion and lens calibration, site location coordinates, length of growing season, sky-region brightness, and atmospheric conditions. GLA requires that each image be registered with respect to the location of due north on the image and the image circular area. This image registration process required that the FC-E8 fish-eye lens be recalibrated due to an actual field of view of 185°, not 180°. The image radius was reduced accordingly so that the 90° zenith angle represented the true horizon. After the image was registered, an analyst derived threshold value was determined between sky (white pixels) and no-sky (black pixels). The GLA software outputs L_e values at the 4th ring (0°-60° degrees) and the 5th ring (0°-75°). In order to assume a projection coefficient of 0.5, L_e should be solved from a gap fraction determined at 57.3°. This can be accomplished in GLA where gap fraction data are returned for the following zenith values: 5.6°, 16.9°, 28.1°, 39.4°, 50.6°, 61.9°, 73.1°, and 84.4°. The gap fraction at 57.3° then can be determined by plotting gap fraction values against the corresponding zenith angle. Solving for L_e from the Beer-Lambert equation results in:

$$L_e = \ln P(\theta) [-2\cos(\theta)] \quad (5)$$

where $P(\theta)$ is the gap fraction at zenith angle θ .

Sampling Design

The elements of uncertainty within the indirect *in situ* optical LAI estimation method (TRAC-DHP) were sampled across four sites in North Carolina (SETRES and Schenck) and Virginia (Appomattox and Brunswick). The woody-to-total area ratio (α) was measured on three sites (SETRES, Brunswick, Appomattox) for *P. taeda*, whereas deciduous α estimates were derived from measurements at Appomattox plus a similar site near Martinsville, Virginia. The needle-to-shoot area ratio (γ_E) was sampled on the SETRES and Brunswick sites only. Inherent natural variation of both the TRAC and DHP parameters, the element clumping index (Ω_E) and the effective LAI (L_e), respectively, were measured only at the Appomattox site. Measurement uncertainty for both Ω_E and L_e was observed on the Schenck Forest site in Raleigh, NC. Specifically, TRAC Ω_E measurement differences associated with intra- and inter-operators were tested along with deviations due to solar zenith angle, atmospheric changes, and changes in the mean element width (MEW) (i.e. shoot). DHP measurements of L_e were also tested for variance associated with increasing diffuse light regimes. DHP inter-operator differences were analyzed from analysis of 30 DHP images by 10 analysts (Figure 22).

$$LAI = (1 - \alpha) \cdot L_e(\gamma_E/\Omega_E)$$

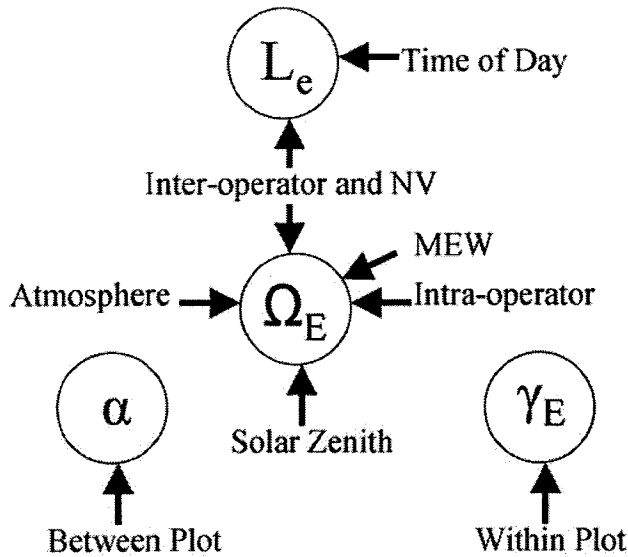


Figure 22. Elements of *P. taeda* uncertainty within the TRAC-DHP indirect (NV = natural variation; MEW = Mean Element Width) *in situ* optical LAI estimation method.

Sampling for Ω_E and L_e at the Appomattox site required establishment of two fundamental field sampling units referred to as quadrants and subplots. A quadrant was a 100 x 100 m grid with five 100 m east-west TRAC sampling transects and five interspersed transects for hemispherical photography (lines A-E). The TRAC transects were spaced at 20 m intervals (north-south), as were the interleaved hemispherical photography sampling transects (Figure 23). A subplot consisted of three 100 m or 50 m transects intersecting at the 50 m center point (25 m for 50 m subplots). The three transects were oriented at 45°, 90°, and 135° to provide flexibility in capturing TRAC measurements during favorable morning and afternoon solar zenith angles (Figure 24).

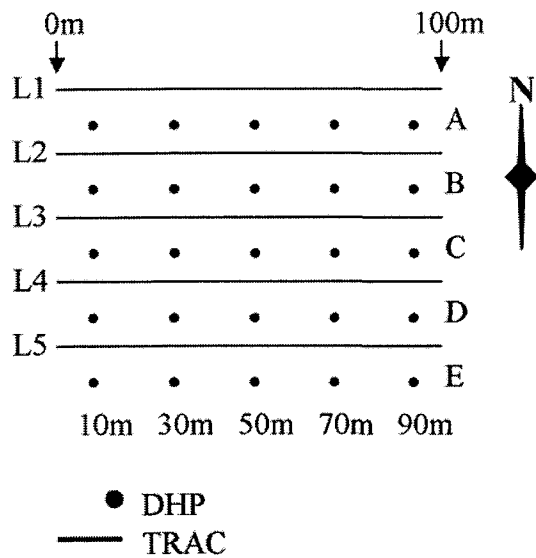


Figure 23. 100 x 100 m quadrant sampling unit.

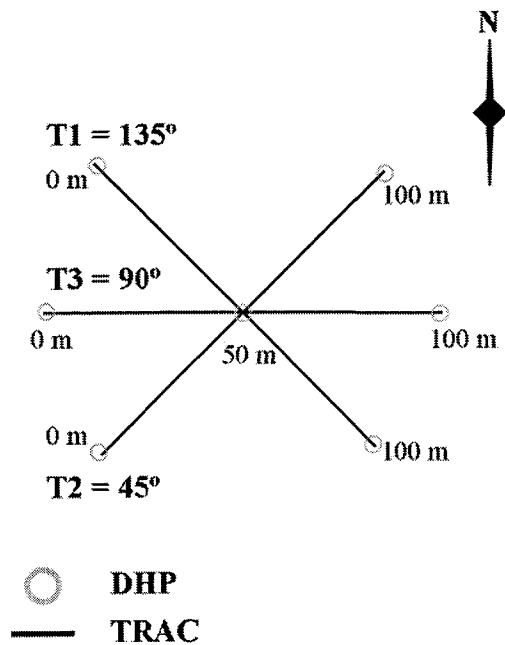


Figure 24. 100 m subplot sampling unit

Quadrants were designed to approximate an LANDSAT ETM⁺ 3 x 3 pixels window. Subplots were designed to increase sample site density and were selected on the basis of LANDSAT ETM⁺

NDVI values to sample over the entire range of variability. Quadrants and subplots were geographically located using real-time (satellite) differentially corrected GPS to a horizontal accuracy of ± 1.0 m. TRAC transects were marked every 10 m with a labeled plastic stake. The stakes were used in TRAC measurements as walking-pace and distance markers. Hemispherical photography transects were staked and marked at the 10, 30, 50, 70, and 90 m locations. Hemispherical photographs were taken at these sampling points.

Subplot (100 m) sampling only was established at both the SETRES site (two subplots), the Brunswick site (one subplot), and the Schenck site (1 subplot). At the Appomattox site, one 100 m and two 50 m subplots were established in the thinned *P. taeda* forest stand. Within the unthinned *P. taeda*, one 100 x 100 m quadrant (Q1P) was located (Table 17). Plot locations were randomly selected (Microsoft Excel RAND command) with the only stipulation required being ease of access to a road or open area, a necessary requirement for obtaining outside PPF readings with the TRAC instrument. Only one transect line of 100 m was established in an east-west direction at the hardwood subplot S1H.

Table 17. Plot coordinates, Appomattox (UTM, NAD 83, Zone 17, meters; U – unthinned, P - thinned)

Plot	Plot Type	Forest Type	GPS	Easting (X)	Northing (Y)
Q1P	Quadrant	Pine (U)	L1_0	688291	4121217
S1H	Subplot	Hardwood	L1_100	688254	4121386
S2P	Subplot	Pine (T)	L1_0	688187	4121705
S3P	Subplot	Pine (T)	L1L2_25	688553	4121370
S4P	Subplot	Pine (T)	L1L2_25	688639	4121372
S5H	Subplot	Hardwood	L1L2_25	688319	4121384
S6H	Subplot	Hardwood	L1L2_25	688258	4121435

TRAC measurements (Ω_E). TRAC derived elemental clumping index (Ω_E) uncertainty was measured on multiple sites and was tested for differences in atmospheric conditions, inter- and intra-operator TRAC operation, solar zenith angle, mean element width, and inherent natural variability.

Summer atmospheric conditions vary significantly in the North Carolina and Virginia regions. To test the effects of varying atmospheric conditions on Ω_E , TRAC measurements were made at the Schenck Forest site directly following the passing of a frontal system that brought clear and stable conditions initially then degraded into the typical hazy, hot, and humid environment typifying this area. The system brought heavy rain on August 5, 2004. TRAC measurements were made at approximately 9:00 am for five days beginning the following day and continuing through August 11, 2004. By limiting the measurement period to this particular time allowed for the collection of PPF to occur within a narrow solar zenith angle range of $60.6^\circ - 55.9^\circ$. A summary of the atmospheric conditions reported at the Raleigh-Durham International Airport (RDU) for these dates can be found in table 18.

Table 18. Weather conditions measured at RDU for the period of 8/5/2004 – 8/12/2004.

Date	Time	Temp (C°)	RH (%)	Sea Level Pressure (mb)	Visibility (km)
8/5/2004	8:51 am	27.8	79	1008.6	6.4
8/6/2004	8:51 am	20	73	1012.5	16.1
8/7/2004	8:51 am	20.6	57	1017.5	16.1
8/8/2004	8:51 am	22.8	61	1021.8	16.1
8/9/2004	8:51 am	23.9	66	1022.5	16.1
8/10/2004	8:51 am	25.6	67	1019.2	16.1
8/11/2004	8:51 am	25.6	76	1015.6	12.9
8/12/2004	8:51 am	23.9	88	1014.0	3.2

Analysis of the data was made in SAS Release 8 (1999) (SAS Institute Inc, Cary, NC) using the PROC AUTOREG procedure. PROC AUTOREG estimates and forecasts linear regression models for time series data when the errors are autocorrelated or heteroscedastic. This procedure tests for a linear trend in time. Descriptive statistics (i.e. mean, variance, standard deviation, standard error) were generated from Microsoft Excel statistical analysis module.

The effect of changes in solar zenith angle on Ω_E was tested at the Schenck Forest site. Multiple TRAC measurements were made between 9:08 am and 10:22 am on August 11, 2004, within a solar zenith angle range from 59.2° to 44.9° . The same statistical procedures used in the

atmospheric conditions analysis were used in this analysis (i.e. SAS PROC AUTOREG, Excel descriptive statistics).

Inter-operator differences were tested between two operators who ran four back-to-back TRAC collections on August 11, 2004 along one 50 m transect Schenck Forest site. These paired dual operator TRAC collections were tested for differences using a paired t-test for two sample means available in the Microsoft Excel statistical analysis module. Microsoft Excel was also used to generate descriptive statistics.

One operator tested for intra-operator differences at the Schenck Forest site between the dates of August 6 through August 11, 2004. The operator made back-to-back TRAC collections along a 50 m transect between the hours of 9:00 am and 10:00 am daily with the exception of an afternoon collection (3:00 pm) on August 7, 2004. A paired t-test generated from Microsoft Excel statistical analysis module tested Ω_E differences for 13 paired trials. Microsoft Excel was also used to generate descriptive statistics.

The primary sampling element within the TRAC algorithm for coniferous species is the shoot and the individual leaf for deciduous species. TRACWin software requires a user defined MEW to determine Ω_E . MEW was varied between 36-46 mm for *P. taeda* on the quadrant Q1P in Appomattox for the date March 6, 2002. This date was chosen for MEW analysis due to the limited obstruction from the leafless understory in the TRAC acquisition of PPFDF through the dominant-codominant *P. taeda* overstory.

Natural variation of Ω_E was measured at the Appomattox validation site on five plots within two *P. taeda* stands, one thinned and the other not, and in one hardwood stand. The primary TRAC sampling length ranged from 20-100 m (Table 19). The theoretical optimal transect length is 10 times the average distance between major foliage structures such as tree crowns. However, obtained values of Ω_E are not compromised by transect length due to forest non-homogeneous structure at both large and small scales (Leblanc et al., 2002). Longer TRAC segments were

processed in the sparsely stocked and recently thinned *P. taeda* stands in order to account for large spacing between the major foliage structures.

Table 19. Natural variability measured over three forest types, Appomattox, Va. (NV = Natural Variation)

Type	Plot	Site	Date	Error Type	Sampling Unit	N
Pine (U)	Q1P	Appomattox	7/30/2002	NV	100 m segments	25
Hardwood	S1H	Appomattox	5/23/2002	NV	20 m segments	5
Pine (T)	S2P	Appomattox	5/23/2002	NV	100 m segments	1
Pine (T)	S3P	Appomattox	5/23/2002	NV	50 m segments	1
Pine (T)	S4P	Appomattox	5/23/2002	NV	50 m segments	1

DHP measurements (L_e). Three components of uncertainty were assessed for L_e : (1) Inter-operator differences, (2) light regime differences, and (3) inherent natural variation. Inter-operator differences between 10 analysts in the selection of appropriate threshold values delineating photosynthetic from non-photosynthetic canopy elements were tested over 30 DHP images acquired in Oregon. Seven of the analysts were participants in a study investigating stream solar exposure in Corvallis, Oregon, while the other three analysts were associated with a LAI research project based in Research Triangle Park, NC (Ringold et al, 2003). A single factor analysis of variance (ANOVA) ($\alpha = 0.05$) was run to test for thresholding differences between analysts.

Light regime differences (L_e) were tested at the Schenck Forest site with five sequential images acquired by one operator between 7:54 pm and 8:38 pm on August 6, 2004. These images were acquired to establish the L_e variability attributed to decreasing diffuse light conditions. DHP images were processed by one analyst with GLA software to arrive at L_e . Descriptive statistics were generated from Microsoft Excel.

Natural variation of L_e was measured in late May and late July 2002 within the three forest types (pine, hardwood, thinned pine) at the 1 km Appomattox validation site (Table 20).

Table 20. L_e natural variability measured over three forest types, Appomattox, Va. (NV = Natural Variation)

Type	Plot	Site	Date	Error Type	Sampling Unit	n
Pine (U)	Q1P	Appomattox	7/29/2002	NV	DHP Image	25
Hardwood	S1H	Appomattox	5/23/2002	NV	DHP Image	3
Pine (T)	S2P	Appomattox	5/23/2002	NV	DHP Image	2
Pine (T)	S3P	Appomattox	5/23/2002	NV	DHP Image	2
Pine (T)	S4P	Appomattox	5/23/2002	NV	DHP Image	4

Needle-to-shoot area measurements (γ_E). Needle-to-shoot area ratios, defined as one-half the needle area to one-half of the shoot silhouette area, were measured from samples taken from two sites, Brunswick and SETRES (Figure 21). The needle-to-shoot area ratio was obtained through laboratory analysis of shoot samples following the methodology of Chen and Black (1992a, b) and Fassnacht et al. (1994). Chen (1996) recommended sampling one tree per crown class in each stand type. *P. taeda* stands within this southeastern region are typically even-aged systems with only dominant and codominant trees comprising the main canopy. Thus, only trees in these two crown classes (dominant and codominant) were sampled at the two sites. A total of three trees, randomly selected, were measured at the Brunswick (1 tree) and SETRES (2 trees) sites. Within each tree, four shoot samples were taken from the lower, middle, and upper sections of each crown. Thus one sampled tree yielded 12 shoot samples. Samples were hydrated and cooled in order to retain leaf moisture.

Woody-to-total area ratio measurements (α). The woody-to-total area ratio accounts for the percentage of woody material contributing to the calculation of gap fraction. In this study, the woody-to-total area ratio was determined through a combined analysis approach isolating and retrieving the surface area measurement of the main stem area with ImageTool (University of Texas Health Science Center in San Antonio, <http://ddsdx.uthscsa.edu/dig/itdesc.html>), then analyzing the main canopy with Leica Imagine 8.6 using an unsupervised clustering algorithm, the Iterative Self-Organizing Data Analysis Technique (ISODATA) (Tou and Gonzales, 1974). Five trees were selected from both sites for analysis. Selection criteria included relative isolation

of the tree of interest, thus reducing vegetation overlap with neighboring canopies. Images were taken with a Sony Digital Cyber-Shot DSC-S85 at 96 dots per inch resolution. Images were brought into ImageTool, calibrated, then the area of both the main stem and the canopy were computed through on-screen digitization. The main canopy image was clipped and imported as a TIFF into Leica Imagine 8.6 and the ISODATA clustering algorithm was employed to separate green vegetation from the sky. This algorithm uses a minimum spectral distance to assign a cluster for each candidate pixel (ERDAS Imagine Field Guide, 4th Edition). Arbitrary cluster means are specified at the initiation of the process, then multiple iterations shift the cluster means in the data. Initial parameters using one standard deviation, 99% convergence, 20 classes, and a maximum of 10 iterations were imputed into the algorithm. In choosing plus and minus one standard deviation from the mean, a total of 33% of the variation was initially assigned to classes 1 and 20. Due to the large amount of variation ascribed to these two classes, the ISODATA algorithm splits and merges these classes over all the iterations. The percent of green vegetation identified from the ISODATA analysis was simply multiplied to the upper crown area computed earlier, to return a percent needle area.

TRAC-DHP LAI variability assessment: Monte Carlo Simulation in *P. taeda* (unthinned).

After the determination of variances surrounding the mean of each input parameter for the modified Beer-Lambert light extinction model, LAI variability was estimated in Q1P (unthinned conifer) through a Monte Carlo simulation drawing values from the uncertainty distributions attributed to each input. Minimum and maximum values for all four inputs (Ω_E , L_e , γ_E , α) were applied to the simulation. Ω_E and L_e uncertainty was not based on the multiple effects tested (i.e. atmospheric, light regime, inter and intra-operator) due to a lack of understanding regarding their interactions (i.e. additive, compensating, multiplicative, etc.). The Monte Carlo simulation was completed through the process of sampling 10000 randomly generated values of the four input parameters from a Gaussian distribution. The random numbers were generated from the software program RandGen (<http://www.lohninger.com/randgen.html>). These values were then applied to

the Modified Beer-Lambert light extinction model to produce 10000 estimates of LAI. From the resulting distribution, mean and standard deviation was calculated using Microsoft Excel statistical analysis package. This standard deviation would later be applied to mean LAI values estimated at Appomattox in 2002.

Appomattox Validation Site TRAC-DHP LAI estimation measurements 2002. TRAC and DHP measurements were made over the Appomattox validation site in 2002 in order to establish mean LAI values for each land cover class. TRAC measurements were made July 30, 2002 between 9:13 am and 9:41 am in the unthinned pine forest class (Q1P). Temperature at the time of the TRAC collect was 30.6°C with clear skies, good visibility (16.1 km), and a relative humidity of 59%. PPFD varied 340 $\mu\text{mol}/\text{m}^2/\text{s}$ from a minimum at the start of the measurements to 1013 $\mu\text{mol}/\text{m}^2/\text{s}$ at the end of the data collection. The solar zenith angle ranged from 57.0° to 51.3° and the solar azimuth changed from 91.1° to 95.6° during this time interval. All five 100 m transect lines were measured once with TRAC. DHP measurements on Q1P were made the previous evening (July 29) at all 25 sampling locations.

TRAC and DHP measurements for the thinned conifer (S1P, S2P, S3P) and the deciduous forest classes (SIH) were made May 23, 2002. TRAC and DHP derived parameters (Ω_E and L_e) were assumed to not differ significantly from values measured in late July or early August due to: (1) the leaf biomass stability of the 82 year old hardwood forest stand and (2) the relatively low LAI values found in the recently thinned pine stand. The thinned pine stand also was in a recovery state where the percentage of understory removal had been significant and would not respond with new growth until the beginning of the next growing season. TRAC measurements were taken at the four plots between 3:52 pm and 5:57 pm. Solar azimuth changed from 255.7° to 276.4°, while the solar zenith angle changed from 38.3° to 62.9° over this time period. On this date, the data collect temperature was 74° with a relative humidity of 29%. The atmosphere was clear with good visibility (16.1 km). One TRAC collection was made on all 4 plots. DHP measurements were made later that evening.

In order to arrive at an overall LAI value for the three sampled forest types, i.e. thinned (S2-4P) and unthinned conifer (Q1P) along with deciduous (S1H) stands, three separate sampling schemes were utilized dictated by stand structure. The sampling unit within the unthinned conifer (Q1P) was the 100 m TRAC transect measurements in conjunction with adjoining DHP measurements (n=5). S1H sampling protocol involved populating 30 m Landsat ETM⁺ cell with 20 m TRAC segment measurements with adjoining DHP measurements (n=4). Finally, due to the sparse stocking of tree stems within the thinned conifer sites (S2-4P), sampling units were TRAC and DHP measurements for the entire subplot (n=3).

Summary: TRAC-DHP *in situ* variability method. Uncertainty analysis was applied to the TRAC-DHP *in situ* indirect optical method of estimating LAI in the southeastern United States. Standard deviations of input parameters to the modified Beer-Lambert light extinction model (Chen et al., 1997) were quantified in the *P. taeda* forest class. A Monte Carlo analysis simulating 10000 randomly generated observations within the parameter variability constraints produced a standard deviation measure of LAI for *P. taeda*. Later, this measure of dispersion was applied to a July 29, 2002 measured mean LAI value in unthinned and thinned *P. taeda* forest class within the Appomattox validation site. Natural variation measured *in situ* at the Appomattox site was recorded for the other forest classes. These uncertainty values were then applied to mean LAI retrieved from the hardwood and thinned *P. taeda* forest classes from measurements made on May 23, 2002.

Process 2: Classification variance between analysts

The second step in the creation of a 1 km² RSM, after the *in situ* LAI estimation was completed, was upscaling the *in situ* LAI measurements per land cover class to pixel or patch based high resolution imagery (20-30 m spatial resolution). Upscaling is commonly accomplished through the establishment of a site-specific relationship between *in situ* LAI and fine resolution satellite reflectance data. In a predominate number of LAI validation studies, MODIS 1 km² cell

sizes are homogeneous with respect to land cover. Within these homogeneous, 1 km² MODIS cells, empirical relationships are developed through sampling across the entire range of LAI. Establishing the NDVI and *in situ* LAI relationship was not possible at the Appomattox site due to the heterogeneous composition of land cover types within the 1 km² area. The Appomattox site had a narrow range of possible LAI values in the dominant land cover type (coniferous), effectively negating the possibility of correlating *in situ* LAI with satellite-derived indices. In this study I ignored the empirical relationship and simply transferred indirect *in situ* optical LAI estimates to the corresponding land cover delineated on the 1 km² RSM. This avoided error associated within the NDVI-*in situ* LAI correlation. The error associated with the NIR and red wavelengths in Landsat ETM⁺ imagery is currently being investigated by researchers at Boston University (Huang et al., 2006).

Quantification of uncertainty within the land cover classification of the 30 m fine resolution imagery was necessary. Methods for this process included the analysis of inter-analyst classification variability, addressing differences between classifications when only training site signature selection was controlled by the analyst. Here, inter-analyst variability was examined between six analysts from the Department of Natural Resources at the University of New Hampshire. Each analyst classified a 100 km² Landsat ETM⁺ image (August 12, 2002), centered on the 1 km² Appomattox validation site (Figure 21), varying only location and number of training sites. These analyst-derived classifications were degraded to coarser resolutions, assigning the dominant land cover to the new cell resolution. Analyst-to-analyst differences were noted at the varying scales (90 m²-1200 m²) as well as overall accuracy assessment results compared to a 19.4 km² reference land cover map digitized from an August 3, 2002 Ikonos panchromatic image (Figure 25). Spectral separability for training site data was analyzed for each of the six classifications. These tests included a Euclidean Distance, Transformed Divergence, and Jeffries-Matusita Distance evaluation.

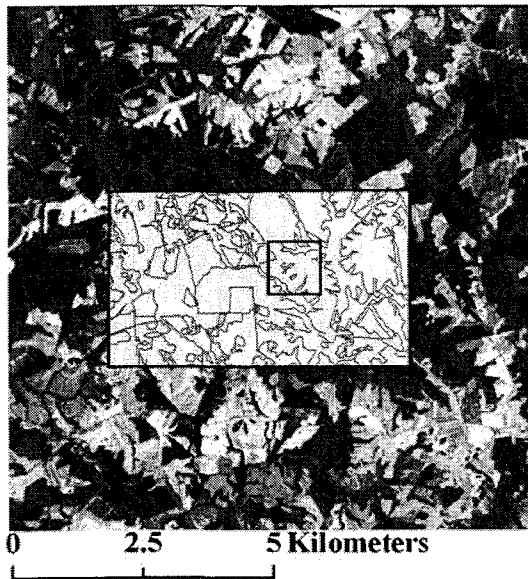


Figure 25. The August 12, 2002 100 km² Landsat ETM⁺ image classified by 6 UNH analysts. The 19.4 km² reference land cover map (yellow) is seen with land cover delineations. The 1 km² MODIS MOD15A2 validation pixel (black box) is inlaid within the reference land cover map.

Landsat ETM⁺ Georectification. An August 12, 2002 full scene Landsat ETM⁺ image (L71016034_03420020812_HDF.LIG) was subset to a 100 km² area, then georectified using the ‘nearest neighbor’ resampling algorithm. Digital orthophoto quarter quadrangles (DOQQs) from 1994-2000 were downloaded from the Virginia Economic Development Project (VEDP) website (<http://gis.vedp.org/quads/search.html>) and used as the reference dataset for the georectification process. Nine control points evenly distributed across the area of interest (AOI) were measured with a Trimble GPS unit employing real-time differentially corrected services (± 1 m horizontal accuracy). Mean x, y deviations were calculated between the image and ground coordinates for both the IKONOS 1 m panchromatic image and the VEDP DOQQs. The VEDP DOQQs were converted from the native MrSid format to the Leica Imagine 8.6 .img format. Within the Leica Imagine 8.6 Image Geocorrection Module, a 2nd order non-linear transformation was applied to correct non-linear distortions. Eleven ground control points (GCPs) were used to georectify this image, fulfilling the requirement of a minimum of six GCPs to define a 2nd order polynomial

(paraboloid). The nearest neighbor resampling algorithm was applied to maintain original digital number (DN) values. The RMSE (2.10 m) within the georectification process was acceptable because it was approximately within one-half pixel. The Landsat ETM⁺, IKONOS 1 m panchromatic, and DOQQ imagery were projected in the Universal Transverse Mercator (UTM) projection with the following projection parameters: zone 17, datum NAD 83 (the North American Datum 1983), and units meters.

Data Exploration. Derivative bands (Table 21) were created and “stacked” to the 6-band Landsat ETM⁺ image. The series of indices that included the infrared (Landsat ETM⁺ Band 4) and the red (Landsat ETM⁺ Band 3) spectral bands were designed to respond to changes in the amount of green biomass and chlorophyll content. In order to achieve band matrix invertibility, a necessary component for divergence analysis, three layer stacks were created using the following band combinations:

- (1) TM123457_NDVI
- (2) TM123457_SR_54
- (3) TM123457_√VI_VI_tNDVI

Histograms for all 6 bands of the 100 km² subset image were evaluated for the minimum, maximum, and mean brightness value, the dynamic range (defined here as ‘the range within approximately two standard deviations of the mean’), the distributional mode, and the closest distributional curve. The data analysis techniques that were chosen for data exploration included derivative band analysis (i.e. ratios, vegetation indices, etc.), principal component analysis, spectral pattern analysis, and divergence analysis.

Table 21. Derivative bands created from original 6-band LANDSAT ETM⁺ imagery.

Band	Abbreviation	Formula
NDVI	NDVI	$(\text{ETM } 4 - \text{ETM } 3)/(\text{ETM } 4 + \text{ETM } 3)$
Simple Ratio	SR	$\text{ETM } 4/\text{ETM } 3$
Ratio 5/4	54	$\text{ETM } 5/\text{ETM } 4$
$\sqrt{\text{VI}}$	$\sqrt{\text{VI}}$	$\sqrt{4/3}$
Vegetation Index ^x	VI	$\text{ETM } 4 - \text{ETM } 3$
tNDVI	tNDVI	$(\text{NDVI}) * 0.5$

Data Analysis: Techniques. The derivative bands (Table 21) chosen for this analysis, with the exception of the Ratio 5/4 index, take advantage of the reflectance characteristics inherent within vegetation and non-vegetation between the red and near infrared (NIR) portion of the electromagnetic spectrum. The combination of healthy green vegetation absorbing incident energy for photosynthesis in the red wavelength and reflecting incident energy in the NIR due to leaf mesophyll structure creates the unique opportunity to distinguish photosynthetic biomass from non-photosynthetic biomass.

Principal Component Analysis allowed for the production of transformed bands with possible better interpretability than the original raw LANDSAT ETM⁺ bands. Typically, more than 98% of the image variation can be explained in the first three PC bands allowing the added benefit of data reduction. In PC analysis, eigenvalues for each band are calculated and the percent variance explained per band is computed by dividing each band eigenvalue by the sum of all eigenvalues.

Spectral Pattern Analysis allowed for the visual inspection of class separability in an image. Signatures of all land cover types (deciduous, coniferous, mix, water, and other vegetation) were created via the Signature Editor. Within the “Seed Properties” dialogue the neighborhood was set to grid, pixel distances were set to 300 and spectral euclidean distances were varied between 7 and 12 pixels. Invertability was achieved with all training sites. Due to the problems of invertability and the lack of significant separation in most land cover except water, all PC bands were eliminated from the analysis for possible inclusion into the classification process.

Prior to selecting the bands for classification, a divergence, a Transformed Divergence and Jeffries-Matusita analysis, were performed on the layerstack images. All techniques were reasonable in evaluating signature separability. The Transformed Divergence exhibited computationally simpler empirical measurements and the Jeffries-Matusita showed a more theoretical soundness due to directly relating to the upper bound of probability classification errors (Richards, 1986).

Data Analysis: Classification. In order to test inter-analyst differences, all classifications differed only with respect to training site location and the number of iterations. Analysts were provided a 4-band (cell resolution = 30 x 30 m) image to classify using a supervised classification approach implementing the parametric maximum likelihood algorithm. The 4-band image was comprised of original and derived bands from the August 12, 2002 LANDSAT ETM⁺ image. The bands chosen for analysis included LANDSAT ETM⁺ bands 5 and 7, \sqrt{VI} , and tNDVI.

Training and data was provided to each analyst. Each received the image to be classified, reference images (Ikonos 1.0 m panchromatic and 1.0 m color infrared (CIR) digital orthophoto quarter-quadrangles (DOQQs)), screen captured images in TIFF image format depicting specific land cover types, and directions. The land cover classes and definitions were as follows:

- LC 1 (Deciduous Forest) – at least 25% of the area is covered by trees and more than 75% of the crown class is deciduous
- LC 2 (Coniferous Forest) – at least 25% of the area is covered by trees and more than 75% of the crown class is coniferous
- LC 3 (Mixed Forest) - at least 25% of the area is covered by trees and neither conifers or deciduous trees have more than 75% of the crown class
- LC 4 (Water) – lakes, ponds, or reservoirs
- LC 5 (Other Vegetation) – areas having less than 25% tree coverage and more than 10% other vegetation such as agricultural lands, urban grasses, and transitional vegetation (i.e., clearcut harvests)

Using the signature editor, training site signatures were collected for all classes, making certain to attain class invertability. The parametric maximum likelihood algorithm was used to assign class values to each pixel.

Classification Assessment. The six analyst-derived classifications were compared to one another (classification-to-classification) at the full 100 km² Landsat ETM⁺ scene. A classification-to-reference comparison was completed within a 19.4 km² area completely contained within the 100 km² Landsat ETM⁺ scene. Here, all six analyst-derived classifications were compared to a reference land cover data set digitized from an August 3, 2002 IKONOS 1 m panchromatic image. Software used in this analysis included the Analytical Tools Interface for Landscape Assessment (ATiILA), and RS Accuracy, both developed at the US EPA Environmental Sciences Division within the Office of Research and Development. ATiILA was developed in Avenue programming language as an ESRI ArcView extension and is designed to accommodate spatial data from a variety of sources. The two primary spatial data types used for analysis were vector (ArcView shapefiles or ArcInfo coverages) and raster (ArcInfo Grid) themes. Landscape metrics were derived from the primary data source, the ArcInfo Grid. The primary reporting unit was the vector polygon. Information contained at the raster level was scaled to the polygon reporting unit of interest. RS Accuracy was designed in Visual Basic programming language to calculate accuracy assessment metrics derived from the comparison of the classified image with the reference data set.

Classification Assessment: Classification-to-Classification Comparison. All classifications were evaluated at eight resolutions (150, 300, 450, 600, 750, 900, 1050, and 1200 m). The purpose of evaluating analyst-derived classification differences at 150 m intervals was to locate the optimal cell resolution where land cover agreement was maximized. The 150 m interval was chosen to correspond within 50 m to the current 1000 m MODIS LAI product and within 50 m of potential future MODIS LAI resolutions: 250 m, 500 m, and 750 m. At each resolution, across all six analyst-derived classifications, the percent total agreement, percent agreement between forest

and non-forest classes, and the percent agreement of deciduous and coniferous within the forest classes were determined.

ArcInfo Grids were created at the resolutions indicated above via the “makegrid” aml (Arc Macro Language) (Appendix B). The “makegrid” aml call creates a polygon grid of a chosen cell size where the lower left coordinates (x, y) are predicated on the lower coordinate (x, y) of an input coverage. The ATtILA extension was loaded into an ArcView project and the “Landscape Characteristics” module is chosen for analysis. For each classification the reporting unit (i.e., polygon generated from the “makegrid” aml) and the classification were inputted into the module. Thus, results returned for each classification included percentages of each land cover type per grid cell of a chosen resolution. The dominant land cover type was determined in Microsoft Excel for each grid cell at each resolution for each of the six classifications. At each of the eight resolutions across all six classifications, the percent total agreement, percent agreement between forest and non-forest classes, and the percent agreement of deciduous and coniferous within the forest classes were determined.

Classification Assessment: Reference Creation and Analysis. A reference land cover dataset was created through the digitization of a 19.4 km² IKONOS 1 m panchromatic image completely contained within the 100 km² Landsat ETM⁺ scene (Figure 25). ArcInfo Grids were created for this 19.4 km² area at the following cell resolutions (m): 30, 90, 150, 300, 450, 600, 750, 900, 1050, and 1200. The ArcView ATtILA algorithm was applied to return land cover percentages per cell resolution beyond the base 30 m resolution. This information was used to calculate the percent land cover homogeneity beyond the 30 m base (90 – 1200 m) in order to evaluate the effect of increasing cell resolution on land cover homogeneity. Within Microsoft Excel, the dominant land cover types were determined per cell resolution. These land cover values were plotted at each cell resolution and transition points were noted where land cover values for each of the five land cover classes deviated from the original 30 m base land cover value. Finally,

average patch size (m²) for each of the five land cover classes was calculated across the 19.4 km² area. Average patch size was calculated in ATtILA assuming a minimum patch size of 90 m².

Classification Assessment: Classification-to-Reference Comparison. Overall accuracy was assessed for all six analyst-derived classifications for nine cell resolutions (90, 150, 300, 450, 600, 750, 900, 1050, and 1200 m). The addition of the 90 m cell resolution was dictated by the need for the analysis of the smallest minimum mapping unit (MMU) beyond one 30 m base. Overall accuracies were determined at the nine selected cell resolutions by comparing the classified land cover cell values with the reference cell values. In order to examine specific areas of confusion within each of the six classifications, error matrices were constructed and analyzed for the 90 m and 150 m resolutions. Error matrices were not created for the coarser cell resolutions (>150 m) due to inappropriate sample sizes (i.e. sample sizes per land cover class less than 50 per class (Congalton and Green, 1999)). Matrices were constructed for each of the six analyst-derived classifications by comparing the classified land cover values with the IKONOS reference land cover values.

Information retrieved from each error matrix included overall accuracy, commission and omission error per land cover class, Kappa coefficient of agreement, and z-tests evaluating pair-wise comparisons between classifications. For each pair of classifications a Z statistic was generated and then compared to the t-value at alpha level of 0.05. However, since a total of 15 pair-wise tests existed in this analysis, the chance for detecting a type I error increased. The definition of a type I error is “the chance of detecting a significant difference when in fact there is not one.” Every additional pair-wise comparison increases this chance of detecting a difference. Thus, a Bonferroni correction was applied to adjust the alpha level downward of each individual test to ensure that the overall risk for a number of tests remained at 0.05. The Bonferroni correction was determined by dividing the alpha level desired (0.05) by the n (15). Thus, the new t-value was 2.573.

Classification Assessment: Training Site Assessment. Spectral separability for training site data was analyzed for each of the six classifications. These tests included a Euclidean Distance, Transformed Divergence, and Jeffries-Matusita Distance evaluation. The Euclidean Distance evaluation is a statistical measure of the spectral distance between the mean vectors of a signature pair. The Euclidean Distance measurement between signatures does not incorporate measures of variation about the mean, but it does give a rough estimate of spectral separation. The Transformed Divergence analysis exhibits computationally simpler empirical measurements than the Jeffries-Matusita analysis. The Jeffries-Matusita analysis displays a more theoretical soundness than the Transformed Divergence in that it directly relates to the upper bounds of classification errors (Richards, 1986). Signatures are said to be totally separable if the calculated divergence is equal to the appropriate upper bound.

Along with the above mentioned divergence measures of separability, bi-spectral box plots were constructed for each operator classification to investigate overlap percentages between classes. For all pair-wise band combinations which included: TM 5-TM7; TM 5- $\sqrt{\text{VI}}$; TM 5-tNDVI; TM 7- $\sqrt{\text{VI}}$; TM 7-tNDVI; $\sqrt{\text{VI}}$ - tNDVI, bi-spectral box plots were created from two measurements of training site (TS) variability for each land cover class: (1) within and (2) between training sites variability. "Within" TS variability was defined as one standard deviation (SD) of the pixel DN values for one training site within one land cover class. The mean SD for all TS for one land cover class returned the outer gray band (A1) depicted in Figure 26. The center (black) ellipse (A2) shown in figure 26 represented the SD of all the mean DN values for all TS for one land cover.

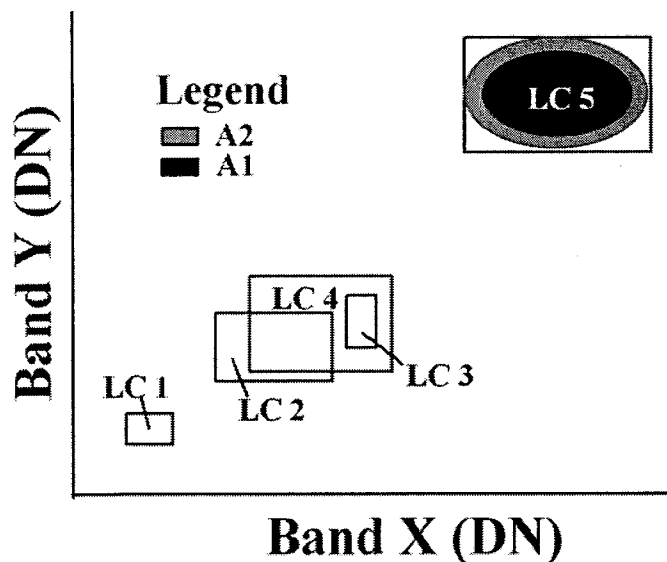


Figure 26. Calculation of the percentage of training site overlap. Each of the 5 land cover (LC) box plots are created from variance associated within each independent training site (A2) and variance measured across all training sites (A1). To arrive at a value A2, DN standard deviations are acquired for each independent training site within a given land cover class. These standard deviations are then averaged to give an overall mean value, resulting in the added variability visualized by the outer gray ring in LC 5. The majority of variability is found in A1, which is a measurement of the standard deviation of the means of each training site contributing to the LC 5 classification.

Process 3: RSM Aggregation and Comparison

The final steps in the creation of a 1 km² RSM prior to the comparison with the MODIS MOD15A2 1 km² LAI cell involved: (1) clipping the six analyst-derived and reference classified maps to the 1 km² bounds of the MODIS cell, (2) aggregating the clipped 1 km² areas to one mean LAI value based on the weighted percentages of each contributing land cover class, (3) determining the mean LAI standard deviation of the six analyst-derived classifications, (4) applying this classification uncertainty to the reference mean LAI value with associated *in situ* variability. Therefore, the final RSM product was a 1 km² cell with one LAI value representing

many contributing land cover LAI values. This one LAI value included three standard deviations of variability incorporating uncertainty estimated from the indirect *in situ* optical estimation of LAI and classification differences between analysts. Finally, the corresponding 1 km² MODIS MOD15A2 LAI cell was retrieved for the date of interest (August 5, 2002) with associated variability.

Appomattox Validation of MODIS MOD15A2 LAI 1 km²cell. Collection 4 MOD15A2 LAI data (2001-2003) was downloaded from the Earth Observing System (EOS) Data Gateway at the NASA Land Processes Distributed Active Archive Center (LP DAAC) (<http://edcimswww.cr.usgs.gov/pub/imswelcome/>). The MODIS MOD15A2 tile encompassing the Appomattox validation site was 1200 x 1200 km (vertical 05, horizontal 11) (Figure 27). A total of 45 dates comprised each year's collection with the first date occurring on January 9 and each subsequent image date 8 days thereafter. The 135 image dates were layer stacked in RSI ENVI Imaging Processing software then reprojected from the native ISIN projection into the UTM projection (units meters, datum NAD 83, zone 17). This MODIS three-year layer stack was then clipped to an 11 x 11 km (121 km²) area with the center cell (row 6, column 6) designated as the Appomattox validation site. The same process was made on the associated MODIS MOD15A2 quality flag data in order to investigate the LAI retrieval algorithm utilized in the production of the MODIS LAI product. Within the data quality flag product, each cell is assigned a numeric value between 0-4 under the following characterization:

- QA Flag 0 – Main RT method used with best possible results
- QA Flag 1 – Main RT method used with saturation
- QA Flag 2 – Main RT method failed due to geometry problems, empirical methods used
- QA Flag 3 – Main RT method failed due to other problems, empirical method used
- QA Flag 4 – Could not retrieve pixel

An initial investigation of the Appomattox validation cell for Julian date (JD) 217 (August 5, 2002) revealed a quality flag value of no retrieval (QA flag 4). There was no LAI retrieval for the JD 217 in 2002. In 2003 JD 217 showed an LAI value of 1.0 indicating some underlying issue affecting the retrieval process. The biome-specific classification map (MOD12Q1) classified this pixel as Savannah (class 4), defined as lands with herbaceous types of cover with tree and shrub cover less than 10% (IGBP classification). A three-year average (2001-2003) of LAI values for the Appomattox validation cell was used to extract one viable LAI value for comparison with the RSM LAI value. An LAI value of 4.8 was found for Julian date 217 (2002) for the Appomattox validation site when extrapolating between the green-up and senescent LAI values (Julian dates: 129 and 273, respectively) (Figure 28). In order to estimate a standard deviation about this MOD15A2 mean of 4.8, a 3 x 3 window average of LAI surrounding the Appomattox validation cell was calculated for 2002. A three-date averaging was made on the data in order to smooth potential outliers from the data. A total of five dates bracketing the targeted Julian date of 217 (Julian dates: 201, 209, 217, 225, 233) were analyzed for variability. Finally, the LAI means of both the RSM and the MOD15A2 Appomattox cell were compared with associated variances of three standard deviations on both sides of the means.

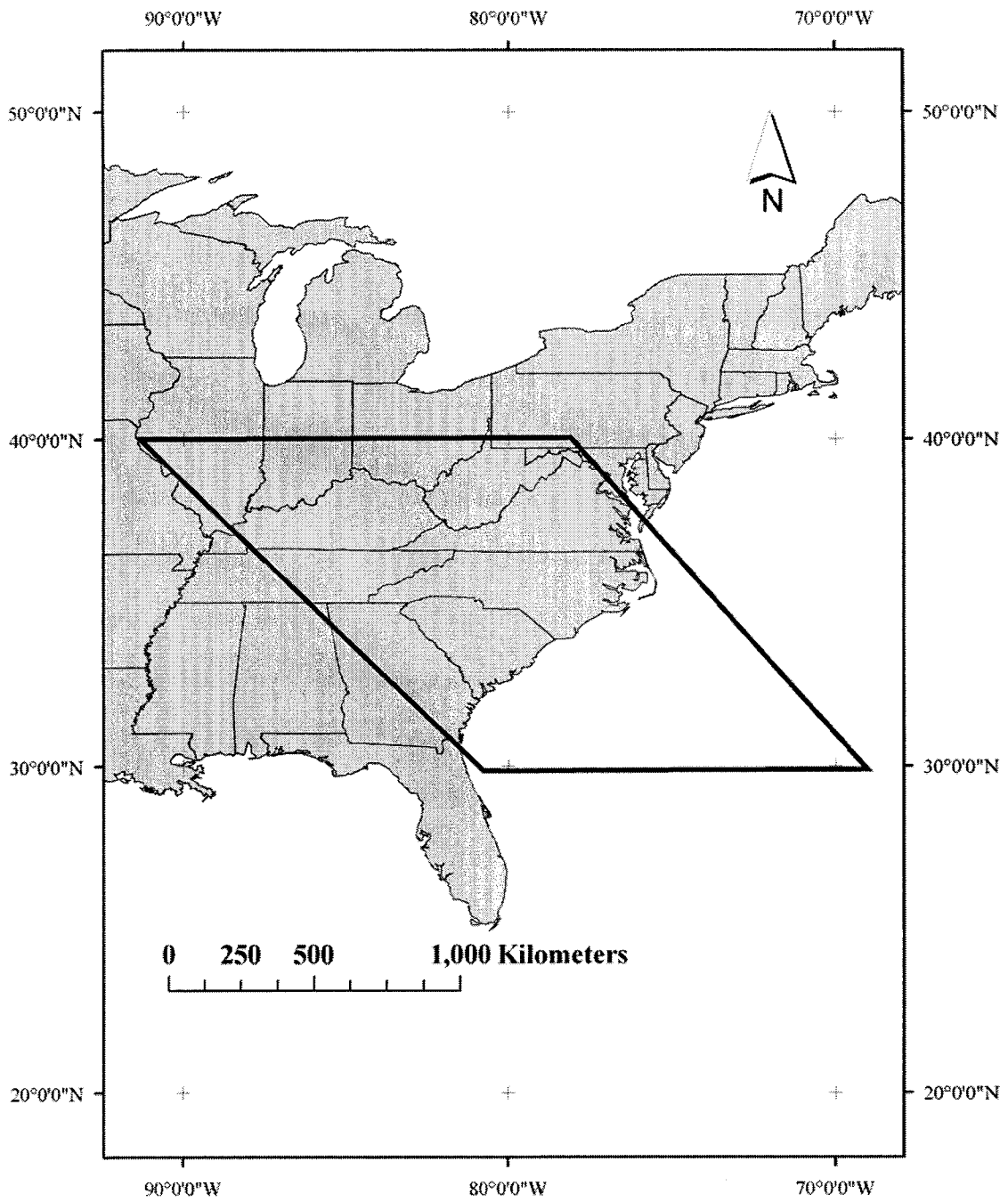


Figure 27. MODIS MOD15A2 LAI Tile (vertical 05, horizontal 11)

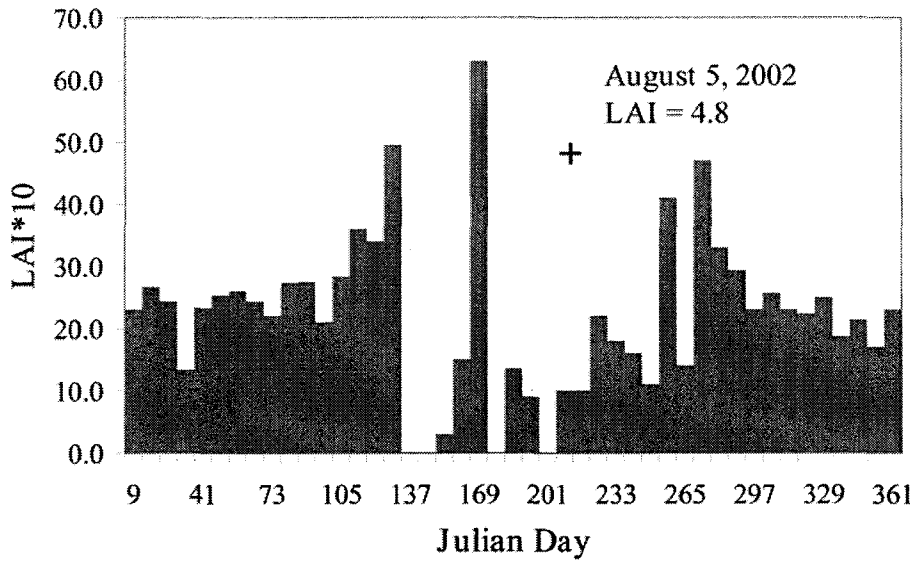


Figure 28. Three-year average of Appomattox validation site MODIS 1 km² cell.

Results

The results section is partitioned to report the results found from the three sections reviewed in the methods. These sections include results for: (1) TRAC-DHP variability, (2) land cover classification variability, and (3) RSM aggregation and comparison.

TRAC-DHP variability analysis

Variability for all four modified Beer-Lambert light extinction model input parameters for *P. taeda* is found in Table 22. The effect of atmospheric changes on Ω_E measurements showed a pattern of possible correlation. (Figure 29). High Ω_E was associated with degraded atmospheric conditions after the passing of the cold front, while lower relative humidity was associated with lower Ω_E values. However the range of Ω_E was exceptionally small ($\Omega_E = 0.02$) implying that the effect of changing atmospheric conditions was relatively insignificant (Figure 30). Results from

the regression analysis indicated that there was no significant linear trend effect with respect to time ($p = 0.96$, $t = -0.06$, $df = 1$).

Inter-operator differences measuring Ω_E were significant ($p = 0.005$, $t = 7.31$, $df = 3$). Intra-operator differences were borderline significant/insignificant ($p = 0.056$, $t = 2.11$, $df = 12$) not warranting a rejection or a non-rejection of the null hypothesis (i.e. Ω_E measured by one operator will return similar values for repeated measurements). Regarding changes in solar zenith angles, no linear trend effect was observed between the measurements of Ω_E ($p = 0.44$, $t = -0.85$, $df = 1$), however a slight decrease in Ω_E was observed with changing solar zenith angle (Figure 30).

A single factor ANOVA showed no significant differences between 10 analysts in the evaluation of 30 hemispherical images ($p = 0.99$, $F = 0.17$, $df = 9$). Regarding light regime differences in the estimation of L_e , no trend was found in the estimation of variability ($\sigma = 0.50$) through a fading light scenario.

The needle-to-shoot area ratio (γ_E) averaged 1.21 over three plots. The largest γ_E was found in the top canopy position (mean $\gamma_E = 1.62$), followed by the bottom canopy position (mean $\gamma_E = 1.05$), then the middle canopy position (mean $\gamma_E = 0.97$). The woody-to-total ratio also presented a wide range of values over three sites, varying between 0.16 and 0.40.

Table 22. *P.taeda* variability for the modified Beer-Lambert light extinction model input parameters.

Parameter	Variability Type	N	Mean	Min	Max	σ
γ_E	Between Plots	2	-	1.00	1.32	-
α	Between Plots	5	-	0.16	0.40	-
L_e	Inter-operator	10	1.16	1.02	1.26	0.076
L_e	Light Regime	5	2.54	2.16	3.29	0.503
Ω_E	Solar Zenith	6	0.94	0.87	0.97	0.041
Ω_E	Atmosphere	5	0.95	0.94	0.96	0.010
Ω_E	Inter-operator	4	0.05	-	-	0.004
Ω_E	Intra-operator	13	0.03	-	-	0.027
Ω_E	MEW	9	-	-	-	0.012

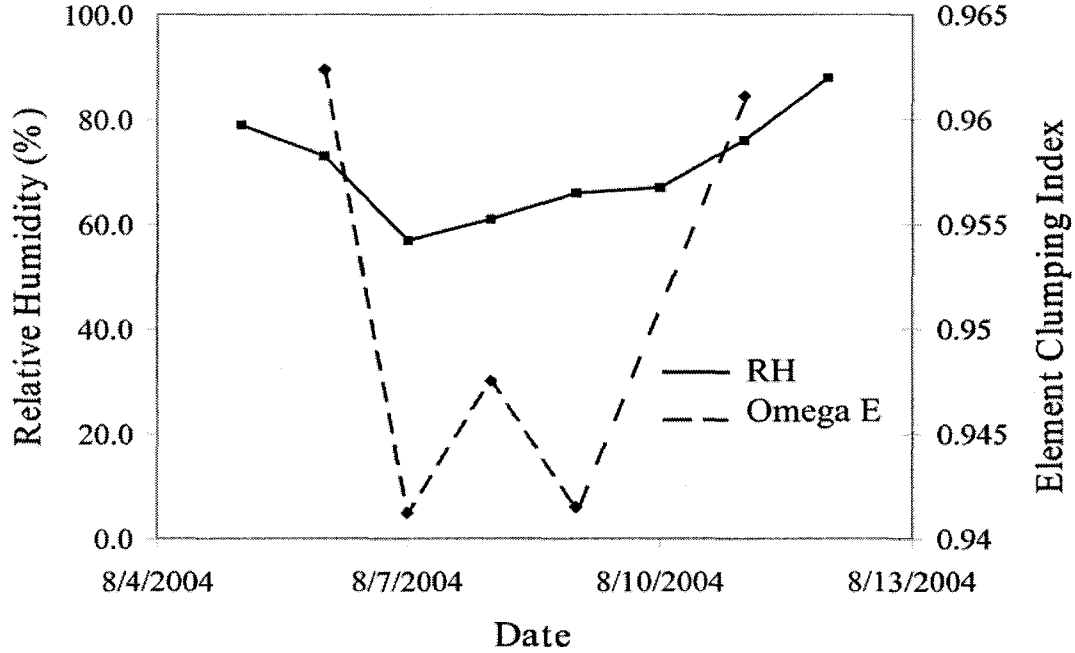


Figure 29. Atmospheric changes and the effect on measured Ω_E

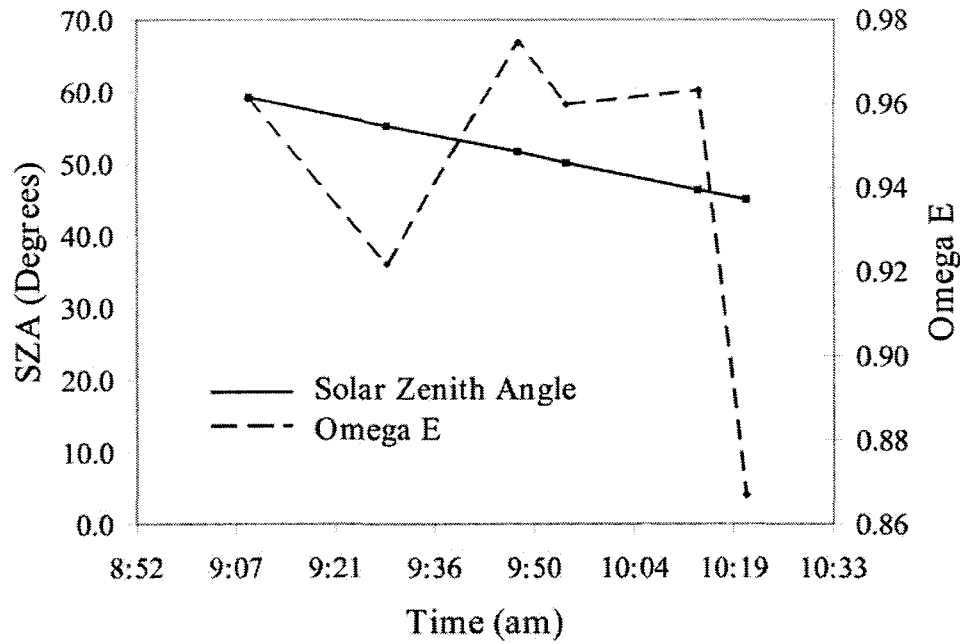


Figure 30. Effect of solar zenith angle changes on Ω_E

The *P.taeda* Monte Carlo simulation at Q1P at the Appomattox validation site applied 10000 randomly selected values of all four input parameters to calculate LAI using the modified Beer-Lambert light extinction model (Table 23). The resulting mean and standard deviation was 2.63 and 0.217 respectively.

Table 23. *P. taeda* inputs for Monte Carlo simulation at Appomattox Q1P (Units [Ω_E] - $\mu\text{mol}/\text{m}^2/\text{s}$)

Parameter	Variability Type	Min	Max
γ_E	Between Plots	1.00	1.32
α	Between Plots	0.16	0.40
L_e	NV	1.81	2.40
Ω_E	NV	0.73	0.95

Next, mean LAI values were measured *in situ* for the multiple forest classes distributed within the Appomattox validation site (Table 24). In order to synchronize land cover types delineated in the classification process, *in situ* measurements from the two coniferous *P. taeda*

stand types (thinned and unthinned) were merged to reflect the LC 2 (coniferous) class. The resulting mean value of LAI was calculated from a weighted average based on the percentage of land cover associated with each conifer type. The standard deviation was assumed the same value found for the unthinned *P. taeda* because the unthinned conifer land cover percentage was twice that of the thinned (46.2% to 27.8%). An LAI value of 0.5 was assumed in a recently harvested conifer component (LC 5 – other vegetation) with sparse vegetation regeneration. This value was chosen to reflect a LAI value lower than that found in the recently thinned conifer component (LAI = 0.83). At the time of the measurements, vegetation was sparse and less than one foot in height. TRAC and DHP measurements could not be made due to the vegetative height constraints. Finally, a mean LAI estimated for a mixed forest class (LC 3) was found by averaging measurements from both the unthinned pine and hardwood measurements.

Table 24. *In situ* LAI measurements on Appomattox validation site 2002.

Forest Class	LC Class	Mean	σ	$3*\sigma$
Hardwood	LC 1	1.89	0.3001	0.9003
Unthinned Pine	-	2.74	0.2173	0.6519
Thinned Pine	-	0.83	None	None
Pine Combined	LC 2	1.50	0.2173	0.6519
Harvested	LC 5	0.50	None	None
Mix	LC 3	2.32	0.2587	0.7761

Land Cover Classification Variability

Classification-to-Classification Comparison. Pixel-to-pixel comparisons were completed at cell resolutions greater than 150 m. Total cell-by-cell agreement between analysts decreased 9.7% from 150 m to 1200 m cell resolution (Figure 31). The highest agreement was observed in the delineation of forest from non-forest pixels between all six analysts across the eight cell resolutions. The cell agreement between deciduous and coniferous forest pixels remained stable up to 600 m then dropped 23.8% between 600 m and 900 m.

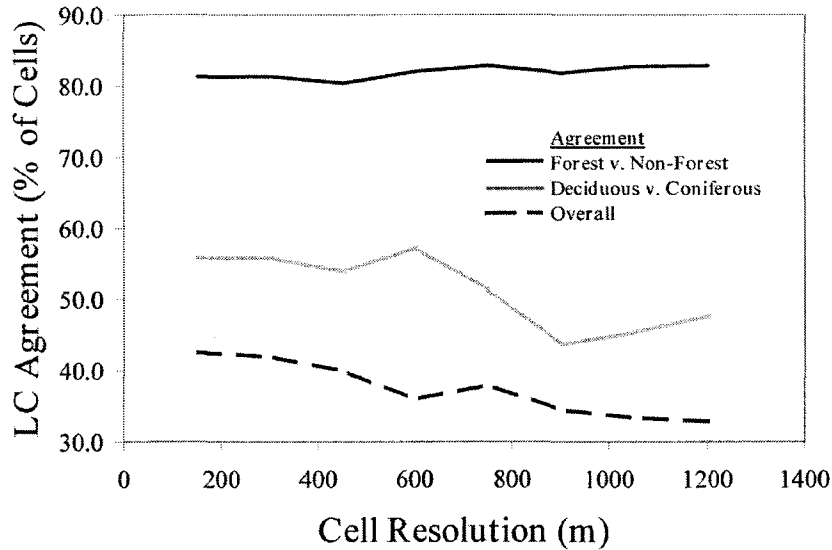


Figure 31. Land cover agreement across eight cell resolutions for six analyst-derived land cover maps.

Reference Creation and Analysis. The percent land cover remained reasonably stable across all land cover classes between 30–150 m cell resolution (Table 25, Figure 32). However, as cell resolution increased the land cover percentages changed significantly mirroring the average patch size statistics generated from the ATtILA algorithm. The transition points for each land cover class were as follows:

- LC 1 (Deciduous) 300 m: 450 m (15.6% increase)
- LC 2 (Coniferous) 450 m: 600 m (12.1% increase)
- LC 3 (Mix) 150 m: 300 m (26.5% decrease)
- LC 4 (Water) 450 m: 600m (100% decrease)
- LC 5 (OV) 450 m: 600 m (41.6% decrease)

The average patch sizes varied between 232.2 m (LC 3) and 476.7 m (LC 1) (Table 26). The significance of the average patch size for this heterogeneous area will be illustrated in the examination of the analyst-derived classifications over the same series of cell resolutions. At cell resolutions greater than 750 m only LC1, LC2, and LC 5 resulted in 100% of the land cover. At the 1250 m cell resolution the land cover percentages were evenly divided between LC 1 and LC 2. Determining the dominant land cover class for each pixel at each stage of increasing cell

resolution required analysis of the underlying 30 m pixel contributions. An analysis of pixel homogeneity assumed that the smaller the cell resolution then the greater the percent homogeneity. Pixel homogeneity is defined as the percent contribution of one land cover type (30 m cell) to a larger cell resolution of interest. Cells 100% one land cover class decreased from 54.7% with the finer resolution (150 m) cell size to 0% at the 600 m cell resolution (Figure 33). From 90 m to 600 m, the percent of cells with one class type between 75% and 99% of the total averaged 28.4%, after which this figure dropped to near-zero percent at the coarser cell resolutions (> 750 m). There was a general increase of cells having one class type at least 51% but less than 75% over decreasing cell resolution up to 750 m, then a decrease at the coarsest resolution (1050 m).

Table 25. Land cover reference data sets by cell resolution.

	Cell Resolution (m)									
	30	90	150	300	450	600	750	900	1050	1200
Cell Area (Ha)	0.09	0.81	2.25	9	20.3	36	56.3	81	110.3	144.0
# Cells	20979	2332	836	180	84	32	21	15	15	8
# Cells Analyzed	20835	2316	830	180	83	32	21	15	15	8
Reference Area (Km ²)	18.8	18.8	18.7	16.2	16.8	11.5	11.8	12.2	16.5	11.5
% LC 1 (Deciduous)	34.5	34.6	33.9	33.3	38.6	43.7	42.9	26.7	26.7	50.0
% LC 2 (Coniferous)	35.2	35.2	35.4	37.8	34.9	40.6	52.4	60.0	53.3	50.0
% LC 3 (Mix)	8.6	8.5	7.8	6.1	2.4	3.1	0	0	0	0
% LC 4 (Water)	1.2	1.1	1.3	1.1	1.2	0	0	0	0	0
% LC 5 (OV)	20.5	20.4	21.6	21.7	22.9	12.5	4.8	13.3	20.0	0

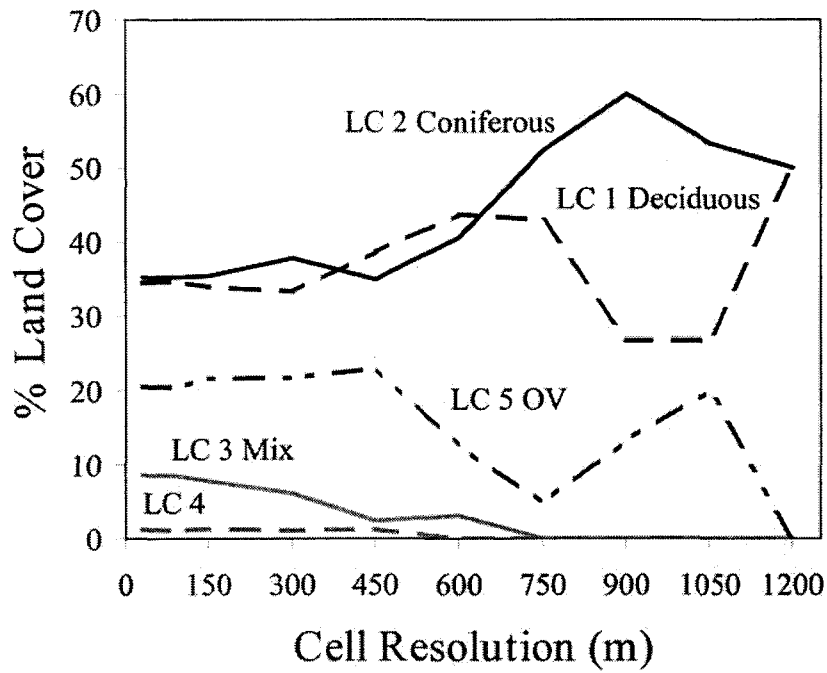


Figure 32. Reference land cover variability across ten cell resolutions.

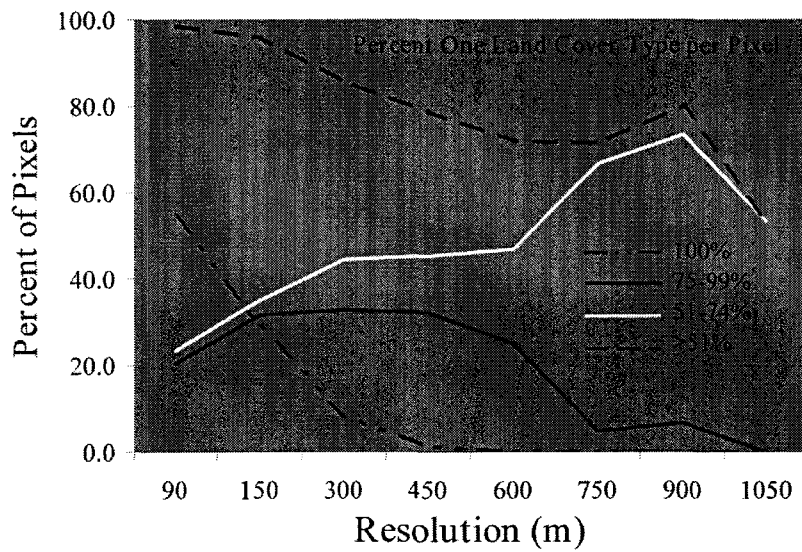


Figure 33. Reference land cover homogeneity analysis over multiple scales.

Table 26. Patch size analysis for 19.4 km² classified Ikonos 1 m (resolution) image. PLPG is the proportion of the largest patch area to the total patch area.

Parameter	All	Deciduous	Coniferous	Mix	Water	Other Veg
Largest (Ha)		241.3	202.4	41.5	21.3	59.7
Avg Size (Ha)		22.7	14.6	5.4	10.8	13.3
PLPG		36.6	30.1	24.8	98.8	14.9
Ave Patch Size (m)	364	476.7	382.6	232.4	328.6	365.2

Classification-to-Reference Comparison. A summary of overall accuracies across all cell resolutions is found in Table 27. Error matrices were developed for each analyst for the 90 m and 150 m cell resolutions. Error matrices were not developed for cell resolutions greater than 150 m due to the low reference sample number per class. Highest accuracies from four out of the six analysts were achieved at the 450 m cell resolution, within proximity of the average patch size determined to be 364 m. The range of accuracies between the six analyst-derived classifications increased from a minimum of 17.1% to a maximum of 46.7% at 900 m (Figure 34).

Table 27. Overall classification accuracy results for six analysts across 8 cell resolutions (150 m – 1200 m) as compared to 19.4 km² reference classification.

Cell Size (m)	Analyst 1	Analyst 2	Analyst 3	Analyst 4	Analyst 5	Analyst 6
1200	37.5	37.5	75.0	37.5	50.0	75.0
1050	40.0	53.3	60.0	40.0	60.0	86.7
900	20.0	66.7	46.7	33.3	53.3	66.7
750	42.9	42.9	57.1	33.3	61.9	66.7
600	46.9	65.6	68.8	43.8	59.4	75.0
450	57.8	67.9	77.1	55.4	75.9	79.5
300	57.9	64.8	69.3	50.6	65.2	73.3
150	58.0	66.0	68.3	55.1	63.8	71.7
90	59.1	62.6	67.9	54.6	63.7	71.7

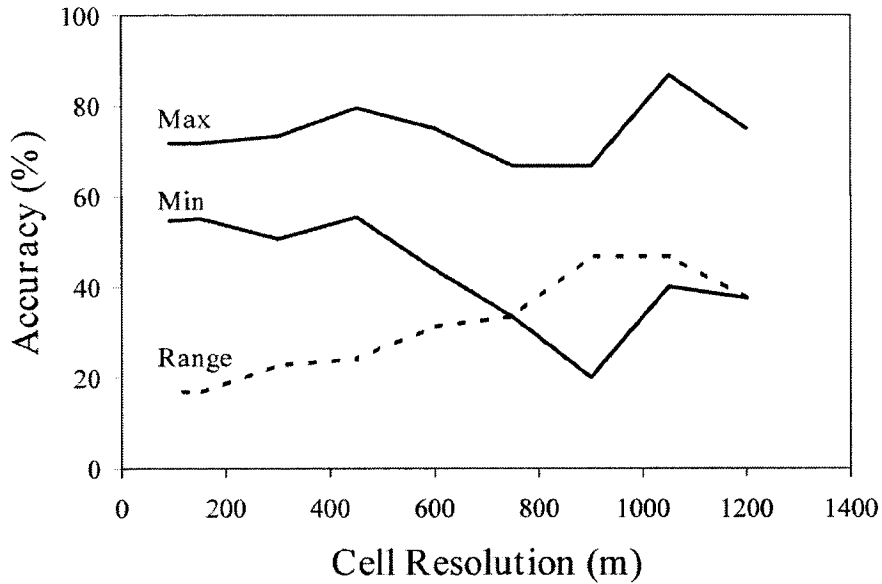


Figure 34. Percent overall agreement between six analyst-derived classifications across varying scales.

Error matrices from the 150 m assessment depicted a range of accuracies from 55.1% to 71.7% (Table 28 a,b). Across classes 1 and 2, omission errors exceeded commission errors, yet the opposite trend occurred with both error types in land cover classes 4 and 5 (Figure 35). LC class 4 (water) had an omission error of 27% with no commission error for all analysts, as would be expected (Table 28 a,b). As expected, the majority of the omission errors for all analysts occurred within the forested classes (deciduous, coniferous, or mix). The kappa analysis revealed that five out of the six analyst derived classifications displayed moderate agreement between the reference data and the classification (Landis and Koch, 1977) (Table 29). The Bonferroni adjusted t-statistic of 2.573 was used to test the 15 pair-wise comparisons of classifications for differences. Seven out of the fifteen pair-wise comparisons showed significant differences (Table 30). Analyst 1 and Analyst 4 classifications, which had the lowest overall accuracies (57.5% and 53.9% respectively), were involved in all the significant differences in the pair-wise comparisons.

Accuracy assessment analysis of the six analyst-derived classifications at the 90 m cell resolution showed insignificant differences with the 150 m matrices (Table 31 a,b) with respect to

omission and commission error and overall accuracy values (Table 32, Figure 36). The kappa analysis revealed the same levels of agreement between the reference data and the classifications as found with the 150 m analysis (Table 32). However, significant differences were found between 10 analyst pair-wise comparisons as compared to the 7 differences associated with the 150 m assessment (Table 33). Also, no significant differences were found for each analyst in a pair-wise test between classifications at 90 m and 150 m (Table 34).

Table 28a. Analyst 1-3 error matrices for 150 m cell resolution. LC = Land Cover (1 – Deciduous, 2 – Coniferous, 3 – Mix, 4 – Water, 5 – Other Vegetation).

		Reference						
		LC1	LC2	LC3	LC4	LC5	% Correct	% Commission
Analyst 1	LC1	188	4	16	1	2	89.1	10.9
	LC2	5	119	3	2	1	91.5	8.5
	LC3	80	137	40	0	59	12.7	87.3
	LC4	0	0	0	8	0	100.0	0.0
	LC5	6	22	2	0	114	79.2	20.8
	% Correct	67.4	42.2	65.6	72.7	64.8	58.0	
	% Omission	32.6	57.8	34.4	27.3	35.2		Kappa = 0.47
Analyst 2	LC1	104	1	13	0	2	86.7	13.3
	LC2	1	212	6	0	2	95.9	4.1
	LC3	136	23	36	2	4	17.9	82.1
	LC4	0	0	0	8	0	100.0	0.0
	LC5	22	52	8	1	169	67.1	32.9
	% Correct	39.5	73.6	57.1	72.7	95.5	66.0	
	% Omission	60.5	26.4	42.9	27.3	4.5		Kappa = 0.55
Analyst 3	LC1	216	19	24	2	21	76.6	23.4
	LC2	4	144	2	1	3	93.5	6.5
	LC3	35	78	29	0	1	20.3	79.7
	LC4	0	0	0	8	0	100.0	0.0
	LC5	12	46	7	0	153	70.2	29.8
	% Correct	80.9	50.2	46.8	72.7	86.0	68.3	
	% Omission	19.1	49.8	53.2	27.3	14.0		Kappa = 0.57

Table 28b. Analyst 4-6 error matrices for 150 m cell resolution. LC = Land Cover (1 – Deciduous, 2 – Coniferous, 3 – Mix, 4 – Water, 5 – Other Vegetation).

		Reference							
		LC1	LC2	LC3	LC4	LC5	% Correct	% Commission	
Analyst 4	LC1	156	35	36	1	5	67.0	33.0	
	LC2	9	107	2	1	3	87.7	12.3	
	LC3	41	61	15	1	19	10.9	89.1	
	LC4	0	0	0	8	0	100.0	0.0	
	LC5	61	72	8	0	149	51.4	48.6	
	% Correct	58.4	38.9	24.6	72.7	84.7	55.1		
	% Omission	41.6	61.1	75.4	27.3	15.3		Kappa = 0.40	
Analyst 5	LC1	202	11	43	1	5	77.1	22.9	
	LC2	6	160	7	1	1	91.4	8.6	
	LC3	50	94	9	1	36	4.7	95.3	
	LC4	0	0	0	8	0	100.0	0.0	
	LC5	5	27	4	0	135	78.9	21.1	
	% Correct	76.8	54.8	14.3	72.7	76.3	63.8		
	% Omission	23.2	45.2	85.7	27.3	23.7		Kappa = 0.52	
Analyst 6	LC1	172	6	35	0	5	78.9	21.1	
	LC2	31	237	18	1	12	79.3	20.7	
	LC3	43	3	5	2	3	8.6	91.4	
	LC4	0	0	0	8	0	100.0	0.0	
	LC5	18	43	6	0	157	70.1	29.9	
	% Correct	64.7	82.0	7.8	72.7	88.7	71.7		
	% Omission	35.3	18.0	92.2	27.3	11.3		Kappa = 0.60	

Table 29. Kappa analysis of all six analyst-derived classifications (150 m cell resolution).

Analyst	Accuracy	Kappa	Agreement
1	58.0	0.47	Moderate
2	66.0	0.55	Moderate
3	68.3	0.57	Moderate
4	55.1	0.40	Poor
5	63.8	0.52	Moderate
6	71.7	0.60	Moderate

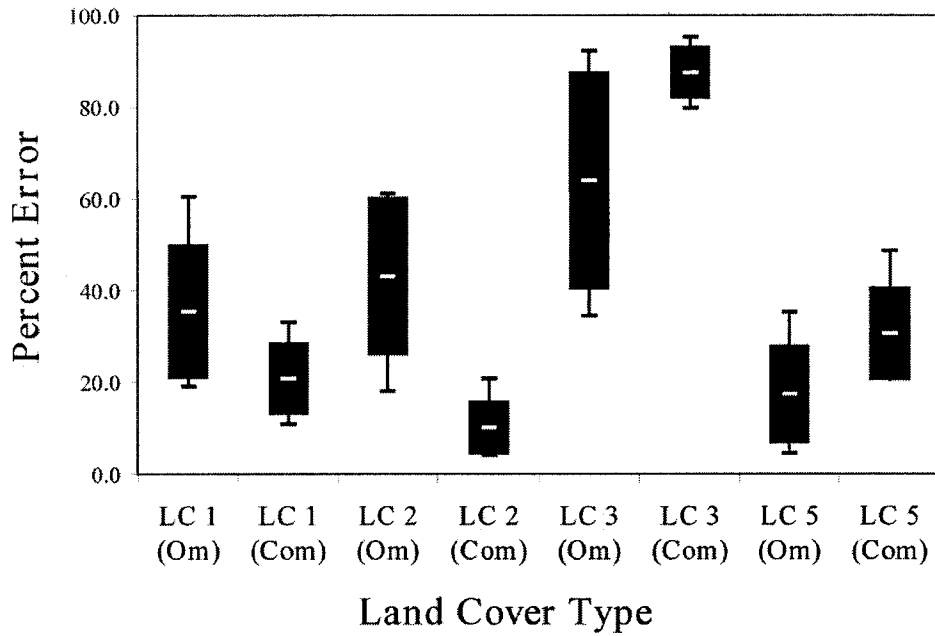


Figure 35. Omission and Commission error for all analyst derived classifications across all land cover classes at the 150 m cell resolution.

Table 30. Testing for significant differences between 15 analyst pair-wise comparisons using a Bonferonni adjusted t-value of 2.58 (150 m).

Analyst:Analyst	Z Statistic	Significant at 95%?
1:2	3.12	Yes
1:3	3.73	Yes
1:4	2.14	No
1:5	1.79	No
1:6	4.71	Yes
2:3	0.66	No
2:4	5.12	Yes
2:5	1.26	No
2:6	1.68	No
3:4	5.67	Yes
3:5	1.89	No
3:6	1.00	No
4:5	3.80	Yes
4:6	6.60	Yes
5:6	2.87	No

Table 31a. Analyst 1-3 error matrices for 90 m cell resolution. LC = Land Cover (1 – Deciduous, 2 – Coniferous, 3 – Mix, 4 – Water, 5 – Other Vegetation).

		Reference						
		LC1	LC2	LC3	LC4	LC5	% Correct	% Commission
Analyst 1	LC1	501	10	63	1	4	86.5	13.5
	LC2	12	360	10	0	6	92.8	7.2
	LC3	222	350	112	1	134	13.7	86.3
	LC4	0	0	0	21	0	100.0	0
	LC5	16	69	3	0	308	77.8	22.2
	% Correct	66.7	45.6	59.6	87.5	68.1	59.1	
	% Omission	33.3	54.4	40.4	12.5	31.9		Kappa = 0.47
Analyst 2	LC1	291	5	46	0	1	84.8	15.2
	LC2	31	531	24	0	9	89.2	10.8
	LC3	354	103	96	3	19	16.7	83.3
	LC4	0	0	0	20	0	100.0	0.0
	LC5	66	144	14	1	432	65.8	34.2
	% Correct	39.2	67.8	53.3	83.3	93.7	62.6	
	% Omission	60.8	32.2	46.7	16.7	6.3		Kappa = 0.51
Analyst 3	LC1	591	42	81	2	36	78.6	21.4
	LC2	14	391	7	1	7	93.1	6.9
	LC3	113	228	85	1	10	19.5	80.5
	LC4	0	0	0	20	0	100.0	0.0
	LC5	34	122	9	0	406	71.1	28.9
	% Correct	78.6	49.9	46.7	83.3	88.5	67.9	
	% Omission	21.4	50.1	53.3	16.7	11.5		Kappa = 0.57

Table 31b. Analyst 4-6 error matrices for 90 m cell resolution. LC = Land Cover (1 – Deciduous, 2 – Coniferous, 3 – Mix, 4 – Water, 5 – Other Vegetation).

		Reference							
		LC1	LC2	LC3	LC4	LC5	% Correct	% Commission	
Analyst 4	LC1	418	83	82	0	3	71.3	28.7	
	LC2	22	266	9	1	19	83.9	16.1	
	LC3	144	162	64	3	61	14.7	85.3	
	LC4	0	0	0	20	0	100.0	0.0	
	LC5	145	190	19	0	367	50.9	49.1	
	% Correct	57.3	37.9	36.8	83.3	81.6	54.6		
	% Omission	42.7	62.1	63.2	16.7	18.4		Kappa = 0.40	
Analyst 5	LC1	558	32	117	0	4	78.5	21.5	
	LC2	17	439	23	2	6	90.1	9.9	
	LC3	168	257	38	2	83	6.9	93.1	
	LC4	0	0	0	20	0	100.0	0.0	
	LC5	20	74	2	0	361	79.0	21.0	
	% Correct	73.1	54.7	21.1	83.3	79.5	63.7		
	% Omission	26.9	45.3	78.9	16.7	20.5		Kappa = 0.52	
Analyst 6	LC1	474	10	94	0	4	81.4	18.6	
	LC2	91	640	60	2	35	77.3	22.7	
	LC3	122	18	18	3	9	10.6	89.4	
	LC4	0	0	0	20	0	100.0	0.0	
	LC5	46	118	5	0	411	70.9	29.4	
	% Correct	64.7	81.4	10.2	80.0	89.5	71.7		
	% Omission	35.3	18.6	89.8	20.0	10.5		Kappa = 0.60	

Table 32. Kappa analysis of all six analyst-derived classifications at the 90 m cell resolution

Analyst	Accuracy	Kappa	Agreement
1	59.1	0.47	Moderate
2	62.6	0.51	Moderate
3	67.9	0.57	Moderate
4	54.6	0.40	Poor
5	63.7	0.52	Moderate
6	71.7	0.60	Moderate

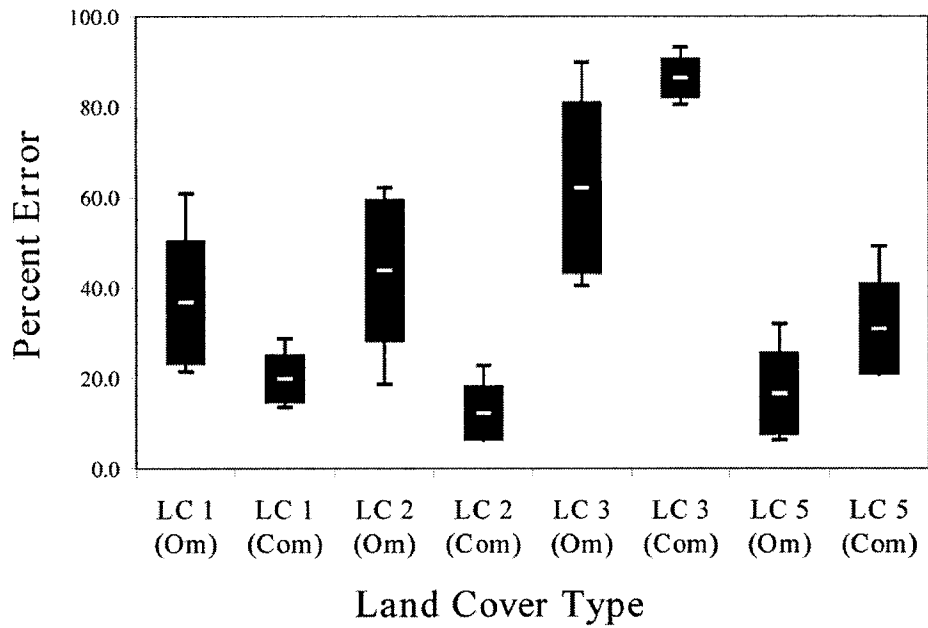


Figure 36. Omission and Commission error for all analyst derived classifications across all land cover classes at the 90 m cell resolution.

Table 33. Testing for significant differences between 15 analyst pair-wise comparisons using a Bonferonni adjusted t-value of 2.573.

Analyst:Analyst	Z Statistic	Significant at 95%?
1:2	2.05	No
1:3	5.31	Yes
1:4	4.06	Yes
1:5	2.30	No
1:6	7.09	Yes
2:3	3.26	Yes
2:4	6.01	Yes
2:5	0.27	No
2:6	5.07	Yes
3:4	9.11	Yes
3:5	2.95	Yes
3:6	1.85	No
4:5	6.21	Yes
4:6	10.78	Yes
5:6	4.74	Yes

Table 34. Testing for significant differences between 90 m and 150 m matrices per analyst using a Bonferonni adjusted t-value of 2.573.

Analyst	Z Statistic	Significant at 95%?
1	0.41	No
2	1.83	No
3	0.19	No
4	0.06	No
5	0.07	No
6	0.04	No

Training Site Assessment. Classification differences between analysts were attributed to training site selection for all five classes. The six analysts chose between 27 and 60 training sites with a minimum of 5 training sites per class (Table 35). Iterations varied between 3 and 5 for all analysts. Across all analysts, spectral pattern analysis revealed that the water and other vegetation classes were widely separated from the each other and the forested classes across all 4 bands (Figure 37). However, the forested classes (deciduous, coniferous, mix) displayed overlap and very little separation across all 4 bands. Separability tests were inconclusive in the prediction of the best classification, however, the lowest accuracy classification was identified with all three tests (Euclidean, Transformed Divergence, and Jeffries-Matusita) (Table 36-38). The percent overlap analysis did detect the top 4 classifications with a minimum overlap ranging between 4.44% and 20.42% (Table 39).

Table 35. Summary of training site data collected by six analysts.

Analyst	TS Total	TS Class 1	TS Class 2	TS Class 3	TS Class 4	TS Class 5	Iterations
1	28	5	8	5	4	6	5
2	27	5	6	6	4	6	3
3	60	12	12	12	12	12	3
4	41	8	10	6	5	12	4
5	30	5	5	5	5	5	4
6	49	5	18	4	3	19	3
Mean	39.2	6.7	9.8	9.8	5.5	10.0	3.7
Min	27	5	5	5	3	5	3
Max	60	12	18	18	12	19	5

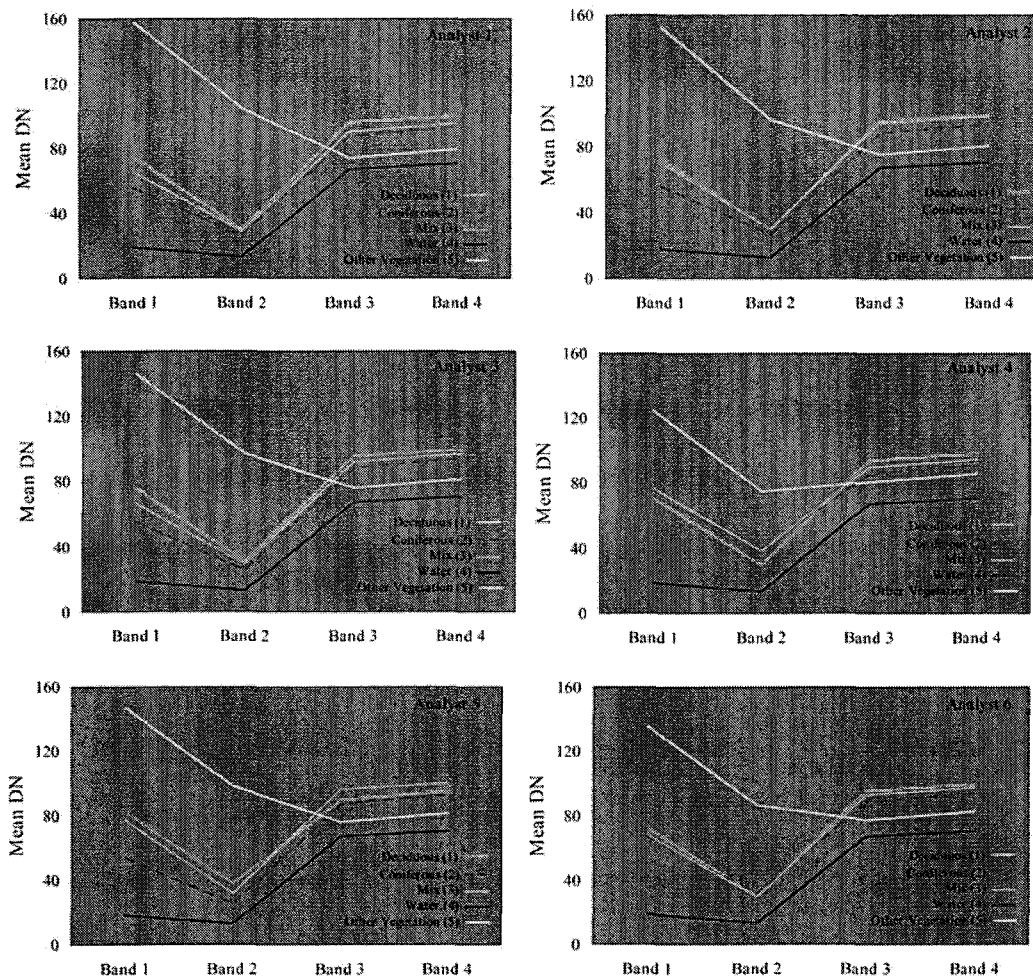


Figure 37. Spectral pattern analysis for training site data collected by six analysts.

Table 36. Training site separability analysis for six analysts employing the Euclidean Distance algorithm. Land cover codes are as follows: (1) Deciduous, (2) Coniferous, (3) Mix, (4) Water, and (5) Other Vegetation. Rank refers to the best separability (1) to the worst (5).

Analyst	Land Cover										AVE	Rank (All)	1v2v3 AVE	Rank (1v2v3)
	1v2	1v3	1v4	1v5	2v3	2v4	2v5	3v4	3v5	4v5				
1	21	12	72	120	8	51	134	60	129	172	77.9	1	13.7	1
2	20	3	70	110	21	51	125	71	108	162	74.1	2	14.7	2
3	24	10	73	103	14	49	121	63	11	157	62.5	5	16.0	5
4	10	3	64	49	9	58	47	65	46	100	45.1	6	7.3	6
5	26	12	75	103	28	49	121	74	95	157	74.0	3	22.0	3
6	15	4	70	86	11	55	96	65	89	138	62.9	4	10.0	4

Table 37. Transformed Divergence analysis for six analysts for training site data.

Analyst	Land Cover									
	1v2	1v3	1v4	1v5	2v3	2v4	2v5	3v4	3v5	4v5
1	2000	2000	2000	2000	1999	2000	2000	2000	2000	2000
2	2000	2000	2000	2000	2000	2000	2000	2000	2000	2000
3	2000	1418	2000	2000	2000	2000	2000	2000	2000	2000
4	2000	1999	2000	2000	1887	2000	1994	2000	1764	2000
5	2000	2000	2000	2000	1998	2000	2000	2000	2000	2000
6	2000	1878	2000	2000	1921	2000	2000	2000	2000	2000

Table 38. Jeffries-Matusita analysis for six analysts for training site data.

Analyst	Land Cover									
	1v2	1v3	1v4	1v5	2v3	2v4	2v5	3v4	3v5	4v5
1	1414	1346	1414	1414	1202	1414	1414	1414	1414	1414
2	1414	1183	1414	1414	1404	1414	1414	1414	1414	1414
3	1412	983	1414	1414	1299	1414	1414	1414	1414	1414
4	1327	1104	1414	1332	1163	1414	1175	1414	1414	1414
5	1413	1343	1414	1414	1404	1414	1414	1414	1414	1414
6	1386	1038	1414	1414	1139	1414	1414	1414	1414	1414

Table 39. Signature overlap (%) for six analysts for training site data.

Analyst	TM5	TM5	TM5	TM5	TM7	SQRT(4/3)	AVE	Rank
	TM7	SQRT(4/3)	tNDVI	SQRT(4/3)	tNDVI	tNDVI		
1	20.7	25.3	42.4	33.4	31.1	28.5	30.2	5
2	4.3	11.2	8.3	10.5	7.6	20.8	10.5	2
3	5.1	12.1	9.7	19.2	14.5	21.0	13.6	3
4	38.4	41.1	40.1	45.8	45.7	48.0	43.2	6
5	3.8	3.4	2.9	1.2	3.5	12.0	4.4	1
6	15.6	27.5	24.4	15.8	15.9	23.3	20.4	4

RSM aggregation and comparison

Aggregation of the 1 km² RSM resulted in a mean LAI value of 1.89. This figure was calculated by multiplying each land cover mean LAI value by the percentage of land occupied within that 1 km² area by that particular land cover class (Table 40). These contributing values were then summed to produce an overall mean LAI for that 1 km² area. To acquire the dispersion of three standard deviations about this mean LAI value (1.89), the same operation described above was completed for each of the land cover classes for the 1 km² cell (Table 41). The same aggregation process was employed on the six analyst-derived land cover classifications for the 1 km² area resulting in an estimated mean LAI (Table 42). The three standard deviations of the mean LAI values generated from the six analyst-derived classifications (0.46) was applied to the previously computed three standard deviation dispersion from the aggregated *in situ* measurements (0.48) to give a total dispersion about the mean of ± 0.93 . Thus the 1 km² RSM LAI distribution about the mean of 1.89 is 0.96-2.83 assuming three standard deviations of variability for both classifier and *in situ* uncertainty.

The MODIS MOD15A2 uncertainty was determined to be an LAI value of 0.22 ($\pm 1 \sigma$). Thus, three standard deviations equated to ± 0.67 LAI, and when distributed about the mean MODIS MOD15A2 value of 4.8 showed a spread of 4.13 to 5.47. MODIS MOD15A2 LAI, then, is approximately 2.5 times larger than the RSM LAI (Table 41). The 4.8 interpolated LAI value from this MODIS-defined savannah land cover compared reasonably well with a 3 x 3 spatial averaging of MODIS LAI cells surrounding the validation site for 2003 (MODIS mean LAI = 5.3). These cells were classified both within the coniferous and deciduous land cover classes.

Table 40. Calculation of RSM mean LAI value from contributing LC types (U – unthinned, T – thinned).

LC Type	LC%	LAI AVE (In Situ)	LC%*LAI AVE
Deciduous	19.2	1.89	36.3
Coniferous (U)	46.2	2.74	126.5
Coniferous (T)	27.8	0.83	23.0
O.V.	6.8	0.50	3.4
TOTAL			189.2
MEAN			1.89

Table 41. RSM and MODIS 1 km² LAI values with uncertainties

	RSM LAI	MODIS LAI
<i>In situ</i> TRAC-DHP (σ)	0.16	-
LC (σ)	0.15	-
MODIS (σ)	-	0.22
[<i>In situ</i> TRAC-DHP (σ)] x 3	0.48	-
[LC (σ)] x 3	0.46	-
[MODIS (σ)] x 3	-	0.67
TOTAL UNCERTAINTY	0.93	0.67
MIN	0.96	4.13
MAX	2.83	5.47
MEAN	1.89	4.80

Table 42. Classification variability between six analyst-derived classifications (LAI)

Analyst	Min	Max	Mean
1	1.16	2.58	1.87
2	0.91	2.19	1.64
3	1.02	2.38	1.78
4	0.88	1.99	1.49
5	1.01	2.43	1.79
6	0.79	2.08	1.53
SD	-	-	0.15
SD*3	-	-	0.46

Discussion

Indirect *in situ* optical estimation of LAI

Differences in the diffuse light regime had a significant effect on the ability of the analyst to choose the correct threshold for determining gap fraction in the determination of L_e . Decreasing light conditions contribute to the decreasing contrast observable between the conifer shoots and the sky. This light regime decrease could be responsible for the significantly high variability found within this parameter. Inter-analyst effects on the thresholding of the 30 images showed little difference between analysts. Therefore, the major element of determining L_e variability lies with the image quality with respect to resolution and contrast.

The element clumping index (Ω_E) was most affected by changes in the solar zenith angle. The element clumping index increased (i.e. less clumping) with increases in solar zenith angle. This result concurs with Chen and Cihlar (1995a) who found a similar increase in Ω_E with increases in solar zenith angle for boreal forests. Chen (1996) found this same pattern within *P. banksiana* and *P. mariana* and explained that conifer architecture provided the best explanation for this pattern of Ω_E change. At nadir, conifer crowns appear solid with small gaps, yet as the sun's incident radiation approaches the horizon, these small gaps break down into whorls or branches. This disintegration of the canopy architecture into subcomponents would tend to make the canopies less clumped. One other factor, the penumbra effect, may, to a lesser extent distort gap visibility by the optical instrument. At the longer angles, multiple penumbra effects mask small gaps within the canopy, ultimately affecting the gap size distribution and thus affecting the gap removal process.

The needle-to-shoot area ratio (γ_E) was by far the most difficult to measure, both in the field and in the lab. Chen (1996) found that this parameter was positively correlated with increases in needle biomass over the course of the growing season. Between five sites measured in Virginia and North Carolina the γ_E varied 24.3%. A 15-25% variation was recorded in γ_E over one growing season (Chen, 1996). The mean γ_E value of 1.21 found in this study fell within the range of γ_E

values reported in the literature for coniferous forest types. A 1.20-1.40 range was recorded for *P. banksiana* (Chen and Cihlar, 1996; Gower et al., 1999). This study only measured γ_E during one time period. It is highly probable that *P. taeda* γ_E measurements would vary significantly through the growing season due to the accretion and loss of loblolly pine needles.

The woody-to-total ratio requires analysis of multiple images and is site and age class specific. Error involved in the measuring process of this technique to acquire α was linked to the difficulty in isolating individual trees. Overlap of adjoining branches would conflate estimates of active photosynthetic area.

As previously explained, unknown interactions confounded computing total variance for both L_e and Ω_E . It is very difficult to control the different elements entering the equations due to the inherent problem of measuring natural systems. The Monte Carlo simulation mean and standard deviation results, 2.63 and 0.22 respectively, closely matched the LAI measurements taken over Q1P (mean = 2.73, σ = 0.09).

Classification differences

The range of classification differences in this study was 16.8% at the 150 m cell resolution. The effect on the overall accuracy of the RSM could be significant with respect to the distribution of misclassified land cover. For example, the lowest overall accuracy was 53.9% (Analyst 4) compared to the highest accuracy of 70.7% (Analyst 6). A significant number of pixels (35.2%) were committed by analyst 4 to the other vegetation (LC 5) category. However, the reference data set showed 21.2% attributed to this LC 5 category. Confusing any of the forested pixels (LAI 1.5-3.0), with other vegetation (LAI < 1.0) could negatively bias the resulting LAI values for MODIS comparison.

Examination of the training site information for all six analysts revealed that class confusion could be predicted using all the separability measures, however gradations of accuracy could not be determined. Also, training site confusion between classes could not be further segmented into

potential omission and commission errors. It was beneficial to utilize all separability measures for determination of the best and worst analyst-derived classification.

Aggregation and comparison

The MODIS MOD15A2 LAI Appomattox cell selected for comparison returned only one LAI value for the three year period 2001-2003. One underlying problem was the MOD12Q1 “Savannah” land cover classification attributed to that cell. This class assumes a herbaceous dominated cover, with tree cover less than 10%. The thinning operation within the 1 km² RSM reduced the conifer tree crown cover to 35-40%, but that forest type only comprised 28% of the 1 km² cell area. Adding the harvested (other vegetation) component of 7% resulted in an area approximately 35% that might be construed by the MOD12Q1 classification algorithm as “Savannah”. However, the remaining cell area (65%) comprised conifer and deciduous forest types. This brings into the discussion the difficulties of ascribing a global data set to a regional scale. As shown, this area is highly heterogeneous, with an average patch size calculated at 13.3 ha or a cell resolution of 364 m. One suggestion to offset these issues at the regional level is to produce a 500 m scale product for both the MODIS LAI and land cover products. One other issue affecting the MODIS LAI algorithm success or failure was the atmospheric conditions prevalent during the summer growing season. Moisture laden air in combination with varying amounts of cloud cover prevented retrieval of LAI values for the MODIS cells. This is evident upon examination of a 3 x 3 km MODIS cell window centered about the 1 km² MODIS Appomattox validation cell. Here, 22.5% of the LAI retrievals were calculated from the back-up empirically-based MODIS LAI algorithm incorporating NDVI (Figure 38). This trend was amplified during the growing season where 35% of the returns were NDVI-based. However, the only reason the back-up algorithm was initiated was that there was questionable red and near-infrared band spectral returns for this particular land cover class. Thus, the values retrieved from the back-up algorithm are already questionable at best.

The overall comparison between the aggregated 1 km² RSM and the MODIS MOD15A2 LAI cell showed a disagreement of 60.6%. This two-fold plus difference in the conifer domain has been noted in unpublished findings around the world. Recent developments in the collection 5 algorithm may alleviate this large discrepancy.

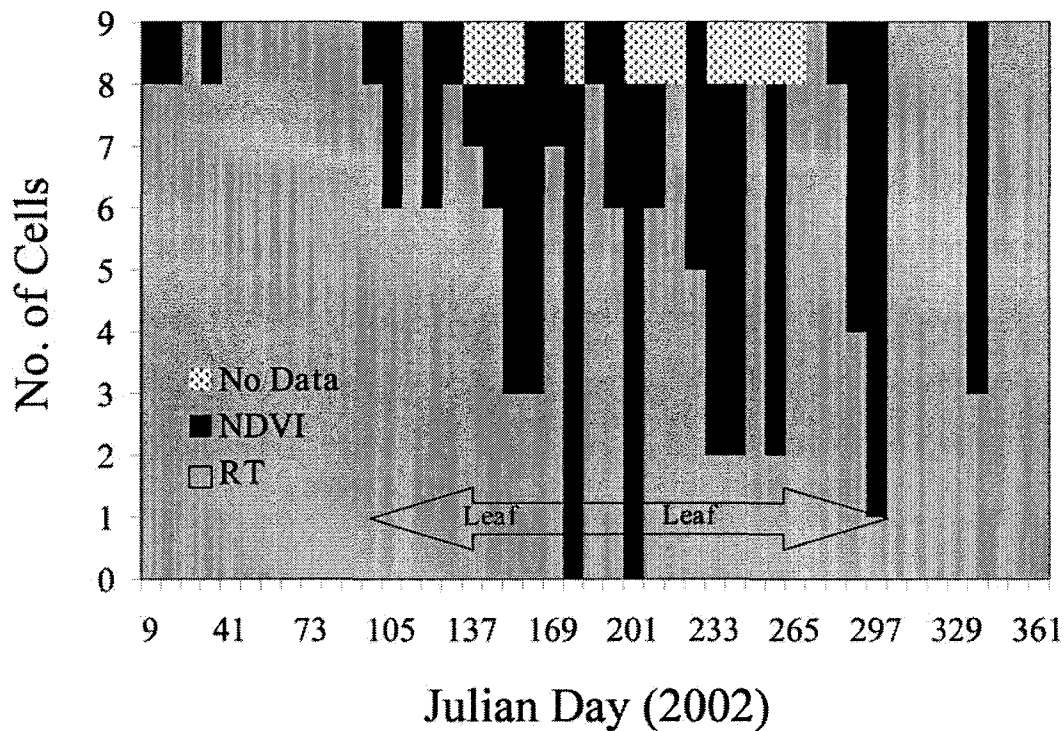


Figure 38. Primary algorithm, back-up algorithm, or failure for MODIS LAI retrieval over 3 x 3 km area (center cell = Appomattox validation site) for 2002.

Conclusions

This research attempts to parameterize *in situ* measurement variability of LAI and classification differences between analysts in the analysis of uncertainty propagation in the creation of a 1 km² RSM. The site chosen for MODIS LAI comparison was a highly

heterogeneous area, typifying the spatial land cover pattern of the southeastern United States. Results from this research indicate *in situ* measurements of *P. taeda* vary within a 0.23 unit of LAI. The mixed pixel issue within the MODIS data set may be resolved by decreasing cell size to 500 m, a resolution comparable to the average patch size found on this landscape. Future research will aim to investigate MODIS LAI returns from MODIS classified coniferous cells with similar spectral responses in the red and NIR wavelengths. Finally, the estimation of LAI from satellite-derived indices and radiative transfer modeling is limited by the spectral saturation of vegetative indices within regions of high LAI.

CHAPTER VII

FINAL CONCLUSIONS

The United States Environmental Protection Agency initiated MODIS MOD15A2 LAI validation research (2002) in the evergreen needle leaf biome, as defined in the MOD12 classification, in a regional study located in the southeastern United States. The validation effort was prompted by the potential use of MODIS LAI inputs into atmospheric deposition and biogenic emission models developed within the US EPA Office of Research and Development. The MODIS LAI validation process involves the creation of a high spatial resolution LAI surface map, which when scaled to the MOD15A2 resolution (1 km) allowed for comparison and analysis with the 1 km MODIS LAI product. Creation of this LAI surface map involved: (1) the collection of *in situ* LAI measurements via indirect optical measurements, (2) the correlation of land cover specific LAI estimates with spectral values retrieved from high resolution imagery (20 m - 30 m), and (3) the aggregation of these 30 m cells to 1 km spatial resolution, matching the resolution of the MODIS product and enabling a comparison of the two LAI values (Morisette et al., 2006). This research assessed the uncertainty associated with the creation of the high-resolution LAI reference map, specifically addressing uncertainty in the indirect *in situ* optical measurements of LAI and the uncertainty in the land cover classification process. Also addressed was the influence of vegetative understory on satellite-derived vegetation indices from the IKONOS sensor.

The TRAC-DHP integrated approach to optical LAI estimation underestimated LAI by 11% when compared to LAI estimates derived from allometric equations developed from whole-tree harvest data on one site (SETRES). In contrast, the method failed at the Brunswick site, presumably due to the lack of Brunswick-specific allometric equations and the possibility of

variable SLA measurements. Parameterization of site-specific inputs into the modified Beer-Lambert light extinction model (i.e., needle-to-shoot area ratio, γ_E and the woody-to-total area ratio, α) would further reduce the disjoint between “true” LAI and estimated LAI.

The ability to detect understory LAI from overall satellite-derived LAI was dependent on image acquisition zenith θ , crown closure, and reflective properties of the understory species. Increasing forest canopy complexity tended to further obscure the vegetative signature from the lower level canopy position. Analysis of off-nadir IKONOS NDVI following a complete understory removal detected a 4.7% reduction in LAI compared to an *in situ* estimated LAI reduction of 9.9% (Appomattox). The detection of LAI reduction at Hertford site was confounded by the optical properties of the predominant understory species, *Ilex opaca*. Only a 1.0% LAI reduction was found in the analysis of IKONOS NDVI when compared to *in situ* estimated LAI (17.6%).

The propagation of uncertainty within the multiple stages of the creation of a fine resolution LAI reference surface map (RSM) yielded an LAI distribution of 0.96-2.83, assuming three standard deviations on both side of the mean value of 1.89. The MODIS LAI distribution, i.e. three standard deviations about the mean, did not intersect the RSM distribution (4.13-5.47, mean = 4.80). This 2.5 times overestimation of LAI by the collection 4 MODIS LAI product has been recorded in other needle-leaf biomes around the world. Collection 5 is expected to correct for this large discrepancy.

The question arises whether LAI can be estimated accurately from three-dimensional radiative transfer modeling when dependence of quality LAI retrievals is based on vegetation indices that saturate at high levels of LAI. This asymptotic increase of NDVI over increasing values of LAI produces more uncertainty in the returned MODIS LAI value. *P. taeda* primarily is established on nutrient and water deficient sites, thus growth is typically sub-optimal, thereby leaf biomass never attains a maximum in a natural setting. Therefore, the NDVI-LAI relationship on the majority of *P. taeda* sites occurs within the linear portion of this correspondence. This is not

the case for deciduous forest stands where high levels of LAI are typical. Another approach to estimating forest productivity in these deciduous stands would be to integrate hyperspectral image analysis of canopy level nitrogen where it was found to be a stronger correlate with productivity than was LAI (Smith et al., 2002).

LITERATURE CITATIONS

Abbaspour, R. A., Delavar, M. R., and Batouli, R. (2003). The issue of uncertainty propagation in spatial decision making. In Proceedings of the Scandinavian Research Conference on Geographical Information Science (pp. 57-65).

Aber, J.D. and Melillo, J.M. (2001). Terrestrial Ecosystems. San Diego, Academic Press, 556 p.

Aerts, J.C.J.H., Goodchild, M.F., and Huevelink, G.B.M. (2003). Accounting for spatial uncertainty in optimization with spatial decision support systems. *Transactions in GIS*, 7, 211-230.

Albaugh, T.J., Allen, H.L., Dougherty, P.M., Kress, L.W., and King, J.S. (1998). Leaf area and above- and belowground growth responses of loblolly pine to nutrient and water additions. *For Sci*, 44, 317-328

Albaugh, T.J., Allen, H.L., Dougherty, P.M., and Johnsen, K.H. (2004). Long term growth responses of loblolly pine to optimal nutrient and water resource availability. *Forest Ecology and Management*, 192, 3-19.

Albaugh, T.J., Allen, H.L., and Kress, L.W. (2005). Root and stem partitioning of *Pinus taeda*. *Trees - Structure and Function*. Publisher: Springer-Verlag GmbH, ISSN: 0931-1890 (Paper) 1432-2285 (Online), DOI: 10.1007/s00468-005-0024-4.

Anderson, M.C. (1964). Studies of the woodland light climate. I. The photographic computation of light conditions. *Journal of Ecology*, 52, 27-41.

Asner, G.P., Scurlock, J.M.O. and Hicke, J.A. (2003). Global synthesis of leaf area index observations: implications for ecological and remote sensing studies. *Global Ecology and Biogeography*, 12, 191-205.

Avery, T. E. and Burkhart, H. (1993). Forest Measurements. New York, McGraw Hill Text. 331 p.

Badhwar, G.D., MacDonald, R.B., Hall, F.G., and Carnes, J.G. (1986). Spectral characterization of biophysical characteristics in a boreal forest: relationship between Thematic Mapper band reflectance and leaf area index for aspen. *IEEE Transactions on Geoscience and Remote Sensing*, GE-24, 322-326.

Barclay, H.J. (1998). Conversion of total leaf area to projected leaf area in lodgepole pine and Douglas-fir. *Tree Physiology*, 18, 185-193.

Baret, F. and Guyot, G. (1991). Potentials and limits of vegetation indices for LAI and APAR assessment (absorbed photosynthetically active radiation). *Remote Sensing of Environment*, 35, 161-173.

- Becker, M. (1971). Une technique nouvelle d'utilisation des photographies hémisphériques pour la mesure du climat lumineux en forêt. *Annales des Sciences Forestières*, 28, 425-442.
- Beer, A. (1853). *Einleitung in die höhere Optik*. Braunschweig. Vieweg und Sohn, 430p.
- Bishop, Y., Fienberg, S., and Holland, P. (1975). *Discrete Multivariate Analysis: Theory and Practice*. MIT Press, Cambridge, Ma.
- Bonhomme, R. (1970). Application de la technique des photographies hémisphériques in situ à la mesure de l'indice foliaire. In: *Techniques d'étude des facteurs physiques de la biosphère*, Paris: INRA, 501-505.
- Bonhomme, R., Varlet-Grancher, C., and Chartier, M. (1974). The use of hemispherical photographs for determining the leaf area index of young crops. *Photosynthetica*, 8, 299-301.
- Bonhomme, R. (1983). The solar radiation: characterization and distribution in the canopy, In: Varlet-Grancher C, Bonhomme R, Sinoquet H, eds. *Crop structure and light microclimate: characterization and applications*. Sciences Update. Paris: INRA Editions, 17-28.
- Bouman, B.A. (1992). Accuracy of estimating the leaf area index from vegetative indices derived from crop reflectance characteristics, a simulation study. *International Journal of Remote Sensing*, 13, 3069-3084.
- Brown, L., Chen, J.M., Leblanc, S.G. and Cihlar, J. (2002). A shortwave infrared modification to the simple ratio for LAI retrieval in boreal forests: An image and model analysis. *Remote Sensing of Environment*, 71, 16-25.
- Buckley, D.S. (1999). Practical field methods of estimating canopy cover, PAR, and LAI in Michigan oak and pine stands. *Northern Journal of Applied Forestry*, 16, 25-32.
- Carlson, T.N. and Ripley, D.A. (1997). On the relation between NDVI, fractional vegetation cover, and leaf area index. *Remote Sensing of Environment*, 62, 241-252.
- Chason, J.W., Baldocchi, D.D., and Huston, M.A. (1991). A comparison of direct and indirect methods for estimating forest canopy leaf area. *Agricultural and Forest Meteorology*, 57, 107-128.
- Chen, J.M. and Black, T.A. (1992a). Foliage area and architecture of plant canopies from sunfleck size distributions. *Agric. For. Meteorol.*, 60, 249-266
- Chen, J.M. and Black, T.A. (1992b). Defining leaf area index for non-flat leaves. *Plant Cell Environ.*, 15, 421-429.
- Chen, J.M., and Cihlar, J. (1995a). Quantifying the effect of canopy architecture on optical measurements of leaf area index using two gap size analysis methods. *IEEE Transactions on Geoscience and Remote Sensing*, 33, 777-787.
- Chen, J.M., and Cihlar, J. (1995b). Plant canopy gap-size analysis theory for improving optical measurements of leaf-area index. *Applied Optics*, 34, 6211-6222.
- Chen, J.M. (1996). Optically-based methods for measuring seasonal variation of leaf area index in boreal conifer stands. *Agricultural and Forest Meteorology*, 80, 135-163.

- Chen, J.M. and Cihlar, J. (1996). Retrieving leaf area index of boreal conifer forests using Landsat TM images. *Remote Sensing of Environment*, 55, 153-162.
- Chen, J.M., Rich, P.M., Gower, S.T., Norman, J.M., and Plummer, S. (1997). Leaf area index of boreal forests: Theory, techniques, and measurements. *Journal of Geophysical Research*, 102, 429-443.
- Cohen, J. (1960). Weighted kappa: Nominal scale agreement with provision for scaled disagreement or partial credit. *Psychological Bulletin*, 70, 213-220.
- Cohen, W.B., Spies, T.A., and Bradshaw, G.A. (1990). Semivariograms of digital imagery for analysis of conifer canopy structure. *Remote Sensing of Environment*, 34, 167-178.
- Cohen, W.B. and Spies, T.A. (1992). Estimating structural attributes of Douglas-fir/western hemlock forest stands from Landsat and SPOT imagery. *Remote Sensing of Environment*, 4, 1-17.
- Colbert, S.R., Jokela, E.J., and Neary, D.G. (1990). Effects of annual fertilization and sustained weed control on dry matter partitioning, leaf area and growth efficiency of juvenile loblolly and slash pine. *Forest Science*, 36, 995-1014.
- Congalton, R., and Green, K. (1999). Assessing the accuracy of remotely sensed data: Principles and Practices. CRC Press, Boca Raton, FL., pp. 137.
- Congalton, R.G., Oderwald, R.G., and Mead, R.A. (1983). Assessing Landsat classification accuracy using discrete multivariate-analysis statistical techniques. *Photogrammetric Engineering and Remote Sensing*, 49, 1671-1678.
- Cutini, A., Matteucci, G, and Mugnozza, G.S. (1998). Estimation of leaf area index with the Li-Cor LAI 2000 in deciduous forests. *Forest Ecology and Management*, 105, 55-65.
- Danson, F.M. and Curran, P.J. (1993). Factors affecting the remotely sensed response of coniferous forest plantations. *Remote Sensing of Environment*, 43, 55-65.
- Deblonde, G., Penner, M., and Royer, A. (1994). Measuring leaf area index with the LI-COR LAI-2000 in pine stands. *Ecology*, 75, 1507-1511.
- Dougherty, P.M., Hennessey, T.C., Zarnoch, S.J., Stenberg, P.T., Holeman, R.T., and Wittwer, R.F. (1995). Effects of stand development and weather on monthly leaf biomass dynamics of a loblolly pine (*Pinus taeda* L.) stand. *For. Ecol. Manage.*, 72, 213-227.
- Dougherty, P.M., Allen, L.H., Kress, L.W., Murthy, R., Maier, C.A., Albaugh, T.J., and Sampson, D.A. (1998). An investigation of the impacts of elevated carbon dioxide, irrigation, and fertilization on the physiology and growth of loblolly pine. In *The Productivity and Sustainability of Southern Forest Ecosystems in a Changing Environment*. Eds. R.A. Mickler and S. Fox. Springer-Verlag, Berlin, pp 149-168.
- Ducrey, M. (1975). Utilization des photographies hémisphériques pour le calcul de la perméabilité des couverts forestiers au rayonnement solaire. I. Analyse technique de l'interception. *Annales des Sciences Forestières*, 32, 73-92.

Elvidge, C.D., Yuan, D., Weerackoon, R.D., and Lunetta, R. (1995). Relative radiometric normalization of Landsat Multispectral Scanner (MSS) data using an automatic scattergram-controlled regression. *Photogrammetric Engineering and Remote Sensing*, 61, 1255-1260.

ERDAS Field Guide fourth edition (1997) 656 p. Atlanta, Ga.

Evans, R. (1989). Photosynthesis and nitrogen relationships in leaves of C3 plants. *Oecologia*, 7, 9-19.

Fassnacht, K.S., Gower, S.T., Norman, J.M., and McMurtrie, R.E. (1994). A comparison of optical and direct methods for estimating foliage surface area index in forests. *Agricultural and Forest Meteorology*, 71, 183-207.

Fassnacht, K.S. and Gower, S.T. (1997). Interrelationships among the edaphic and stand characteristics, leaf area index, and aboveground net primary production of upland forest ecosystems in north central Wisconsin. *Canadian Journal of Forest Research*, 27, 1058-1067.

Field, C., and Mooney, H.A. (1986). The photosynthesis-nitrogen relationship in wild plants. In *On the economy of plant form and function*. Edited by T.J. Givnish. Cambridge University Press, Cambridge, 25-55.

Flores, F. (2003). Using remote sensing data to estimate leaf area index and foliar nitrogen of loblolly pine plantations. PhD dissertation, North Carolina State University, Raleigh, North Carolina, 115 p.

Foody, G.M. (2000). Estimation of sub-pixel land cover composition in the presence of untrained classes. *Computers and Geosciences*, 26, 469-478.

Fournier, R.A., Mailly, Walter, J.N., and Soudani, K. (2003). Indirect measurement of forest canopy structure from in situ optical sensors. In: *Remote sensing of forest environments: concepts and case studies*, Chapter 4, pp 77-113 (Wulder, M.A. and S.E. Franklin editors).

Franklin, J. (1986). Thematic Mapper analysis of coniferous forest structure and composition. *International Journal of Remote Sensing*, 7, 1287-1301.

Franklin, S.E., Lavigne, M.B., Deuling, M.J., Wulder, M.A., and Hunt, E.R. (1997). Estimation of forest leaf area index using remote sensing and GIS for modelling net primary production. *International Journal of Remote Sensing*, 18, 3459-3471.

Gates, D.M., Keegan, J.J., Schleiter, J.C., and Weidner, V.R. (1965). Spectral property of plants, *Applied Optics*, 4, 11-20.

Gausmann, H.W., Allen, W.A., and Cardenas, R. (1969). Reflectance of cotton leaves and their structure. *Remote Sensing of Environment*, 1, 110-122.

Geron, C.D., Guenther, A.B., and Pierce, T.E. (1994). An improved model for estimating emissions of volatile organic-compounds from forests in the eastern United-States. *Journal of Geophysical Research-Atmospheres*, 99, 12773-12791

- Gholz, H.L., Fritz, F.K., and Waring, R.H. (1976). Leaf area differences associated with old growth forest communities in western Oregon Cascades. *Canadian Journal of Forest Research*, 6, 49-57.
- Gholz, H.L. (1982). Environmental limits on above-ground net primary production, leaf-area, and biomass in vegetation zones of the Pacific Northwest. *Ecology*, 63, 469-481.
- Gitelson, A.A. (2004). Wide dynamic range vegetation index for remote quantification of biophysical characteristics of vegetation. *Journal of Plant Physiology*, 161, 165-173.
- Gough, C., Seiler, J.R., Johnsen, K.H., and Sampson, D.A. (2004). Seasonal Photosynthesis in Fertilized and Nonfertilized Loblolly Pine. *Forest Science*, 50, 1-9.
- Gower, S.T., and Norman, J.M. (1991). Rapid estimation of leaf-area index in conifer and broad-leaf plantations. *Ecology*, 72, 1896-1900.
- Gower, S.T., Kucharik, C.J., and Norman, J.M. (1999). Direct and indirect estimation of leaf area index, fAPAR, and net primary production of terrestrial ecosystems. *Remote Sensing of Environment*, 70, 29-51.
- Gower, S.T., Vogel, J.G., Norman, J.M., Kucharik, C.J., Steele, S.J., and Stow, T.K. (1997). Carbon distribution and aboveground net primary production for aspen, jack pine, and black spruce stands in Saskatchewan and Manitoba, Canada. *Journal of Geophysical Research*, 103, 29 029-29 041.
- Gower, S.T., Vogt, K.A., and Grier, C.C. (1992). Carbon dynamics of Rocky-Mountain Douglas-Fir - Influence of water and nutrient availability. *Ecological Monographs*, 62, 43-65.
- Gregoire, T.G., Valentine, H.T., and Furnival, G.M. (1995). Sampling methods to estimate foliage and other characteristics of individual trees. *Ecology*, 76, 1181-1194.
- Grier, C.C., Lee, K.M., and Archibald, R.M. (1984). Effect of urea fertilization on allometric relations in young Douglas-fir trees. *Canadian Journal of Forest Research*, 14, 900-904.
- Hall, R.J., Davidson, D.P., and Peddle, D.R. (2003). Ground and remote estimation of leaf area index in Rocky Mountain forest stands, Kananaskis, Alberta. *Canadian Journal of Remote Sensing*, 29, 411-427.
- Hennessey, T.C., Dougherty, P.M., Cregg, B.M., and Wittwer, R.F. (1992). Annual variation in needlefall of a loblolly pine stand in relation to climate and stand density. *Forest Ecological Management*, 51, 329-338.
- Herbert, M.T., and Jack, S.B. (1998). Leaf area index and site water balance of loblolly pine (*Pinus taeda* L.) across a precipitation gradient in East Texas. *For. Ecol Manage.*, 105, 273-282.
- Huang, D., Yang, W., Tan, B., Rautiainen, Zhang, P., Hu, J., Shabanov, N., Linder, S., Knyazikhin, Y., and Myneni, R.B. (2006). The importance of measurement error for deriving accurate reference leaf area index maps and validation of the MODIS LAI product. *IEEE Transactions on Geoscience and Remote Sensing* (In press).

Huemmrich, K.F. and Goward, S.N. (1997). Vegetation canopy PAR absorbance and NDVI: and assessment for ten tree species with the SAIL model. *Remote Sensing of Environment*, 61, 254-269.

Huemmrich, K.F., Privette, J.L., Mukelabai, M., Myneni, R.B., and Knyazikhin, Y. (2005). Time-Series Validation of MODIS Land Biophysical Products in a Kalahari Woodland, Africa. *International Journal of Remote Sensing*, accepted.

Huete, A.R. (1988). A soil-adjusted vegetation index. *Remote Sensing of Environment*, 25, 295-309.

Huevelink, G.B.M. (1998). Geographic Information Technologies in Society, NCGIA Core Curriculum GIScience, <http://www.ncgia.ucsb.edu/giscc/units/u098/u098.html>, posted February 05, 1998.

Hunter, G.J., and Goodchild, M.F. (1997). Modelling the uncertainty of slope and aspect estimates derived from spatial databases. *Geographical Analysis*, 29, 35-49

Hurlbert, S.H., (1984). Pseudoreplication and the design of ecological field experiments. *Ecological Monographs*, 54, 187-211.

Jensen, J.R. (2000). *Remote sensing of the environment: An earth resource perspective*. Upper Saddle River, NJ, Prentice-Hall. 544 p.

Johnsen, K.H., Wear, D., Oren, R., Teskey, R.O., Sanchez, F., Will, R., Butnor, J., Markewicz, D., Richter, D., Rials, T., Allen, H.L., Seiler, J., Ellsworth, D., Maier, C., Samuelson, L., Katul, G., and Dougherty, P. (2001). Meeting global policy commitments: Carbon sequestration and southern pine forests. *Journal of Forestry*, 99, 14-21.

Jonckheere, I., Fleck, S., Nackaerts, K., Muys, B., Coppin, P., Weiss, M., and Baret, F. (2004). Review of methods for in situ leaf area index determination - Part I. Theories, sensors and hemispherical photography. *Agricultural and Forest Meteorology*, 121, 19-35.

Jonckheere, I., Muys, B., and Coppin, P. (2005). Allometry and evaluation of in situ optical LAI determination in Scots pine: a case study in Belgium. *Tree Physiology*, 25, 723-732

Jones, H.G. (1992). *Plants and microclimate*. 2nd edn. Cambridge: Cambridge University Press.

Knyazikhin, Y., Martonchik, J.V., Diner, D.J., Myneni, R.B., Verstraete, M.M., Pinty, B., and Gobron, N. (1998). Estimation of vegetation canopy leaf area index and fraction of absorbed photosynthetically active radiation from atmosphere-corrected MISR data. *J. Geophys. Res.*, 103: 32239-32256.

Kucharik, C. J., Norman J.M., and Gower, S.T. (1998). Measurements of branch area and adjusting leaf area index indirect measurements. *Agricultural and Forest Meteorology*, 91, 69-88.

Lambers, H., and Poorter, H. (1992). Inherent variation in growth rate between higher plants: A search for physiological causes and ecological consequences. *Adv. Ecolog. Res.*, 23 187-261

Landis, J., and Koch, G. (1977). The measurement of observer agreement for categorical data. *Biometrics*, 33, 159-174.

- Landsberg, J.J. and Gower, S.T. (1997). Applications of Physiological Ecology to Forest Management. San Diego, Academic, 354 p.
- Law, B.E., Van Tuyl, S., Cescatti, A., and Baldocchi, D.D. (2001). Estimation of leaf area index in open-canopy ponderosa pine forests at different successional stages and management regimes in Oregon. *Agricultural and Forest Meteorology*, 108, 1-14.
- Le Dantec, V., Dufrene, E., and Saugier, B. (2000). Interannual and spatial variation in maximum leaf area index of temperate deciduous stands. *For. Ecol. Manage.*, 134, 71-81.
- Leblanc, S.G. (2002). Correction to the plant canopy gap size analysis theory used by the Tracing Radiation and Architecture of Canopies (TRAC) instrument. *Applied Optics*, 41, 7667-7670.
- Leblanc, S.G., Chen, J.M., and Kwong, M. (2002). Tracing radiation and architecture of canopies. TRAC Manual. Version 2.1.3. Natural Resources Canada, Canada Centre for Remote Sensing, Ottawa ON, Canada, 25 p.
- Leblanc, S.G. and Fournier, R.A. (2005). Towards a better understanding of in-situ canopy measurements used in the derivation and validation of remote sensing leaf area index products. International Symposium of Remote Sensing of Environment, Saint Petersburg, Russia. Proceedings Paper, 4 pp.
- Leblon, B., Gallant, L., and Grandberg, H. (1996). Effects of shadowing types on ground-measured visible and nearinfrared shadow reflectances. *Remote Sensing of Environment*, 58, 322-328.
- Maier, C.A., Johnsen, K.H., Butnor, J., Kress, L.W., and Anderson, P.H. (2002). Branch growth and gas exchange in 13-year-old loblolly pine (*Pinus taeda*) trees in response to elevated carbon dioxide concentration and fertilization. *Tree Physiology*, 22, 1093-1106.
- McDonald A.J., Gemmill, F.M., and Lewis, P.E. (1998). Investigation of the utility of spectral vegetation indices for determining information on coniferous forests. *Remote Sensing of Environment*, 66, 250-272.
- Mencuccini, M. and Grace, J. (1995). Climate influences the leaf -area sapwood area ratio in Scots pine. *Tree Physiology*, 15, 1-10.
- Morisette, J.T., Nickeson, J.E., Davis, P., Wang, Y.J., Tian, Y.H., Woodcock, C.E., Shabanov, N., Hansen, M., Cohen, W.B., Oetter, D.R., and Kennedy, R.E. (2003). High spatial resolution satellite observations for validation of MODIS land products: IKONOS observations acquired under the NASA Scientific Data Purchase. *Remote Sensing of Environment*, 88, 100-110.
- Morisette, J.T., Baret, F., Privette, J.L., Myneni, R.B., Nickeson, J., Garrigues, S., Shabanov, N., Weiss, M., Fernandes, R., Leblanc, S., Kalacska, M., Sánchez-Azofeifa, G., Chubey, Rivard, M.B., Stenberg, P., Rautiainen, M., Voipio, P., Manninen, T., Pilant, A., Lewis, T., Iames, J., Colombo, R., Meroni, M., Busetto, L., Cohen, W., Turner, D., Warner, E., Petersen, G.W., Seufert, G., and Cook, R. (2006). Validation of global moderate-resolution LAI Products: a framework proposed within the CEOS Land Product Validation subgroup. *IEEE Transactions of Geoscience and Remote Sensing*, (In Press).

Murthy, R. and Dougherty, P.M. (1997). Effect of carbon dioxide, fertilization and irrigation on loblolly pine branch morphology. *Trees* 11,485–493.

Myers, V. I. (1970). Soil, water, and plant relations. *Remote sensing with Special Reference to Agriculture and Forestry*, National Academy of Sciences, Washington, D.C., 253-297.

Myneni, R., Knyazikhin, Glassy, J., Votava, P., and N. Shabanov (2003). User's Guide FPAR, LAI (ESDT: MOD15A2) 8-day Composite NASA MODIS Land Algorithm.

Nemani, R., Pierce, L., and Running, S. (1993). Forest ecosystem processes at the watershed scale: Sensitivity to remotely sensed leaf area index estimates. *International Journal of Remote Sensing*, 14, 2519-2534.

Neumann, H.H., Den Hartog, G., and Shaw, R.H. (1989). Leaf area measurements based on hemispheric photographs and a leaf-litter collection in a deciduous forest during autumn leaf-fall. *Agricultural and Forest Meteorology*, 45, 325-345.

Nilson, T. (1971). A theoretical analysis of the frequency of gaps in plant stands. *Agricultural Meteorology*, 8, 25-38.

Pearson, J.A., Fahey, T.J., and Knight, D.H. (1984). Biomass and leaf area in contrasting lodgepole pine forests. *Canadian Journal of Forest Research*, 14, 259-265.

Peterson, D.L., Spanner, M.A., Running, S.W., and Teuber, K.B. (1987). Relationship of Thematic Mapper Simulator data of leaf area index of temperate coniferous forests. *Remote Sensing of Environment*, 22, 323-341.

Peterson, D.L., and Running, S.W. (1989). Applications in forest science and management. *Theory and Application of Optical Remote Sensing*, G. Asrar. New York, Wiley, 429-473 p.

Pierce, L.L., and Running, S.W. (1988). Rapid estimation of coniferous leaf-area index using a portable integrating radiometer. *Ecology*, 69, 1762-1767.

Qi, J., Chehbouni, A., Huete, A.R., Kerr, Y.H., and Sorooshian, S. (1994). A modified soil adjusted vegetation index. *Remote Sensing of Environment*, 48, 119-126.

Rautiainen, M. and P. Stenberg (2005). Application of photon recollision probability in coniferous canopy reflectance simulations. *Remote Sensing of Environment*, 96, 98 – 107.

Reich, P.B., Koike, T., Gower, S.T., and Schoettle, A.W. (1995). Causes and consequences of variation in conifer leaf life-span. *Ecophysiology of Conifers*, W.K. Smith, and T.M. Hinkley. San Diego, Academic, 225-254 p.

Rich, P.M. (1990). Characterizing plant canopies with hemispherical photographs. *Remote Sensing Reviews*, 5, 13-29.

Richards, J. A. (1986). *Remote Sensing Digital Image Analysis: An Introduction*, Springer-Verlag, Berlin.

Ringold, P.L., Sickie, J.V., Rasar, K., and Schacher, J. (2003). Use of hemispherical imagery for estimating stream solar exposure. *Journal of the American Water Resources Association*, 39, 1373-1384.

- Rondeaux, G., Steven, M., and Baret, F. (1996). Optimization of soil-adjusted vegetation indices. *Remote Sensing of Environment*, 55, 95-107.
- Roxburgh, J.R. and Kelly, D. (1995). Uses and limitations of hemispherical photography for estimating forest light environments. *New Zealand Journal of Ecology*, 19, 213-217
- Running, S.W. and Coughlan, J.C. (1988). A general-model of forest ecosystem processes for regional applications. 1. Hydrologic balance, canopy gas-exchange and primary production processes. *Ecological Modelling*, 42, 125-154.
- Running, S.W., Peterson, D.L., Spanner, M.A., and Teuber, K.B. (1986). Remote-sensing of coniferous forest leaf-area. *Ecology*, 67, 273-276.
- Sampson, D.A., Albaugh, T.J., Johnsen, K.H., Allen, H.L. and Zarnoch, S.J. (2003). Monthly leaf area index estimates from point-in-time measurements and needle phenology for *Pinus taeda*. *Can. J. For. Res.*, 33, 2477-2490.
- Sampson, D.A., and Allen, H.L. (1995). Direct and indirect estimates of leaf area index (LAI) for lodgepole and loblolly pine stands. *Trees*, 9, 119-122.
- Schultz, R.P. (1997). Loblolly pine: the ecology and culture of loblolly pine (*Pinus taeda* L.). Washington, D.C., U.S. Department of Agriculture, Forest Service, 493 p.
- Shabanov, N.V., Knyazikhin, Y., Baret, F., and Myneni, R.B. (2000). Stochastic modeling of radiation regime in discontinuous vegetation canopies. *Remote Sensing of Environment*, 74, 125-144.
- Smith, M.L., Ollinger, S.V., Martin, M.E., Aber, J.D., Hallett, R.A., and Goodale, C.L. (2002). Direct estimation of aboveground forest productivity through hyperspectral remote sensing of canopy nitrogen. *Ecological Applications*, 12, 1286-1302.
- Smith, N.J., Chen, J.M., and Black, T.A. (1993). Effects of clumping on estimates of stand leaf area index using the LICOR LAI-2000. *Canadian Journal of Forest Research*, 23, 1940-1943.
- Smolander, H., and Stenberg, P. (1996). Response of LAI-2000 estimates to changes in plant surface area index in a Scots pine stand. *Tree Physiol.*, 16, 345-349.
- Snell, J.A.K., and Brown, J.K. (1978). Comparison of tree biomass indicators- DBH and sapwood area. *Forest Science*, 24, 455-457.
- Soil Survey Division, N.R.C.S., United States Department of Agriculture. 2001. Official soil series descriptions. USDA-NRCS Soil Survey Division, <http://www.statlab.iastate.edu/soils/osd>.
- Spanner, M.A., Brass, J.A., and Peterson, D.L. (1984). Feature selection and the information content of Thematic Mapper simulator data for forest structural assessment. *IEEE Transactions on Geoscience and Remote Sensing*, 22, 482-489.
- Spanner, M.A., Pierce, L.L., Peterson, D.L., and Running, S.W. (1990a). Remote sensing of temperate coniferous forest leaf area index: The influence of canopy closure, understory vegetation and background reflectance. *International Journal of Remote Sensing*, 11, 95-111.

- Spanner, M.A., Pierce, L.L., Running, S.W., and D.L. Peterson (1990b). The seasonality of AVHRR data of temperate coniferous forests: relationship with LAI. *Remote Sensing of Environment*, 33, 97-112.
- Stenback, J.M., and Congalton, R.G. (1990). Using Thematic Mapper imagery to examine forest understory. *Photogrammetric Engineering and Remote Sensing*, 56, 1285-1290.
- Stenberg, P., DeLucia, E.H., Schoettle, A.W., and Smolander, H. (1995). Photosynthetic light capture and processing from cell to canopy. In *Resource Physiology of Conifers*. Eds. W.K. Smith and T.M. Hinckley. Academic Press, New York, pp 3-38.
- Stenberg, P., Linder, S., Smolander, H., and Flower-Ellis, J. (1994). Performance of the LAI-2000 plant canopy analyzer in estimating leaf area index of some Scots pine stands. *Tree Physiology*, 14, 981-995.
- Stow, T.K., Allen, H.L., and Kress, L.W. (1992). Ozone impacts on seasonal foliage dynamics of young loblolly pine. *Forest Science*, 38, 102-119.
- Sword, M.A., Chambers, J.L., Tang, Z., Dean, T.J., and Goelz, J.C. (2002). Long-term trends in loblolly pine productivity and stand characteristics in response to stand density and fertilization in the Western Gulf Region. Citation for proceedings: Outcalt, Kenneth W., ed. 2002. Proceedings of the eleventh biennial southern silvicultural research conference. Gen. Tech. Rep. SRS-48. Asheville, NC: U.S. Department of Agriculture, Forest Service, Southern Research Station. 622 p.
- Tan, B., Hu, J., Zhang, P., Huang, D., Shabanov, N., Weiss, M., Knyazikhin, Y., and Myneni, R.B. (2005). Validation of Moderate Resolution Imaging Spectroradiometer leaf area index product in croplands of Alpiilles, France, *J. Geophys. Res.*, 110, D01107, doi:10.1029/2004JD004860.
- Teskey, R.O., Bongarten, B.C., Cregg, B.M., Douherty, P.M., and Hennessey, T.C. (1987). Physiology and genetics of tree growth response to moisture and temperature stress: An examination of the characteristics of Loblolly pine (*Pinus taeda* L.). *Tree Physiology*, 3, 41-61.
- Tian, Y., Woodcock C.E., Wang Y., Privette J.L., Shabanov N.V., Zhou L., Zhang Y., Buermann W., Dong J., Veikkanen B., Hame T., Andersson K., Ozdogan M., Knyazikhin Y., and Myneni, R.B. (2002). Multiscale analysis and validation of the MODIS LAI product - II. Sampling strategy. *Remote Sensing of Environment*, 83, 431-441.
- Tou, J.T., and Gonzalez, R.C. (1974). *Pattern Recognition Principles*. Addison-Wesley Pub. Co., Reading, Ma.
- Turner, D.P., Cohen, W.B., Kennedy, R.E., Fassnacht, K.S., and Briggs, J.M. (1999). Relationships between leaf area index and Landsat TM spectral vegetation indices across three temperate zone sites. *Remote Sensing of Environment*, 70, 52-68.
- Vose, J., and Allen, H.L. (1988). Leaf area, stemwood growth, and nutrition relationships in loblolly pine. *For. Sci.*, 34, 547-563.
- Vose, J.M. (1988). Patterns of leaf area distribution within crowns of nitrogen- and phosphorus-fertilized loblolly pine trees. *For. Sci.*, 34, 564-573.

- Wilson, W.J. (1963). Estimation of foliage denseness and foliage angle by inclined point quadrats. *Aust. J. Bot.*, 11, 95-105.
- Williams, D.L. (1991). A comparison of spectral reflectance properties at the needle, branch, and canopy level for selected conifer species. *Remote Sensing of Environment*, 35, 79-93.
- Wulder, M.A., LeDrew, E.F., Franklin, S.E., and Lavigne, M.B. (1998). Aerial image texture information in the estimation of northern deciduous and mixed wood forest leaf area index (LAI). *Remote Sensing of Environment*, 64, 64-76.
- Yang, W., Tan, B., Huang, D., Rautiainen, M., Shabanov, N.V., Wang, Y., Privette, J.L., Huemmrich, K.F., Fensholt, R., Sandholt, I., Weiss, M., Ahl, D.E., Gower, S.T., Nemani, R.R., Knyazikhin, Y., and Myneni, R.B. (2005). MODIS Leaf Area Index Products: From Validation to Algorithm Improvement. *IEEE Transactions on Geoscience and Remote Sensing*, (In Press).
- Yoder, B.J. and Waring, R.H. (1994). The normalized difference vegetation index of small Douglas-fir canopies with varying chlorophyll concentrations. *Remote Sensing of Environment*, 49, 81-91.
- Yu, S., Chambers, J.L., Zhenmin, T., and Barnett, J.P. (2003). Crown characteristics of juvenile loblolly pine 6 years after application of thinning and fertilization. *Forest Ecology and Management*, 180, 345-352.
- Zhang, S., Hennessey, T.C., and Heinemann, R.A. (1997). Acclimation of loblolly pine (*Pinus taeda*) foliage to light intensity as related to leaf nitrogen availability. *Canadian Journal Forest Research*, 27, 1032-1040.

APPENDICES

Appendix A. Point-in-Time LAI Estimation (Sampson et al., 2003)

Validation of the TRAC-DHP indirect optical technique for estimating stand level LAI requires a comparison to an assumed “truth” baseline. Validation data was provided by NCSFNC where stand-level foliage biomass (g/ha) was converted to LAI from estimates of specific leaf area (cm²/g) (SLA), defined as the ratio of green leaf area to oven dry weight (65°C). Sampson et al. (2003) developed a technique for deriving monthly LAI estimates from point-in-time measurements of foliage biomass based on the needle phenology of *P. taeda*. This method alleviated the need for coordination of the indirect optical measurements with the direct sampling of LAI. LAI was estimated over four control plots each from both sites for the year 2003.

Based on *P. taeda* leaf accretion and abscission phenology, three years of point-in-time stand-level foliage biomass were required to initialize the monthly estimates of 2003 LAI. Sampson et al. (2003) found that *P. taeda* varied twofold interannually with a minimum LAI in March-April and a maximum in September. Needle abscission and accretion were found to impact a current year foliage cohort beginning at bud initiation (July) and continuing through the third year, though only 7-9% of the foliage could be attributed to that third year. Sampson et al. (2003) determined that monthly estimates of LAI could be found with the parameter inputs of relative needle accretion and abscission (monthly), therefore monthly LAI for 2003 was estimated as:

$$LAI_n = C_{LAI(c)}(A_{Cn} - A_{Bn}) + C_{LAI(c-1)}(1 - A_{Bn+12}) + C_{LAI(c-2)}(1 - A_{Bn+24}) \quad (1)$$

where LAI_n is stand LAI (m²m⁻²) for month n (1-12); $C_{LAI(c)}$, $C_{LAI(c-1)}$, and $C_{LAI(c-2)}$ are the cohort LAI values for 2003, 2002, and 2001, respectively; A_{Cn} is the relative needle accretion for month n ; and A_{Bn} is the relative needle abscission for month n . Daily LAI was calculated by evenly dividing the monthly change in LAI among all the days between the monthly estimates.

Three years of cohort LAI (C_{LAI}), years 2001-2003, were determined through the primary inputs of stand-level foliage biomass and SLA. Stand-level foliage biomass was estimated from age and treatment specific whole tree regression equations developed at the SETRES location following the methods presented in Albaugh et al. (1998) and (2004). These site and plot specific regression equations were based on destructive harvests from multiple years (1992, 1994, 1996, 1998, 2003) and included tree diameter and height as independent variables (Albaugh et al. 2005). Sampling SLA required the collection of foliage samples (Brunswick 2003, SETRES 2002) from four trees per site (1 foliage sample = 20 fascicles) and from six crown locations per tree, yielding 24 total foliage samples collected on both sites. SLA was calculated by measuring the projected green leaf area (Delta-T Devices) and oven dry weight. This ratio (cm^2/g) was averaged over all samples at each site. Treatment-invariant estimates of SLA multiplied by foliage biomass (grams dry mass of foliage per square meter of ground, g/m^2) from three crown levels (top, middle, and bottom) yielded estimates of LAI. The formula for empirical estimates of LAI estimated from foliage biomass and treatment-invariant SLA is summarized as follows (Sampson et al., 2003):

$$LAI = \frac{[(fol(i) * cbf_b * SLA_b) + (fol(i) * cbf_m * SLA_m) + (fol(i) * cbf_t * SLA_t)]}{10000} \quad (2)$$

where $fol(i)$ is total foliage mass (g/m^2), cbf is the crown biomass fraction at three crown positions (bottom, middle, and top), and SLA is treatment invariant SLA at three canopy positions (bottom, middle, and top). For the control plots at both SETRES and Brunswick sites, $cbf_{b,m,t}$ and $SLA_{b,m,t}$ was (0.41, 0.41, 0.18) and (36.65, 32.49, 30.47 cm^2g^{-1}), respectively.

Appendix B. MakeGrid AML

```
&args in out size
&if [null %in%] or [null %out%] or [null %size%] &then
&return &error USAGE: &r makegrid <in_cover> <out_cover> <cellsize>
&describe %in%
&s xmin = %dsc$xmin%
&s xmax = %dsc$xmax% + %size%
&s ymin = %dsc$ymin%
&s ymax = %dsc$ymax% + %size%
generate %out%
fishnet
%xmin% %ymin%
%xmin% %ymax%
%size%,%size%
0,0
%xmax% %ymax%
quit
build %out%
projectcopy cover %in% cover %out%
&return
```